THE STRUCTURAL BASIS FOR LIPID-DEPENDENT UNCOUPLING OF THE NICOTINIC ACETYLCHOLINE RECEPTOR

Jiayin Sun

Dissertation submitted to the Faculty of Graduate and Postdoctoral Studies, Department of Biochemistry, Microbiology, and Immunology in partial fulfillment of the requirement for a Masters of Science in Biochemistry.

University of Ottawa
Ottawa, Ontario, Canada
July, 2016

© Jiayin Sun, Ottawa, Canada, 2016

Abstract

In lipid membranes lacking activating lipids, the nicotinic acetylcholine receptor adopts an uncoupled conformation that binds ligand, but does not transition into an open conformation. Understanding the mechanisms of lipid-dependent uncoupling is essential to understanding lipid-nAChR interactions, which may be implicated in pathological conditions such as nicotine addition. Here, I tested two structural features of a proposed uncoupling method to elucidate the mechanism of lipid-dependent uncoupling. First, infrared measurements and electrophysiological characterization performed in prokaryotic homologues indicate that lipid sensitivity is largely controlled by the most peripheral α-helix in the transmembrane domain, M4. My data show that tighter association of M4 with the adjacent M1 and M3 transmembrane α-helices decreases a receptor's propensity to adopt a lipid-dependent uncoupled conformation. Second, I indirectly tested the hypothesis that uncoupling results from a conformational change at the extracellular/transmembrane domain interface that leads to an increased separation between the two domains and ultimately to a constriction of the channel pore. Finally, biophysical studies presented in this dissertation shed light on the complex binding of a number of non-competitive channel blockers to the nicotinic acetylcholine receptor channel pore in both the resting and desensitized states. The data provide further insight into the structural rearrangements that occur upon uncoupling of ligand binding and gating in the nicotinic acetylcholine receptor.

Acknowledgements

This work would not have been possible without the continued support of many people, toward whom I would now like to express my sincere gratitude.

- First and foremost, I would like to thank my graduate supervisor, Dr. John Baenziger. The reason I joined this lab was because I admired your sincere dedication to doing ‘good science.’ Despite the many frustrations of life in the lab, I am thankful to have worked with you, and I hope that some of your integrity has permanently rubbed off on me.

- To my parents, who always got on my back when I began to drag my feet. Thank you for your unwavering support, and for understanding that I am still just finding my way in the world.

- To my boyfriend, Justin Chiao. I wish you would let me brag about you more. I know of no one else who has your steadfast patience and consideration, and I am endlessly thankful for all the times you listened to me vent my frustrations or simply stepped back and gave me the space I needed. Thank you for the intellectual conversations, for your reasonableness, for your gentleness, and most of all, for your love.

- To my lab buddies who shared my frustrations and successes: Jaimee Domville, Claire Edrington, Daniel Giguère, Camille Hénault, Annie Jiang, Charlotte Searle-Wagner, and Daniel Therien. Special thanks to Camille, who is always ready with a helpful suggestion, and who always manages to somehow magic-hands the AKTA and electrophysiology rig back into working condition. I literally could not have collected my data without you.

- To the lab of Dr. Jean Gariepy at Sunnybrook, for the use of their ITC machine. Special thanks to Dr. Marzena Cydzik, who toughed through some frustrating days of experiments with me like a champ and who taught me to keep a cool head and try, try, try again.

- To Dr. Corrie daCosta. I don’t think we’ve actually ever talked in real life, but the paper (electronic) trail of meticulously documented data and protocols you left behind was invaluable to my growth as a scientist. Thank you for showing me how to do some darn good science.

- To Dr. Jeffrey Keillor, for generously synthesizing and providing the TID.

Preface

Most of the work presented in this document has been published or has been submitted for publication, with the last segment being an experimental chapter.

Chapter 2

Casey L. Carswell, **Jiayin Sun**, and John E. Baenziger. (2015) Intramembrane aromatic interactions influence the lipid sensitivities of pentameric ligand-gated ion channels. *J. Biol. Chem.* **290**, 2496-2507.

Chapter 3

Jiayin Sun, Frederique Comeau, and John E. Baenziger. (2016) Fluorescent channel blockers exhibit distinct pharmacologies for uncoupled, resting, and desensitized nicotinic acetylcholine receptors. *BBA-Biomembranes.*1859(2), 146-154.

Chapter 4

Experimental chapter. Pore pharmacology of reconstituted nAChR.

Table of Contents

Abstract .... **ii**

Acknowledgements .... **iii**

Preface .... **iv**

Table of Contents .... **v**

List of Figures .... **viii**

List of Tables .... **x**

List of Abbreviations .... **xi**

Chapter 1 – Introduction **1**

1. General Introduction 2
2. Neurotransmission 3
    - The neuron 3
    - Membrane potential 6
    - Action potentials 6
    - The synapse 8
    - pLGICs and neurotransmission 8
3. The Nicotinic Acetylcholine Receptor 12
    - nAChR subtypes 12
    - Structure of the nAChR and other pLGICs 13
    - Gating 20
    - The coupling interface 26
    - Conformations of the nAChR 29
    - Modulators of nAChR function 32
4. Lipid Sensitivity and Uncoupling 37
    - nAChR lipid sensitivity 37
    - Lipid-nAChR interactions 37
    - Lipid-dependent uncoupling 38
    - M4 lipid-sensor model of lipid-dependent uncoupling 39

ELIC and the uncoupled model 40
Broader implications of nAChR lipid sensing and uncoupling 48
5. Research Aims and Organization of Dissertation 52

Chapter 2 – Intramembrane Aromatics Influence Lipid Sensitivity 53
1. Rationale 54
2. Methods...55
Preparation of ELIC proteoliposomes 55
Fourier Transform Infrared Spectroscopy (FTIR) 56
Electrophysiology 57
3. Results...57
Aromatic additions between M1/M3 and M4 decrease peptide backbone hydrogen exchange 57
Aromatics increase TMD Stability 63
Aromatic additions between M1/M3 and M4 promote coupling in ELIC............68
4. Discussion 71
5. Conclusion...74

Chapter 3 – Alterations to Pore Conformation in Uncoupling (manuscript) 76
1. Preface...77
2. Introduction...77
3. Methods...82
Materials 82
Preparation of reconstituted nAChR..82
Fourier transform infrared spectroscopy...82
Equilibrium ^{3}H-ACh binding...82
Fluorescence spectroscopy..83
4. Results...83
The uncoupled nAChR in PC membranes 83
No detectable binding of ethidium to the pore of the uncoupled nAChR 89
No detectable binding of CrV to the pore of the uncoupled PC-nAChR..............97

5. Discussion 101

Chapter 4 – Pore Pharmacology of Membrane-Reconstituted nAChR 105

1. Rationale 106
2. Methods..109
    - Preparation of reconstituted nAChR 109
    - Fluorescence spectroscopy..109
    - Isothermal calorimetry 110
3. Results..110
    - Local anesthetics occupy more than one pore site 110
    - Displacement of ethidium and CrV by an antidepressant 121
    - TID does not compete for ethidium/CrV sites 124
    - Ethidium and CrV bind desensitized nAChR at different but overlapping loci ..125
    - Calorimetric measurement of NCA binding to nAChR......................128
4. Discussion 134
5. Conclusion 142

Chapter 5 - General Conclusions...143

1. M4 acts as a Lipid Sensor 144
2. nAChR Pore Conformations 145
3. Final Remarks 146

References...148

Appendices...160

A. CHAPS Correction for Free Crystal Violet 161
B. Supporting Data for CrV Binding Experiments..166

Curriculum Vitae 175

List of Figures

Chapter 1

Figure 1.1 Schematic of a neuron 5
Figure 1.2 Schematic of events at a synapse following an action potential 10
Figure 1.3 pLGIC structure....15
Figure 1.4 Schematic and structure of the ligand-binding site 18
Figure 1.5 Structure of the *Torpedo* nAChR pore 22
Figure 1.6 pLGIC gating motions....25
Figure 1.7 Coupling interface in a *Torpedo* nAChR subunit....28
Figure 1.8 Schematic of pLGIC conformational equilibrium....31
Figure 1.9 Allosteric binding sites in pLGICs....35
Figure 1.10 Working model of lipid-dependent uncoupling 42
Figure 1.11 Coupling interface of the nAChR and ELIC 45
Figure 1.12 Transmembrane aromatics in the nAChR and prokaryotic homologues....47
Figure 1.13 Structural comparison of the nAChR and ELIC pore 50

Chapter 2

Figure 2.1 Homology model of ELIC with added aromatics....59
Figure 2.2 Infrared spectra of ELIC-3 62
Figure 2.3 Stacked thermal denaturation plots of ELIC and ELIC-3 65
Figure 2.4 Representative thermal denaturation curves....67
Figure 2.5 Dose-response of ELIC-3....70

Chapter 3

Figure 3.1 Structural comparison of the nAChR and ELIC....80
Figure 3.2 Structure and function of membrane-reconstituted nAChR....85
Figure 3.3 Ethidium binding to reconstituted nAChR....91
Figure 4.4 Kinetic ethidium binding experiments to different conformations of nAChR....95
Figure 4.5 Crystal violet binding to reconstituted nAChR 99

Chapter 4

Figure 4.1 Molecular structures of noncompetitive antagonists 108
Figure 4.2 Competition between local anesthetics and ethidium in desensitized nAChR.........113
Figure 4.3 Competition between local anesthetics and CrV in desensitized nAChR 117
Figure 4.4 Competition between local anesthetics and CrV in resting nAChR.........................120
Figure 4.5 Competition binding of bupropion 123
Figure 4.6 Competition binding of TID 127
Figure 4.7 Competition binding between ethidium and CrV in desensitized nAChR...............130
Figure 4.8 Tetracaine binding to resting aso-nAChR 133
Figure 4.9 TID binding to resting aso-nAChR 136
Figure 4.10 NCA binding sites in the nAChR pore 139

Appendix A

Figure A.1 CrV fluorescence intensity in the presence and absence of nAChR 163
Figure A.2 Free vs. added CrV 165

Appendix B

Figure B.1 Kinetic CrV binding experiments to reconstituted nAChR 168
Figure B.2 Emission scans of CrV bound to resting aso-nAChR...171
Figure B.3 Peak emission of CrV bound to nAChR with increasing concentrations of α-BTX
....173

List of Tables

Chapter 3

Table 3.1 Scatchard analysis of ^{3}H-ACh binding to reconstituted nAChR 87

Table 3.2 Binding of ethidium and crystal violet to reconstituted nAChR 92

Chapter 4

Table 4.1 Competition binding of noncompetitive antagonists to reconstituted nAChR..........114

List of Abbreviations

^1H	Hydrogen
^2H	Deuterium
^2H_2O	Deuterium oxide
5-HT_3R	5-hydroxytryptamine (serotonin) receptor
α-BTX	α-bungarotoxin
ACh	Acetylcholine
AChBP	Acetylcholine binding protein
aso	Asolectin lipids
Aso-ELIC	ELIC reconstituted into asolectin lipids
Aso-GLIC	GLIC reconstituted into asolectin lipids
Aso-nAChR	nAChR reconstituted into asolectin lipids
au	Arbitrary units
B_{max}	Maximum number of binding sites
Carb	Carbamylcholine
CHAPS	3-((3-cholamidopropyl)dimethylammonio)-1-propanesulfonate
Chol	Cholesterol
Cl^-	Chloride ion
C=O	Carbonyl group
CrV	Crystal violet
Cryo-EM	Cryo-electron microscopy
D	Desensitized conformation
DDM	Dodecylmaltoside
Dib	Dibucaine

EC_{50}	Concentration at which half maximal activity is achieved
ECD	Extracellular domain
EDTA	Ethylenediaminetetraacetic acid
ELIC	A pLGIC isolated from *Erwinia chrysanthemi*
FTIR	Fourier transform infrared spectroscopy
$GABA_A$	Gamma-aminobutyric acid
GLIC	A pLGIC isolated from *Gloeobacter violaceus*
GluCl	Glutamate-gated chloride channel
GlyR	Glycine receptor
HEPES	4-(2-hydroxyethyl)-1-piperazineethanesulfonic acid
IC_{50}	Concentration at half maximal inhibition
ICD	Intracellular domain
IPTG	Isopropyl-β-D-thiogalactopyranoside
ITC	Isothermal calorimetry
K^+	Potassium ion
K_d	Dissociation constant
K_{eq}	Equilibrium constant
K_i	Inhibition constant
M1	Transmembrane α-helix 1
M2	Transmembrane α-helix 2
M3	Transmembrane α-helix 3
M4	Transmembrane α-helix 4
MBP	Maltose binding protein
MWC	Monod-Wyman-Changeux model of allostery
$N\text{-}^1H$	Peptide hydrogen

N-^{2}H	Peptide deuterium
Na$^+$	Sodium ion
nAChR	Nicotinic acetylcholine receptor
NAM	Negative allosteric modulator
NCA	Noncompetitive antagonist
NSRI	Norepinephrine selective reuptake inhibitor
O	Open conformation of the nAChR
PA	phosphatidic acid
PAM	Positive allosteric modulator
PC	phosphatidylcholine
PC-ELIC	ELIC reconstituted into phosphatidylcholine membranes
PC-GLIC	GLIC reconstituted into phosphatidylcholine membranes
PC-nAChR	nAChR reconstituted into phosphatidylcholine membranes
PCP	Phencyclidine
pLGIC	Pentameric ligand-gated ion channel
R	Resting conformation
SEM	Standard error of the mean
SSRI	Selective serotonin reuptake inhibitor
TCP	Tenocyclidine
T_d	Temperature at which half denaturation occurs
TEA	Tetraethylammonium
TID	3-trifluoromethyl-3-(*m*-iodophenyl)diazirine
TM	Transmembrane
TMD	Transmembrane domain

TQS	4-(naphthalene-2-yl)-3a,4,5,9b-tetrahydro-3H-cyclopenta[c]quinoline-8-sulfonamide
TRB	*Torpedo* Ringer buffer
TRIS	(hydroxymethyl)aminomethane
U	Uncoupled conformation of the nAChR

Chapter 1

Introduction

1. General Introduction

The survival of living organisms, from single-celled bacteria to mammals, requires the ability to perceive and respond to changes in their environment. In humans, as in many other species, these demands are satisfied by the existence of a nervous system: a sophisticated biological control system for information flow within the body of the organism. The mammalian nervous system has a role in both conscious behavior, such as voluntary command of motor function and thought, and unconscious behavior, such as autonomous breathing and sensory processing. Disruptions in the functioning of this system through disease states or normal aging have major consequences for physical and/or mental health. The study of the nervous system, and in particular of the brain, is therefore of great interest both in the context of health and in the understanding of human consciousness.

A fully in-depth understanding of our nervous system requires knowledge not just on the systemic level, but also at the cellular and molecular level. Considerable research has focused on the specific events occurring at the synapse, the site of information transfer between neurons. My particular interest lies in a superfamily of membrane-bound neurotransmitter receptors that mediate the transformation of a chemical signal released from one neuron to an electrical signal at the next cell. These receptors are crucial to the normal functioning of the brain and are amenable to modulation by a host of endogenous and exogenous factors. Accordingly, their dysfunction has been implicated in many neurological disease states.

The research presented in this dissertation focuses on a member of this family of receptors, the acetylcholine-gated nicotinic receptor (nAChR). The nAChR from the electric fish *Torpedo californica* and *Torpedo marmorata* is the prototypical member of this class of receptor, and has been used extensively as a model for the study of their structure and function. The broad goal of this work was to investigate the structural correlates of nAChR lipid sensitivity and to characterize in more detail the structure of a novel, lipid-influenced uncoupled conformation adopted by the nAChR in certain membrane environments. The research presented is prefaced by a review of neurotransmission, our current understanding of nAChR structure and function, and what is known to date of the uncoupled conformation.

2. Neurotransmission

The neuron. Information is transmitted through the nervous system in the form of chemical and electrical signals, and is relayed by highly specialized cells called neurons. Neurons may be classified into several subtypes based on their specific morphology, but they share a number of key structural components (Figure 1.1): 1) a widely branched network of filamentous projections collectively referred to as dendrites; these function as the site for information reception, 2) the cell body or soma, which receives electrical signals from individual dendrites, 3) the axon hillock, where electrical signals are integrated, and 4) a specialized projection called the axon, which extends from the axon hillock. Neurons typically possess only one axon, less branched than its dendritic arboration, through which the electrical signal is propagated in (generally) unidirectional fashion from the soma down to small, bud-like projections off the axon called axon termini. Neurotransmitter-loaded vesicles are stored here and fuse with the plasma membrane upon depolarization, releasing their contents into the extracellular space (see *Action potentials*, below). Axons in the central nervous system and peripheral nervous system are ensheathed in insulating myelin, which enhances the propagation

Figure 1.1

Schematic diagram of the neuron showing major structural components involved in neurotransmission.

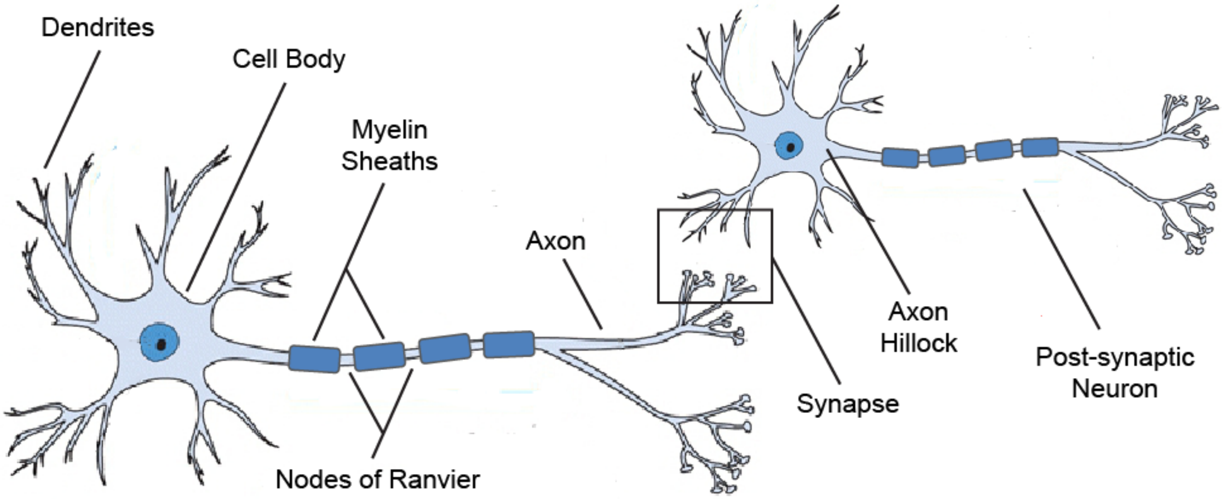
Dendrites
Cell Body
Myelin Sheaths
Axon
Nodes of Ranvier
Synapse
Axon Hillock
Post-synaptic Neuron

speed of electrical signals and is largely lipid by composition. This myelin sheath is provided by nearby supporting cells, or glia (oligodendrocytes and Schwann cells in the central and peripheral nervous system, respectively).

Membrane potential. The neuronal cell membrane is largely composed of phospholipids, creating a barrier between the intra- and extracellular compartments that is impermeable to most large polar or charged species. Movement of ions across the membrane is mediated by pumps and channels. The membrane-bound Na^+/K^+ ATPase exchanges 3 Na^+ ions to the extracellular compartment for 2 K^+ ions to the intracellular compartment per ATP hydrolyzed, resulting in a large concentration gradient across the membrane for both ions (Na^+ is concentrated to ~145mM extracellularly and 5mM intracellularly, and K^+ to 5mM extracellularly and 140mM intracellularly) and a net loss of positive charge from the cell interior. K^+ leak channels, however, allow the efflux of K^+ ions down its concentration gradient until the negative charge inside the cell exerts an inward driving force equal to the outward driving force generated by the concentration gradient. These events collectively result in the accumulation of positive charge outside the cell, leading to a resting membrane potential for the neuron at approximately -70mV (intracellular relative to extracellular).

Action potentials. Signals are passed through neurons in the form of electrical events called action potentials, which result from rapid and transient changes in local membrane potential. In most neurons found in the central nervous system, an action potential is initiated by stimulus from an upstream neuron. Incoming signals are received at a neuron's dendrites as a depolarization event (a shift in membrane potential towards positive potential due to the influx of cations into the cell) corresponding in size to the frequency and strength of the stimulus. Due to the high degree of branching in dendritic arboration, a neuron can simultaneously receive input from many sources.

These input signals are summated spatially and temporally as they converge at the axon hillock. If the combined signal at this structure causes local depolarization of the membrane above an excitation threshold of roughly -55mV, voltage-sensitive sodium channels open, allowing the rapid influx of Na^+ ions down their electrochemical gradient. The Na^+ ions diffuse down the axon and depolarize nearby segments of the membrane. This leads to the opening of additional sodium channels, rapid influx of Na^+ ions, and ultimately propagation of the signal down the axon. In the event that the summated signal at the hillock does not reach the excitation threshold, the action potential is not triggered and the axon remains electrically silent.

Na^+ influx after the threshold potential is reached locally depolarizes the cell membrane to nearly +50mV, close to the Na^+ equilibrium potential of +60mV. The rising membrane potential inactivates voltage-gated Na^+ channels and activates voltage-gated K^+ channels, allowing K^+ ions to flux out of the cell along their concentration gradient, leading to repolarization of the membrane. Because the K^+ channels close slowly, K^+ efflux continues until near to the equilibrium potential of K^+, at which point the local membrane is hyperpolarized at -90mV. During the after-hyperpolarization period, all voltage-gated channels have closed, and resting membrane potential is restored by activity of the Na^+/K^+ ATPase and K^+ leak channels, as discussed previously (see *Membrane potential*, above).

An action potential is followed by an absolute refractory period of 1-2 ms during which the inactivated voltage-gated Na^+ channels are unable to respond to further stimuli, and then by a relative refractory period of about 3-4 ms during which excitability is gradually restored as they regain an activatable conformation. During this period, a second action potential can be elicited if a stronger stimulus is applied. The refractory period coincides with hyperpolarization and the subsequent return to resting membrane potential.

Refraction after depolarization ensures that the electrical signal travels unidirectionally, as recently depolarized membrane cannot be immediately excited again. Myelination by glial cells insulates axon segments and allows for saltatory conduction. Depolarization spread is maintained during myelinated stretches of axon without the need for voltaged-gated Na^+ channels, which are concentrated at bare segments called nodes of Ranvier. In highly developed nervous systems, myelination allows for rapid signal transduction over long distances.

The synapse. Communication between most cells of the nervous system occurs at a synapse or synaptic cleft – a space of roughly 20-40 nm that separates the axon terminus of a pre-synpatic neuron from the dendrite or sometimes soma of a post-synaptic cell (Figure 1.2). Following an action potential in the pre-synaptic cell, a wave of depolarization travels down the axon to the axon termini, where positive membrane potential results in the fusion of docked, neurotransmitter-containing vesicles with the plasma membrane. Neurotransmitter molecules are released into the synaptic cleft and diffuse across the synapse to bind receptors on the post-synaptic membrane, which commonly function as ion channels and/or activate intracellular second messenger systems, leading to a post-synaptic response.

pLGICs and neurotransmission. The activity of any particular synapse is dependent on the identity and quantity of the neurotransmitters at that synapse, and on the specificity of the post-synaptic receptors, amongst other factors. At mammalian chemical synapses, the post-synaptic response may be initiated by the action of a family of proteins called pentameric ligand-gated ion channels (pLGICs). These receptors contain five subunits in a donut-like arrangement, forming a membrane-spanning pore that transiently gates open upon binding of neurotransmitter. Broadly, pLGICs can be classified as cation-selective (with members including the nicotinic acetylcholine

Figure 1.2

Schematic diagram of a synapse indicating the sequence of events that lead to the transmission of an electrical signal between neurons.

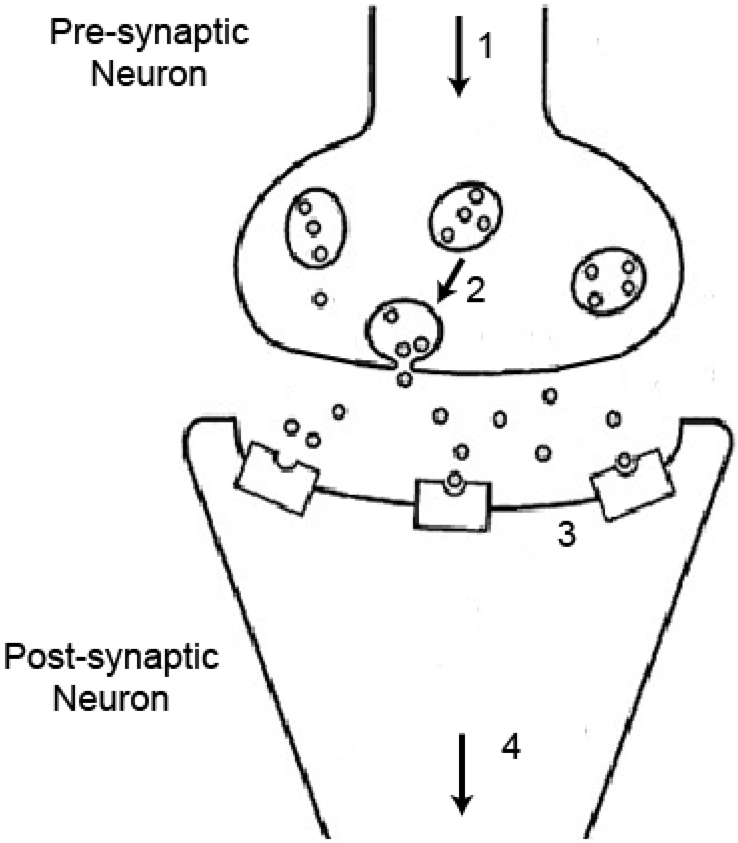
Pre-synaptic Neuron
1
2
3
Post-synaptic Neuron
4

1. Action potential depolarizes membrane to axon terminal

2. Neurotransmitter is released to synaptic cleft by exocytosis

3. Neurotransmitter diffuses across synaptic cleft and binds to receptors on post-synaptic membrane; ions flux into post-synaptic neuron

4. Ion flux causes hyperpolarization/depolarization of post-synaptic membrane

receptor (nAChR) and 5-hydroxytryptamine receptor 3A (5-HT_3R)) or anion-selective (such as the glycine receptor (GlyR) or the type-A γ-aminobutyric acid receptor ($GABA_AR$). Cation-selective channels facilitate the movement of positively charged ions, most commonly Na^+, K^+, and/or Ca^{2+}, across the cell membrane. Under normal physiological conditions, this results in an inward flux of positive charge, causing post-synaptic depolarization. Anion-selective channels under similar conditions cause displacement of Cl^- toward the intracellular compartment, hyperpolarizing the post-synaptic membrane and rendering it less excitable.

Changes in pLGIC function can have profound effects on synaptic behaviour which can be readily seen even at the clinical level. For example, several point mutations have been found in one subunit of the high-affinity neuronal-type nAChR that increase the activity of the receptor and lead to a genetically transmissible form of epilepsy (1). More broadly, alterations in the activity of pLGICs have been implicated in nearly all neuronal diseases and syndromes, including Alzheimer's Disease, Parkinson's Disease, schizophrenia, and even Autism Spectrum Disorder (2-5).

Given the important role played by pLGICs in neuronal signal transmission and the obvious consequences of alterations in their function, the relationship between their structure, function, and pharmacology presents an important and urgent field of study. This document addresses novel advances in the understanding of pLGIC structure and function in the context of the lipid membrane microenvironment. The following chapter briefly reviews the current literature on pLGIC structure and function and lays detailed context for the research described in later chapters.

3. The Nicotinic Acetylcholine Receptor

The nicotinic acetylcholine receptor (nAChR) was the first vertebrate pLGIC identified and is the best-studied to date, as it can be readily purified in significant quantities from the electroplaque organ of the electric rays *Torpedo californica* and *Torpedo marmorata* (6). Its availability and the consequent wealth of literature behind it has made the *Torpedo* nAChR the prototypic pLGIC, and sequence alignments using *Torpedo* nAChR as a template has facilitated the discovery of other pLGICs. Data from the nAChR have contributed greatly to the current understanding of pLGIC structure and function. Interest in the mechanisms of nAChR function stems both from its value as a model for understanding broadly the activity of mammalian pLGICs and from its involvement in human disease states, which may become more readily treatable as an increased understanding of nAChR pharmacology is gained.

nAChR subtypes. In mammals, nAChRs are found in both the central and peripheral nervous systems, and are broadly categorized as either neuronal and muscles types based on their specific subunit composition and stoichiometry. Seventeen homologous nAChR subunits have been identified to date, coding for subunits $\alpha1$-$\alpha10$, $\beta1$-$\beta4$, γ, δ, and ε. Neuronal nAChRs alone comprise several subtypes and are expressed not only in nervous tissue, but also in the lung epithelium and some immune cells, amongst others (7). In the brain, the majority of detectable nAChRs are expressed as homopentamers composed of solely $\alpha7$ subunits or as heteropentamers composed of $\alpha4$ and $\beta2$ subunits in $(\alpha4)_3(\beta2)_2$ (high agonist affinity) or $(\alpha4)_2(\beta2)_3$ (low agonist affinity) stoichiometry (8). Rarer combinations of $\alpha3\beta4$, $\alpha3\beta2$, and $\alpha\beta2\beta3$ subunits can be found in specific brain tissues (9). Muscle type nAChRs are found in the peripheral nervous system and have the subunit composition $(\alpha1)_2\beta\gamma\delta$ or $(\alpha1)_2\beta\varepsilon\delta$; the γ subunit is embryonic and is replaced by the ε subunit in adult tissue.

Structure of the nAChR and other pLGICs. Before recent advances in x-ray crystallography and the discovery of prokaryotic pLGICs amenable to crystallization, the cryo-electron microscopy (cryo-EM) structure of the nAChR (refined to 4Å in 2005 by Unwin, (10)) and the high-resolution crystal structures of the acetylcholine binding protein (2.70Å, from Brejc et al., homologous to the extracellular domain (ECD) of the nAChR (11)), guided studies into the structure of pLGICs. Now, high resolution crystal structures have been obtained for the prokaryotic homologues GLIC, from *Gloeobacter violaceus*, and ELIC, from *Erwinia chrysanthemi*, as well as for the glycine receptor, the glutamate-gated chloride channel (GluCl), the mouse 5-HT$_3$ receptor, and the GABA$_A$ receptor (12-17). In all cases, the pLGICs adopt a similar secondary, tertiary and quaternary fold (Fig. 1.3), although the prokaryotic homologues lack a cytoplasmic domain. While the main focus of my work is on the nAChR, some of the research described in this thesis is centered on the two prokaryotic homologues GLIC and ELIC, which will be discussed in more detail later (see *Lipid Sensitivity and Uncoupling* and Chapter 2).

The nAChR shares a global architecture with the other members of the pLGIC superfamily of five subunits arranged pseudosymmetrically around a central pore (Figure 1.3). Considered individually, each subunit contains a β-sheet-rich N-terminal extracellular portion of approximately 200 residues, a 4-α-helical transmembrane segment of about 150 residues, and a variable C-terminal intracellular segment that forms contacts with the cytoskeleton (note that the intracellular domain is absent in the prokaryotic homologues GLIC and ELIC). Residues in the intracellular domain (ICD) have been linked to gating kinetics and assembly/trafficking (19). The receptor spans approximately 150Å along its longest axis, with 60-70Å being attributed to the extracellular domain (ECD) and about 40Å attributed to the transmembrane domain (TMD) (10).

Figure 1.3

Structure of pLGICs. (A) Cryo-EM structure of the *Torpedo* nAChR at 4Å with the extracellular domain (ECD) labeled in red, the transmembrane domain (TMD) labeled in blue, and the intracellular domain (ICD) labeled in green. Right panel shows a top down view of the ECD (top) and TMD (bottom). Individual subunits are labeled and coloured for clarity. The α-helices are labeled in the TMD view (bottom right). (B) Crystal structures of ELIC (left) and GLIC (right) for comparison. Gating residues are highlighted in yellow spheres for all structures. Figure modified from (18).

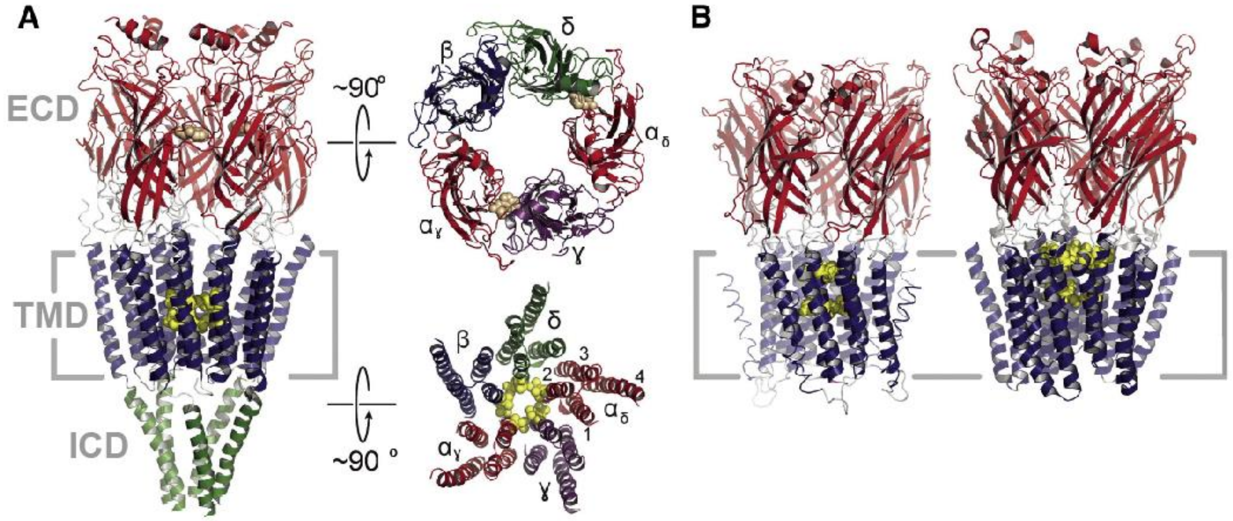
A
ECD
TMD
ICD
~90°
β
δ
α_δ
α_γ
γ
~90 °
3
4
2
1
B

The ECD of each subunit contains 10 β-strands, referred to as β1-β10. These are organized into two anti-parallel β-sheets of six strands (β1, β2, β3, β5, β6, and β8) proximal to the channel pore and four strands (β4, β7, β9, and β10) distal to the pore. These two sheets twist around each other to form a β-sandwich fold with a hydrophobic core. The presence of a highly conserved 13-residue segment between strands β6 and β7 flanked by two disulphide bridge-forming cysteine residues has led vertebrate pLGICs to also be collectively called "Cys-loop receptors." Notably, however, these cysteines are not present in prokaryotic pLGICs, despite otherwise remarkable topological similarity.

The ECD also houses the ligand binding site, which is found at the interface between adjacent subunits, of which one forms the principal (+) face and the other the complementary (-) face (Figure 1.4) (20). In the muscle type nAChR, the α subunits are (+) and the adjacent δ and γ/ε subunits are (-). Each muscle type nAChR therefore contains two sites that are able to bind the endogenous ligand acetylcholine. Residues at the subunit interface are frequently aromatic, but are poorly conserved between subunits. This observation suggests fairly low specificity in subunit assembly, but provides a possible explanation for differences in function between receptor subtypes (11). Initial insights into ligand binding were derived from the high resolution apo- and ligand-bound crystal structures of the soluble acetylcholine binding protein, homologous to the nAChR ECD. Key features of this mechanism have since been observed to be conserved across all vertebrate pLGICs examined to date (14, 15, 17, 21).

Ligand binding is coordinated by residues found on loops connecting the β-strands of the ECD. Loops A (β3- β4), B (β7- β8), and C (β9- β10) are contributed by the (+) subunit and contain conserved aromatic residues (called the "aromatic cage") that interact with the charged quaternary amine of acetylcholine via cation-π interactions (Figure 1.4) (21-24). Loop C extends tangentially

Figure 1.4

Structure of the ligand binding site. (A) Schematic of the ligand binding site in the *Torpedo* nAChR indicating principle (+) and complementary (-) subunits. Cartoon from (18). (B) Structure of the acetylcholine binding protein in complex with the agonist carbamylcholine (red spheres). Only two subunits are shown for clarity. Loops from the principle subunit are depicted in purple (loop C, which caps the bound agonist, is highlighted in yellow), and loops contributed by the complementary face are shown in orange. Aromatic residues key to ligand binding (aromatic box) are shown as blue sticks.

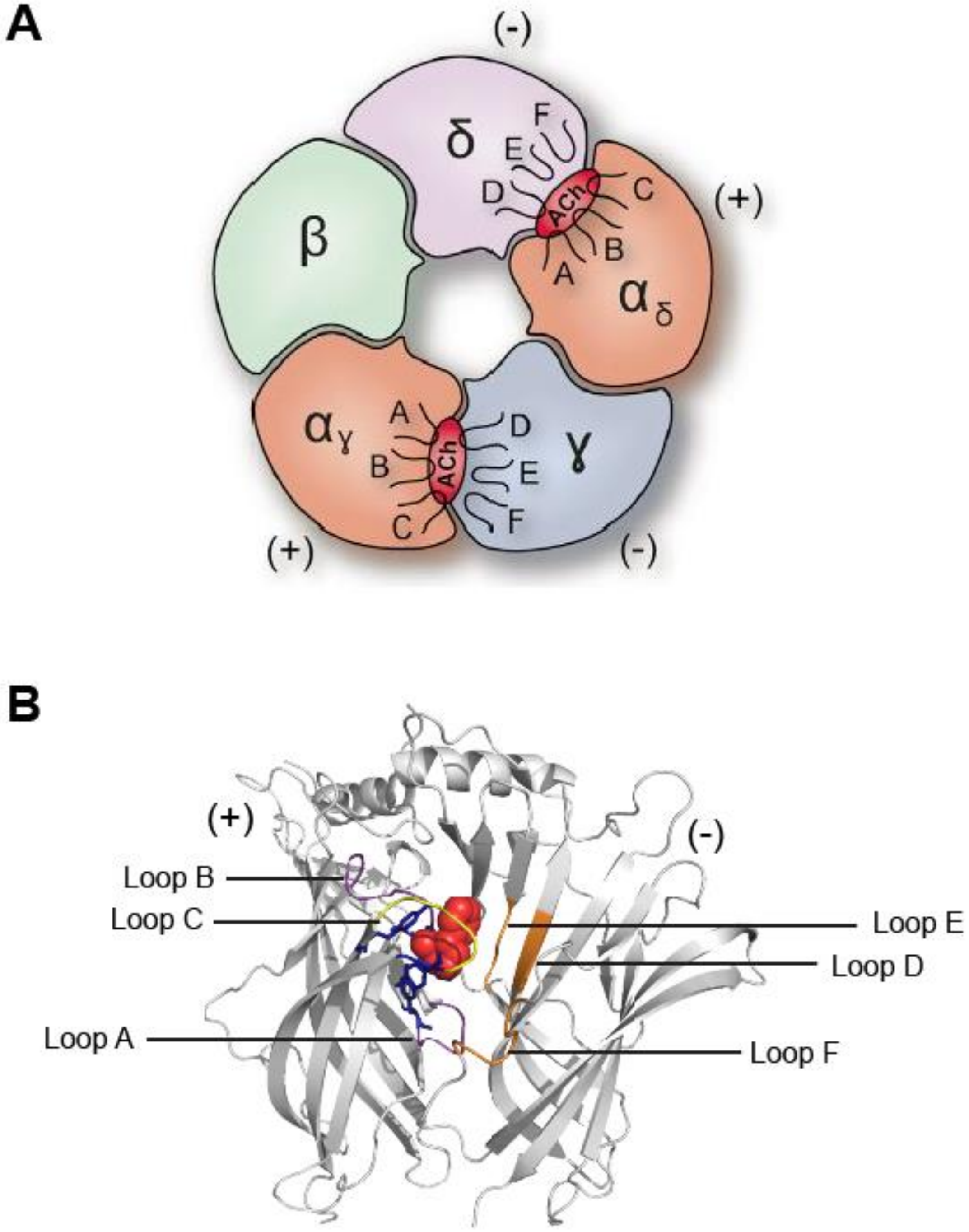
A
(-)
δ
F
E
D
ACh
C
(+)
β
B
A
α δ
αγ
A
D
B
ACh
E
γ
C
F
(+)
(-)
B
(+)
(-)
Loop B
Loop C
Loop E
Loop D
Loop A
Loop F

from the ligand binding site in the resting state, but moves to cap the site in the agonist-bound state (25). The (-) subunit contributes residues from loops D, E (actually found to be β-sheets rather than loops), and F (β6- β7) to the ligand binding site (26-27). These residues vary by subunit and account for differences in ligand affinity between nAChR subtypes.

The ion conduction and channel gating function of the nAChR is localized to the TMD, where the five subunits form a donut structure around a central pore that conducts ions in the open state (Figure 1.3). Each subunit contains four α-helical segments labeled M1-M4. Examined as a whole, the TMD of the pentameric nAChR can be divided into three concentric rings. The innermost ring is formed by the M2 segments from each subunit; these line the channel pore and contribute residues that form the selectivity filter of the channel. The next ring is formed by M1 and M3, and the outermost ring by the M4 α-helices of each subunit, which project radially outwards toward the hydrophobic lipid bilayer environment. Notably, M2 is completely shielded from the environment by the outer rings, and M4, in the outermost ring, is highly lipid exposed.

The intracellular domain (ICD) of the nAChR has been shown to play a role in both ion conductance and channel gating kinetics. The ICD lacks a clear central opening such as found in the ECD or TMD, and likely allows ions to exit the ion conduction pathway through intersubunit gaps, or windows, which are near in diameter to the channel pore and lined with negatively charged residues that contribute to channel selectivity for cations (10).

Gating. The function of the nAChR is fundamentally dependent on its ability to control ion flux through its conducting pore. Cations are drawn to the extracellular mouth of the channel and through the channel pore into the intracellular compartment, passing through rings of pore-lining residues (Figure 1.5). Following the convention where the first residue of M2 is denoted 0’, ions entering from the ECD vestibule first encounter a ring of polar residues at 20’ to guide them into the channel. Hydrophobic residues occupy positions 16’ to 9’. The 6’ position is occupied by a ring of conserved Ser/Thr, and an anionic residue at -1’ (usually Glu, in cationic channels) acts as the charge selectivity filter.

The nAChR structure from Cryo-EM reveals a lack of clear protein density in the channel pore, suggesting an energetic rather than physical barrier to ion flow in the closed state of the receptor (10). At its narrowest point near the middle of the membrane, the closed channel measures roughly 6Å in diameter – too narrow to allow the passage of a hydrated Na^+ or K^+ ion (effective diameters of 8Å and 6Å, respectively). The putative gating region is formed by two rings of highly conserved hydrophobic residues one turn apart on the M2 α-helix (αLeu251 at 9’ and αVal255 at 13’). These residues form part of a hydrophobic stretch along the pore of about 8Å. Ions can only pass through the closed pore if they reduce their effective radius by shedding their hydration shell. However, the hydrophobic pore-lining residues along the gate cannot contribute to hydrophilic interactions with a dehydrated ion, and thus cannot energetically compensate for the loss of the ion’s hydration shell. The hydrophobic residues of the channel gate therefore impose a large energetic penalty for the passage of ions across the closed channel, and need only small adjustments in pore diameter to open the pore enough to allow passage of a hydrated ion (10).

Gating in pLGICs is governed by allosteric transitions initiated by ligand binding in the ECD and ending in conformational change in the TMD pore some 50Å away. In cryo-EM studies of agonist-induced changes at the agonist binding site in the AChBP, Unwin had previously reported a ‘strained’ conformation for the α subunits in which the inner β sheets of the ECD were twisted about 15Å anticlockwise relative to non-α subunits (28). Ligand binding caused a relaxation of this strained conformation to a non-α-like state. More recently, crystal structure of

Figure 1.5

Side surface view of the *Torpedo* nAChR pore (PDB code 2BG9) with one subunit removed for clarity. Pore-lining M2 α-helices are coloured in blue; negatively charged residues are highlighted in red, and hydrophobic gating residues are in yellow. Left: a ribbon diagram showing the relative positions of pore-lining residues, colour-coded as on right. The dotted lines show the approximate limits of the lipid membrane. Figure from (18).

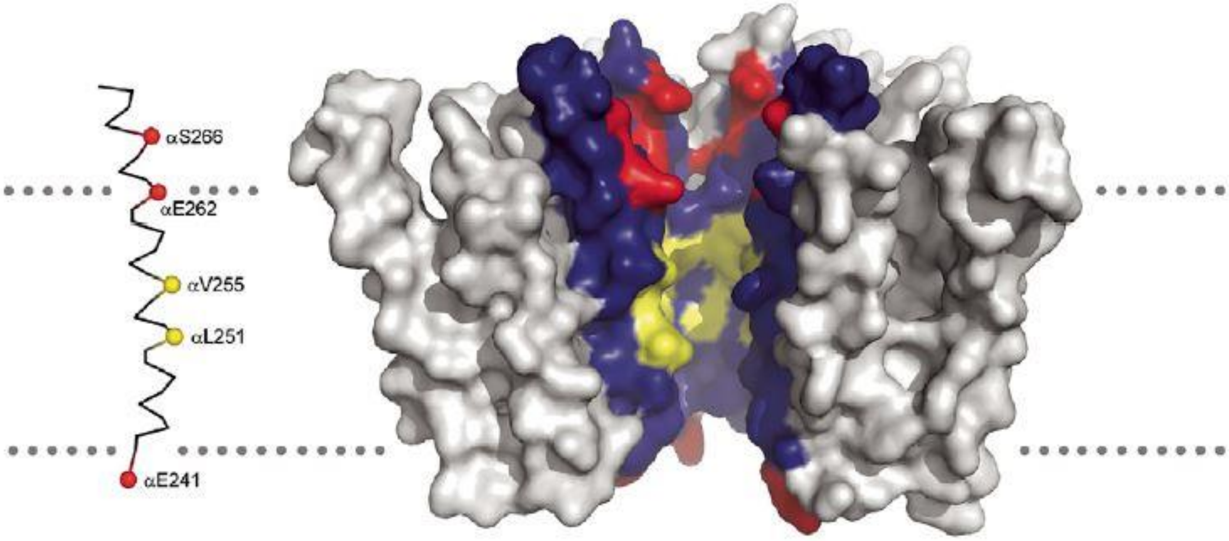
αS266
αE262
αV255
αL251
αE241

both putatively open and closed conformations have been obtained for GLIC (open at pH 4 (29); closed at pH 7 (30)), the eukaryotic glutamate-gated chloride channel (GluCl; open with the partial agonist ivermectin bound (15); closed in apo state (31)), and the glycine-gated chloride channel (GlyR; open with agonist glycine bound; closed with competitive antagonist strychnine bound (14)). A comparison of these structures illustrates an anticlockwise twist of the ECD β-sheets in opening (Figure 1.6). This is notably different from what was observed with the AChBP, and is likely because the ECD in full-length receptors is tethered to the TMD by the inner β-sheets, where Unwin had reported the highest degree of rotational movement in the AChBP.

At the level of the channel pore, the available data suggest a lateral rotation of the transmembrane α-helices relative to the pore axis, with the greatest movement occurring between locations 9' and 16' (32). In particular, GluCl structures from Althoff's group suggest that ivermectin stabilizes the open state by wedging in between helices M1 and M3 of adjacent subunits, causing a conformational change in the M2-M3 linker that rotates M2 to widen the channel pore (15). Ivermectin binds an analogous position in the GlyR to potentiate agonist effects, but crystal structures of GlyR bound with glycine/ivermectin and glycine alone show no significant difference in the positioning of the TMD α-helices (see *Modulators of nAChR function*; 14, 33). The movements observed in the GluCl structure are thus likely a result of opening transitions, rather than steric effects from ivermectin binding. Notably, in the GLIC structures (Fig. 1.6), the TMD twist results in a lateral translation of the α-helices, rather than a rotation. Overall, however, the data reveal clear trends in the mechanism of receptor opening: a counter-clockwise twisting of subunits at the ECD reduces the diameter of the ECD vestibule, while a lateral translation or clockwise twist of α-helices in the TMD increases the pore diameter to allow the passage of ions (32).

Figure 1.6

pLGIC transitions illustrated in GLIC. (A) Overlay of GLIC crystallized at pH 4 (open, orange; PDB 4HFI) and at pH 7 (closed, grey; PDB 4NPQ). Red arrows show direction of gate-opening transition motions. Four subunits are shown, with one in cartoon representation. (B) and (C) show transition movements in the ECD and TMD, respectively.

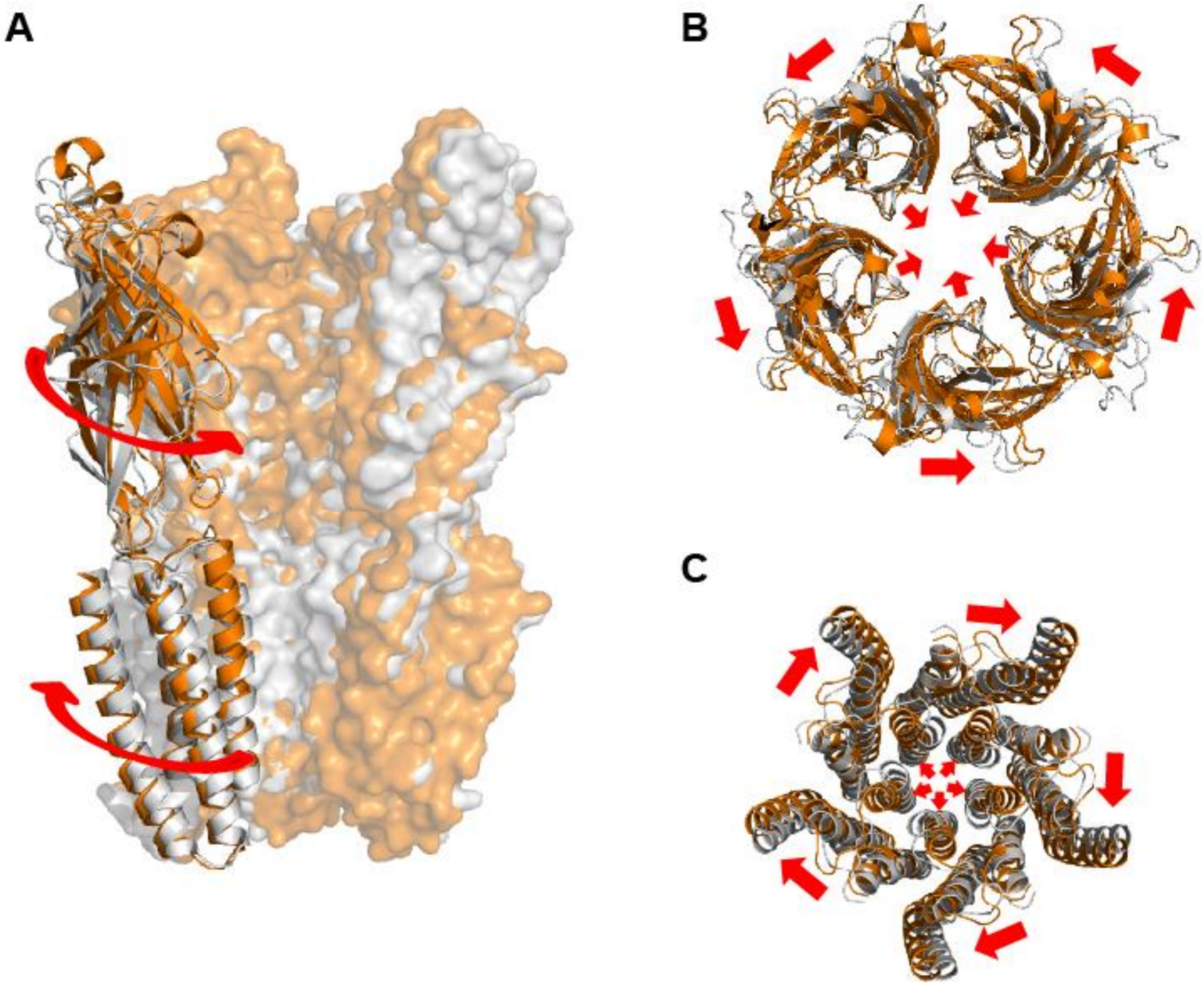
A
B
C

The coupling interface. The translation of agonist binding in the ECD to channel opening in the TMD is mediated by interacting loops at the interface between the two domains. Using single channel measurements of receptors carrying mutations in the α-subunit coupling interface, Lee and Sine identified what they called the principle pathway for signal transduction in the nAChR (34). In brief, the agonist-induced capping motion of the α-subunit C-loop propagates to the β-10 strand, from where the protruding side chain of Arg209 (*Torpedo* nAChR sequence) forms a salt bridge with Glu45 on the β1-β2 linker. This salt bridge is notably conserved across all Cys-loop receptors, and mutations in either residue result in impairments in gating. Glu45 and the adjacent Val46 form a clamp around the conserved Pro272 on the M2-M3 linker, whose *cis-trans* conformation is directly related to channel opening (Figure 1.7). Val46 and Pro272 additionally interact with Ser269, also on the M2-M3 linker. Other mutations within this linker alter channel kinetics without altering ligand affinity. Contacts between the Cys-loop, the β8-β9 linker, and the C-terminal post-M4 segment also make minor contributions to gating (35-36).

Loop complementarity at the ECD/TMD interface is critical for proper folding and interaction of the two domains. Structural studies of the prokaryotic homologue GLIC show that the β6-β7 loop (the Cys-loop in eukaryotic receptors) is poorly resolved in a structure of the ECD alone, but adopts a well-folded conformation in the presence of its TMD (37). Mismatch or weak interactions at the ECD/TMD interface likely disrupts the transmission of conformational change from the ligand binding site to the channel pore, uncoupling ligand binding from gating (*Lipid-dependent uncoupling*). In 2004, Bouzat et al. demonstrated that a chimera that preserved the pLGIC fold could be formed between the AChBP and the 5-HT$_3$ TMD with no change in interface loops (38). This chimera, however, did not gate open in response to agonist binding. A functional AChBP/5-HT$_3$ chimera was generated after replacement of the β1-β2, β6-β7, and β9- β10 loops of

Figure 1.7

Contacts at the coupling interface in *Torpedo* nAChR (PDB 2BG9). The β6-β7 loop is in green, the M2-M3 linker in blue, the M4 C-terminus in orange, and the β1-β2 loop in red. Interacting residues are labeled.

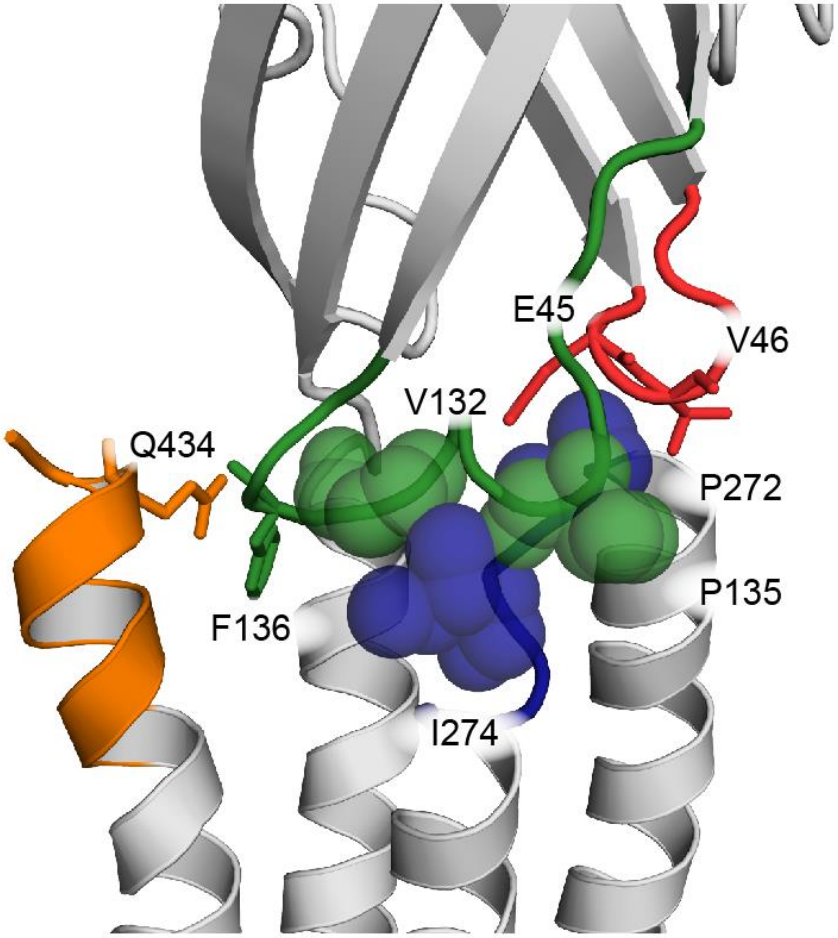
E45
V46
V132
Q434
P272
P135
F136
I274

the AChBP sequence with the corresponding 5-HT_3 loops. Amongst full-length receptors, however, residues and/or interactions at the interface are generally highly conserved, and functional ECD-TMD chimeras between many different members of the pLGIC superfamily can be generated with minimal changes to interface loop sequences (39-42).

Conformations of the nAChR. The allosteric nature of nAChR function is well described by the Monod-Wyman-Changeux (MWC) model of protein allostery. Briefly, this model postulates that a modulatable protein exists at any time in equilibrium between two or more distinct conformations, and that modulators exert their action through selectively stabilizing one conformation over another (43). Ligand-gated ion channels are classically thought to have three major conformations – an unliganded and non-conductive resting/basal state (R), a liganded and conductive open/active state (O), and a liganded and non-conductive desensitized state (D) – with harder-to-detect sub-conformations (D_1, D_2, etc.) postulated based on analyses of channel kinetics (Figure 1.8) (44). In native membranes, the *Torpedo* nAChR is stabilized in a roughly 80:20 ratio between resting and desensitized states (45). Single channel measurements of gain-of-function mutants of the muscle type nAChR from mouse muscle cells show spontaneous openings in the absence of agonist, indicating that the channel is in equilibrium with the open conformation as well (46).

Channel gating occurs rapidly in response to ligand binding to the resting conformation of the receptor. This shifts the conformational equilibrium toward the open state, allowing ion flow across the membrane. Upon prolonged exposure to ligand, the protein undergoes a transition on the order of milliseconds to seconds to the desensitized state, which does not flux ions. At low concentrations of agonist, the receptor may proceed directly to a desensitized conformation without opening (47). Eventual dissociation of the agonist shifts the equilibrium away from the

Figure 1.8

Conformational equilibrium of the nAChR between the liganded open state (O), unliganded resting (R), liganded desensitized (D), and uncoupled (U) conformations. The nAChR only fluxes ions in the open conformation, and after prolonged exposure to agonist, transitions to the liganded desensitized state. Figure from (18).

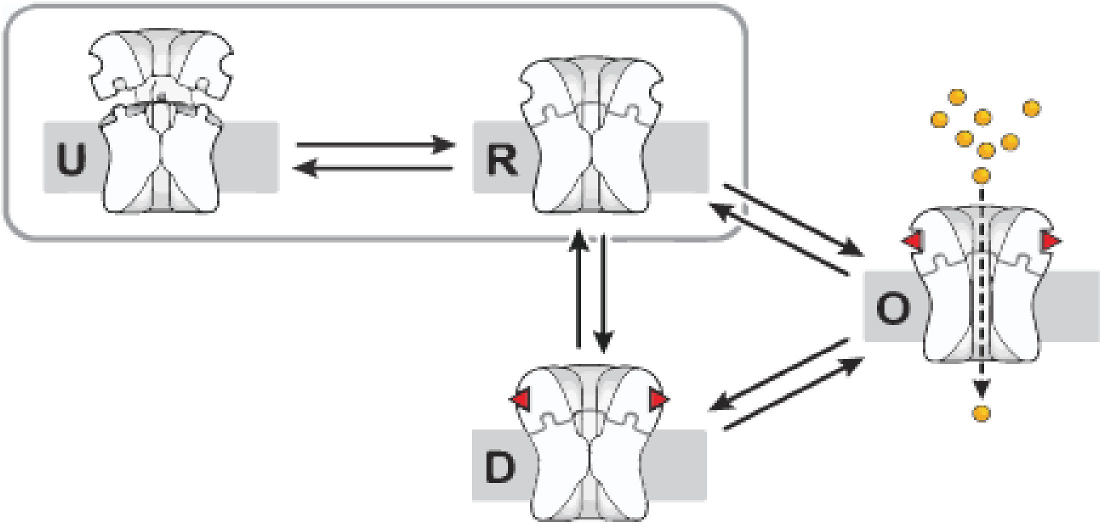
U
R
O
D

desensitized state and back to the resting state.

Modulators of nAChR function. The conformational equilibrium, and therefore function, of the nAChR is modulatable by both endogenous and exogenous compounds, making it a prime target for pharmaceuticals in the treatment of disease (reviewed in 48-49). Other than direct agonists and antagonists which exert their actions at the agonist binding site, drugs may also act elsewhere upon the receptor to affect its function. In the context of neuronal nAChRs, modulators are generally classified as positive allosteric modulators (PAMs) or negative allosteric modulators (NAMs). In addition, receptor function is affected by the binding of noncompetitive antagonists (NCAs) that block the channel pore.

Positive allosteric modulators potentiate the effect of agonist binding and are therefore often called co-agonists or non-competitive agonists (50). These drugs are further functionally subdivided into type I, which enhance the agonist response without altering desensitization kinetics (such as morantel and genistein (51-52)), and type II, which stabilize the open state and often slow desensitization (notable mentions include PNU-120596, TQS, and ivermectin (53-55)). PAMs also exist which display characteristics of both subclasses, or else possess PAM effects on some nAChR subtypes and NAM effects on others.

Negative allosteric modulators, in contrast, may stabilize non-conducting conformations of the receptor, decrease agonist affinity, or increase the receptor's desensitization rate. In addition to synthetic compounds, several endogenous compounds, such as neurosteroids and some fatty acids, have also been shown to have NAM effects (56).

PAMs and NAMs exert their influences from a variety of locations, including non-canonical intersubunit interfaces in the ECD (51, 57), the coupling region between the ECD and the TMD (58), and within the helices of the TMD (54, 60). These sites vary in chemistry across subunits, leading to variable sensitivities of nAChR subtypes to modulation by allosteric modulators. Of these varied sites, the intrasubunit TMD site is one of the most prominent and best-described in literature, and is ‘conserved’ across many pLGICs. For example, the neuronal α7 nAChR binds the potentiator PNU-120596, which slows desensitization, in a cavity formed by the M1, M2 and M4 α-helices (54). An analogous site in the $GABA_A$ and glycine receptors binds neurosteroids and volatile anesthetics (58, 61-62), the anesthetic propofol binds a similar site in the prokaryotic homologue GLIC (63), and the GluCl receptor binds its partial agonist ivermectin in the same general location (15). This site has been proposed in the nAChR to be a non-annular lipid-binding site for neurosteroids, cholesterol, and similar sterols (see *Lipid-nAChR interactions*; 64). Compounds binding at the intrasubunit TMD site likely influence TMD α-helical packing and thus affect gating and coupling (see Chapter 1.4 *M4 lipid sensor model of uncoupling*).

In the context of the work presented in this dissertation, I am most interested in a separate class of drugs referred to as non-competitive antagonists (NCAs), which bind to the pore of the receptor channel to inhibit cation flux (Figure 1.9 B). NCAs bind to the nAChR in a conformationally selective manner, and by probing their pharmacology, a better understanding of pore structure can be achieved (see Chapter 3). Known NCAs of the nAChR include barbiturates, dissociative anesthetics (such as phencyclidine and ketamine), local anesthetics (such as lidocaine and procaine), certain antidepressants (including some selective serotonin reuptake inhibitors (SSRIs) and tricyclic antidepressants), and various others (65-68). Structurally, many of these compounds contain aromatic moieties and tertiary or quaternary amines that may facilitate their binding to the cation-selective and hydrophobic channel interior. The endogenous ligand of the nAChR, acetylcholine, as well as other ligands such as nicotine, epibatidine, and tubocurare also

Figure 1.9

Representative pLGIC allosteric sites. (A) Side view (top) and top-down view (bottom) of a single subunit of GLIC with the anesthetic propofol, shown in red, bound in an intrasubunit site (3P50). (B) TMD of ELIC with memantine (green) bound in the pore (4TWD), shown in a side view (top) and top-down view (bottom). Pore-lining M2 α-helices are shown in blue.

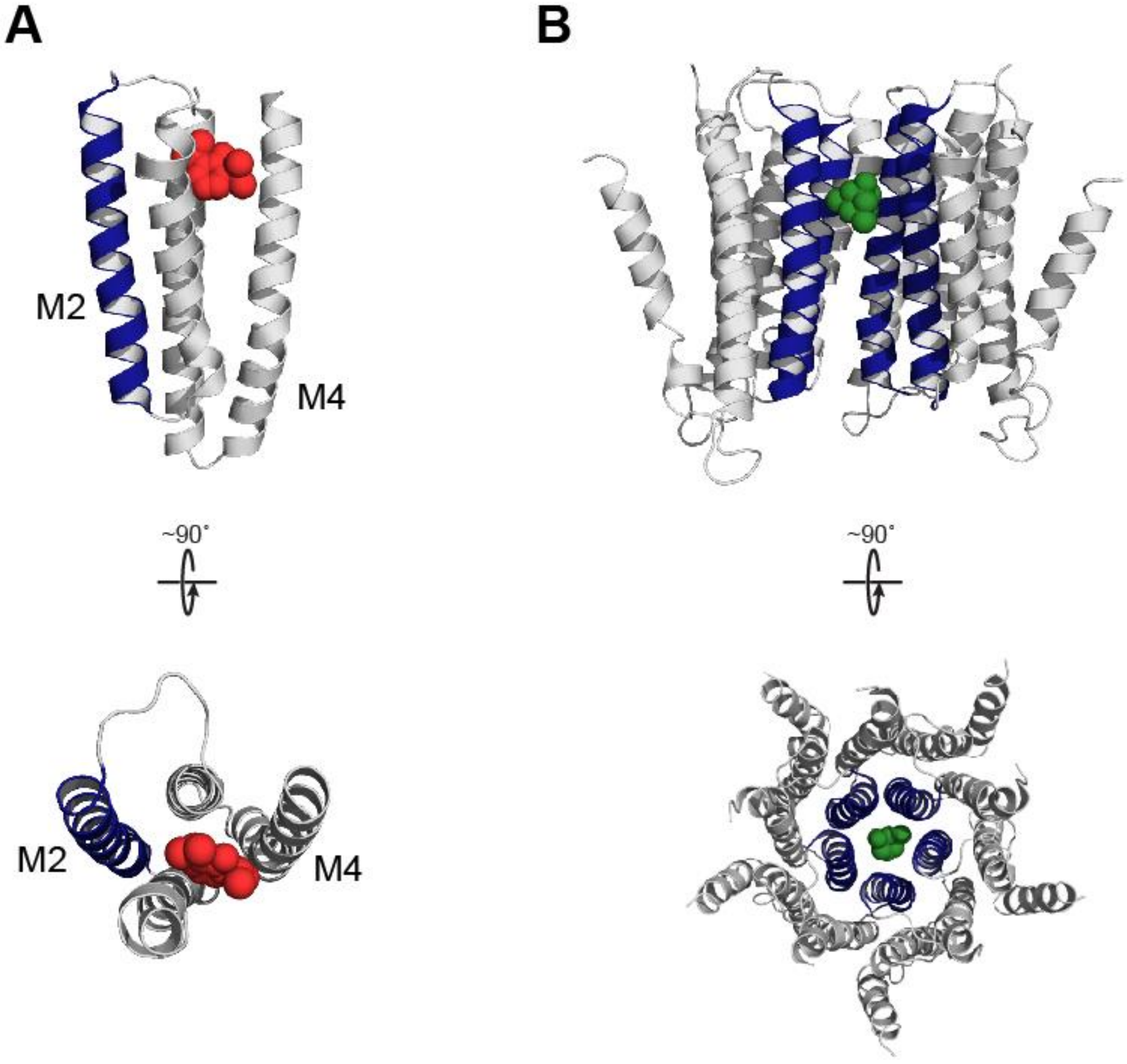
A
B
M2
M4
~90˚
~90˚
M2
M4

share an amino group capable of carrying a positive charge that is essential for binding to the agonist site. Consequently, high concentrations of many NCAs are able to compete for the agonist site, though usually with lower affinity than for the pore site.

NCAs display varied binding affinities depending on receptor subtype, highlighting structural differences in the pore-forming regions that may also be reflected in their different conductances and kinetics. Certain compounds bind across a wide spectrum of receptors; for example, all mammalian cation-conductive pLGICs undergo pore-block by quaternary ammonium cations (69). A classic example of this is tetraethylammonium (TEA), which additionally blocks voltage-gated potassium channels and is active on the prokaryotic pLGIC GLIC (70-72). Notably, the converse is also true when pore structural similarity is low. The local anesthetic lidocaine, which is a classic NCA of the nAChR, was crystallized bound to a different prokaryotic homologue, ELIC, at a non-pore transmembrane site between the rings of M2 and M1/M3 at the interface of two adjacent subunits (72). Lidocaine altered ELIC channel kinetics in a unique fashion, as compared to simple pore-block in Cys-loop receptors.

4. Lipid Sensitivity and Uncoupling

nAChR lipid sensitivity. The ability of the nAChR to undergo conformational transitions is highly sensitive to lipids. The first interest in lipid-nAChR interactions arose from early attempts to isolate functional *Torpedo* nAChRs from their native membranes. As the nAChR is an integral membrane protein, this process required detergent solubilization prior to both purification and reconstitution into model lipid membranes. Initial attempts, however, led to receptors that bound agonist, but did not undergo agonist-induced conformational transitions (73-75). Functional nAChR samples were finally obtained only after it was established that lipids are required throughout solubilization and purification in order to stabilize nAChR structure and function. (76). In fact, lowering the lipid to protein ration below 45:1 (mol:mol) during purification resulted in irreversible inactivation of the nAChR (77). In addition, the ability of the nAChR to undergo conformational transitions is highly dependent on the specific lipid species in the reconstituted membrane environment. Anionic and neutral lipids optimally support receptor function, though the nAChR appears to have loose requirements for the specific type of anionic or neutral lipid (78-81). Both anionic lipids and neutral lipids are abundant in native *Torpedo* membranes (~15% and ~35% molar ratio, respectively), suggesting that membrane compositions that support receptor function likely mimic the native membrane environment (82-83).

Lipid-nAChR interactions. Lipid-nAChR interactions are likely complex and have been proposed to occur through several different mechanisms. Most anionic and/or neutral lipids are able to support nAChR function to some extent, making it unlikely that lipids act on the nAChR through a highly specific mechanism – i.e. through specific lipid binding sites (84). Studies using spin-labeled lipids show that the receptor discriminates in favour of both anionic and neutral lipids. Specifically, the nAChR interacts with lipids in its vicinity, slowing their rotational and translational movements (85). A proportion of these lipids were found to be ‘immobilized’, leading to the suggestion that the receptor is encircled by a ring, or ‘annulus,’ of lipids that have the highest affinity for the lipid/receptor interface. Phosphatidic acid and cholesterol, which are particularly effective at stabilizing functional nAChR, have the highest degree of immobilization, suggesting that the nAChR selectively associates with lipids that promote its function (86). Data from fluorescence quenching studies and molecular dynamics simulations propose that non-annular sites within the nAChR TMD may also exist for the specific binding of cholesterol, although there is no direct experimental evidence for this (87, 64).

As phosphatidic acid and cholesterol both increase ordering of the lipid membrane, it was proposed that nAChR function may also be affected by membrane bulk properties (78, 84). Although membrane fluidity has been shown to have only minor effects on nAChR function (88), recent data showed that altering the thickness of phosphatidylcholine (PC) membranes shifts the conformational equilibrium of the nAChR between functional and non-functional states, providing evidence that membrane bulk properties also have an effect on nAChR function (89).

Recent studies also show that the nAChR can influence its own lipid microenvironment. The introduction of nAChR to lipid membranes increases membrane order, which may feed back into receptor function (90). This effect is strikingly higher for membranes containing anionic lipids than for those lacking them. In addition, the *Torpedo* nAChR co-purifies with phospholipase C activity, suggesting that the receptor or a closely associated factor is able to modify the identity of lipid species in its immediate vicinity (91). More recent experiments show that signaling by synthetic diacylglycerol derivatives downstream of phospholipase C activity increase nAChR surface expression (92).

Lipid-dependent uncoupling. The nAChR reconstituted into PC membranes (PC-nAChR) in the absence of anionic lipids and cholesterol adopts a non-functional conformation. Cryo-EM images and Fourier-transform infrared (FTIR) spectra both indicate that PC-nAChR adopts a native-like pentameric fold with similar thermostability to the nAChR in functional membranes, consistent with previous observations that the lipid membrane has little effect on overall receptor structure (93-95). The lipid environment therefore likely affects nAChR function by influencing receptor conformation dynamics.

Characterization of PC-nAChR in terms of the classical resting-open-desensitized conformational equilibrium, however, initially yielded conflicting results. Photolabeling studies using the hydrophobic probe 3-trifluoromethyl-3-(*m*-[125I]iodophenyl) diazirine ([^{125}I]TID), which preferentially labels lipid-exposed residues, revealed similar labeling patterns for PC-nAChR as for desensitized nAChR. These studies suggested that the non-functional PC-nAChR is not stabilized in a resting conformation and may be non-functional because it is stabilized in the desensitized conformation (90). In fact, other biophysical tools have shown that the nAChR reconstituted into a mixture of PC and phosphatidylserine is stabilized primarily in the desensitized state (96). The desensitized nAChR, however, is characterized by high affinity binding for both agonists, such as acetylcholine, and channel blockers, such as ethidium bromide (97-99). Subsequent studies revealed that PC-nAChR binds acetylcholine with low, resting-state-like affinity, and it is unclear whether it binds ethidium at all (94). It was thus proposed that PC-nAChR adopts a conformation distinct from the classical resting, open and desensitized conformations. As PC-nAChR is able to bind agonist, but does not flux cations, it was suggested that there is a functional uncoupling of ligand binding from gating – PC-nAChR thus adopts a novel “uncoupled” conformation.

M4 lipid-sensor model of lipid-dependent uncoupling. A key question that arises from the observation that lipids affect nAChR function is how the receptor senses and changes its conformation in response to its lipid environment. We and other have proposed that the lipid sensitivity of the nAChR involves the M4 α-helix in the TMD, on account of its highly lipid-exposed position on the periphery of the receptor (100-102). Mutations of the lipid-facing residues in M4 in *Torpedo* and mammalian muscle-type nAChRs affect its channel-opening response to agonist, despite being distant from both the ligand binding site and the channel pore (103-106). Molecular dynamics simulations also suggest that the orientation of M4 is at least partially dependent on bulk membrane properties (101-102). Lipids in the nAChR's vicinity (annular lipids) may therefore preferentially stabilize certain orientations of M4 to affect the conformational equilibrium and gating.

Our working model of the uncoupled conformation proposes that in the absence of anionic lipids and cholesterol, M4 does not interact effectively with the adjacent transmembrane α-helices, M1 and M3, leading to ineffective interactions between the M4 C-terminus and the β6-β7 loop (Fig. 1.10). In the absence of this interaction, the β6-β7 loop may be poorly positioned for interaction with the M2-M3 loop – an interaction which plays a key role in signal transduction from the ligand binding site to the gate – resulting in weak coupling and an increased physical separation at the ECD/TMD interface. In support of this mechanism, uncoupling is accompanied by an increase in the solvent exposure of previously buried regions of the polypeptide backbone (94).

ELIC and the uncoupled model. The crystal structure of the prokaryotic homologue ELIC recapitulates key structural features of the working model of the uncoupled nAChR. The ELIC structure preserves the broad topological architecture common to all pLGICS (though it lacks an ICD), but shows marked differences at its coupling interface relative to the cryo-EM structure of the *Torpedo* nAChR. In the nAChR structure, the M4 C-terminus extends beyond the level of the lipid bilayer to interact with the β-β7 loop, locking the M4 into an upright position against the adjacent α-helices M1 and M3. The β1-β2 and β6-β7 loops form 'clamps' around the M2-M3 linker in the TMD, promoting tight interactions between the ECD and TMD (Fig. 1.11). In the

Figure 1.10

The lipid-dependent uncoupling model implies that activating lipids such as anionic lipids and cholesterol are necessary for coupling of ligand gating to channel gating by promoting a conformation of the M4 α-helix that allows the post-M4 segment (orange) to effectively interact with the Cys-loop or β6-β7 loop (green) and tether the ECD and TMD. The M2-M3 linker is shown in purple, β1-β2 is shown in light blue, and loop C of the agonist binding site is shown in yellow, with an important tryptophan residue displayed in stick format. Figure from (94).

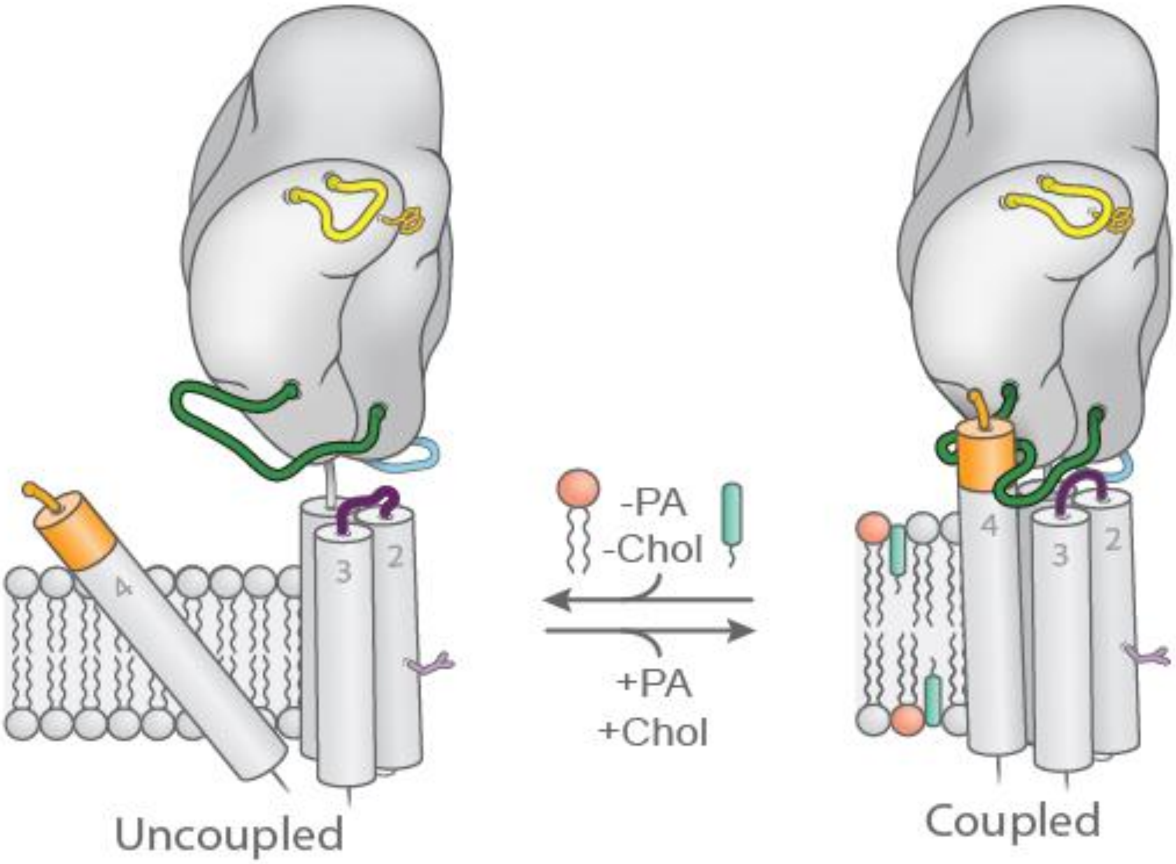

-PA
-Chol
+PA
+Chol
4
3
2
Uncoupled
Coupled

Figure 1.11

Coupling interface of nAChR and ELIC. Residues in the β6-β7 loop (green) and in the β1-β2 loop (red) interact tightly with residues in the M2-M3 linker (blue) in the nAChR (A; from Fig. 1.7), but not in ELIC (B). An interaction between the post-M4 (orange) and the β6-β7 loop is shown for the nAChR; no equivalent interaction can be observed in ELIC. Note that the final 5 residues of the post-M4 are missing in the ELIC crystal structure.

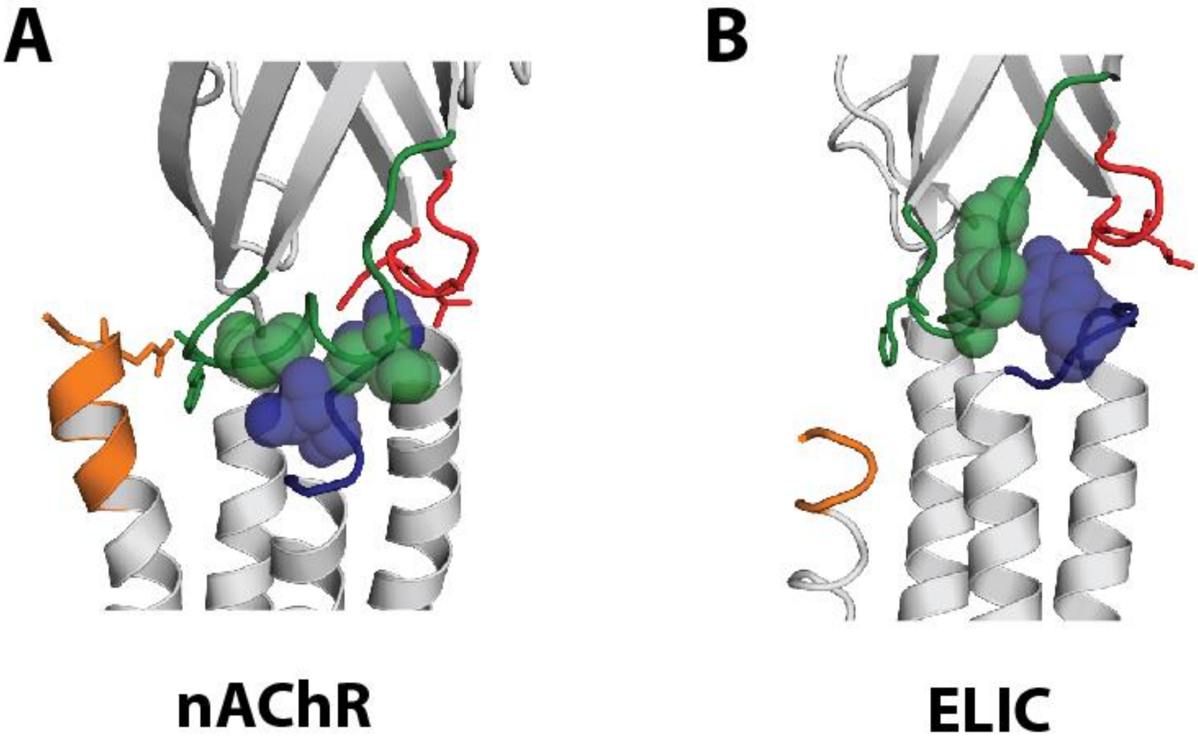
A
B
nAChR
ELIC

ELIC structure, M4 is disengaged from the TMD bundle and its final five residues are unresolved, suggesting weak or no interactions between the C-terminus of M4 and either M1/M3 or the β6-β7 loop. The β1-β2 and β6-β7 loops interact weakly with the M2-M3 linker of the TMD, leading to a physical separation between the ECD and TMD. It is possible that detergent-solubilization of ELIC for crystallization may lead to the formation of an uncoupled conformation, as does detergent-solubilization of the nAChR in the absence of lipids (18). Indeed, ELIC crystallized in both the presence and absence of agonist shows no difference in pore diameter, suggesting that crystallized ELIC is functionally uncoupled (107-108).

Interestingly, crystal structures of a close homologue, GLIC, exhibits tight binding of M4 to M1/M3 along its entire length. Aromatic interactions have been shown to energetically drive the binding of M4 to M1/M3 during folding of the homologous glycine receptor (109). We noted that ELIC has fewer aromatic interactions at the M4-M1/M3 interface than GLIC (Fig. 1.12), and so hypothesized that the reduced number of aromatic residues at this interface may weaken M4-M1/M3 interactions in ELIC relative to GLIC, thus rendering the ELIC TMD more sensitive to the perturbing effects of detergent solubilization in the absence of stabilizing lipids. In light of the uncoupling model, we also suggested that weaker M4-M1/M3 interactions may render ELIC more susceptible to uncoupling, thus making ELIC function more sensitive to its membrane environment. The work I contributed toward testing this hypothesis is presented in Chapter 2.

It is also interesting to note that the first structure of ELIC, which was obtained in the absence of agonist and is thus presumed to be in a closed conformation, exhibits a pore diameter that is much smaller than the pore diameters of the closed GLIC, nAChR and other pLGIC structures (Fig. 1.13) (108). In light of the possibility that ELIC may have been crystallized in an uncoupled conformation, we hypothesized that a constricted channel pore may be a structural

Figure 1.12

TMD aromatics in the nAChR and its prokaryotic homologues. The TMD segment of a single subunit is shown for ELIC (left, PDB code 2VL0), GLIC (center, PDB code 3EAM), and the refined cryo-EM structure of *Torpedo* nAChR (right, PDB code 2BG9) from a side-on view (top) and a top-down view (bottom). Aromatic residues at the M4-M1/M3 interface are shown as yellow sticks. Figure from (110).

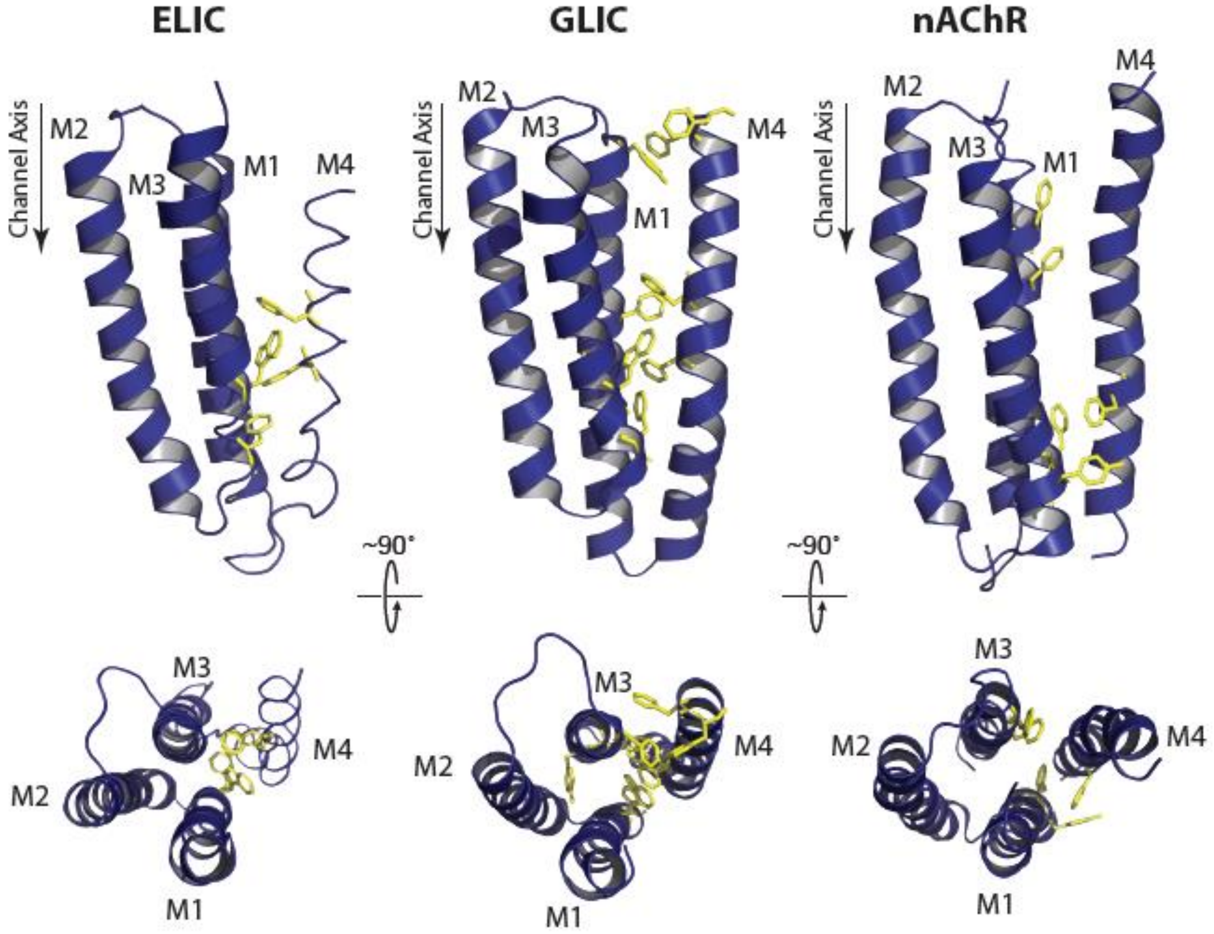
ELIC
GLIC
nAChR
Channel Axis
M2
M3
M1
M4
Channel Axis
M2
M3
M1
M4
Channel Axis
M2
M3
M1
M4
~90°
~90°
M3
M4
M2
M1
M3
M4
M2
M1
M3
M4
M2
M1

Figure 1.13

Structural comparison of the nAChR and ELIC pore. A side view showing M2 and M3 from two nonadjacent subunits (left), with the gating residues αL251 and αV255 in the nAChR (PDB code 2BG9) and L238 and F245 in ELIC (2VL0) highlighted as yellow spheres. The right panel shows a bird's-eye view of the pore-forming M2 α-helices from all subunits, illustrating the constricted diameter of the channel pore in ELIC.

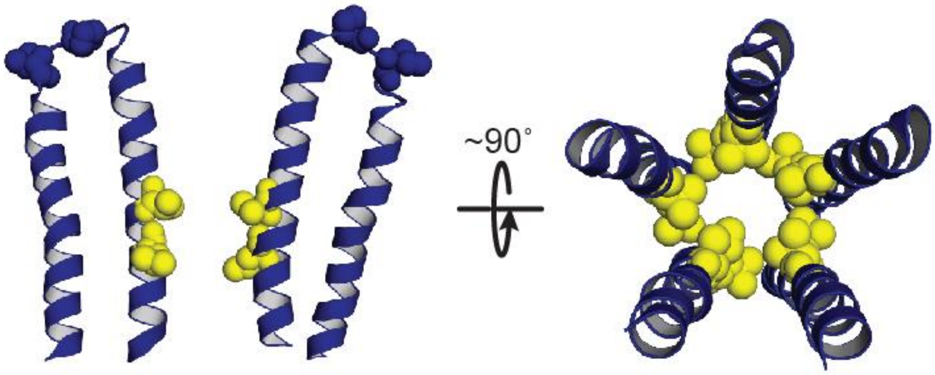

nAChR

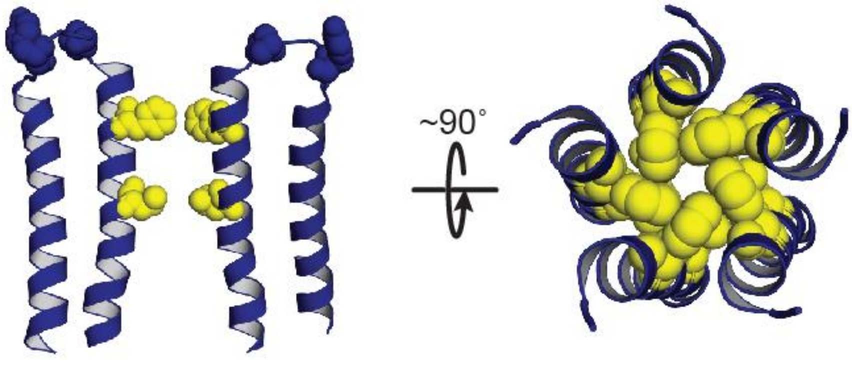

ELIC

feature of the uncoupled conformation.

Previous data have offered little definitive insight into the structure of the uncoupled TMD. The functional probe ethidium binds the pore of the uncoupled PC-nAChR with much lower affinity than the desensitized nAChR. As the resting nAChR binds ethidium with low affinity (94), the pore of the uncoupled PC-nAChR may adopt a resting-like conformation. In contrast, the ELIC structure suggests an alternative TMD conformation, in which there is a tight constriction of the pore. A constricted pore might limit the binding of channel blockers, such as ethidium bromide, thus accounting for the relatively low affinity of PC-nAChR for ethidium noted above. This hypothesis is explored in Chapter 3.

Broader implications of nAChR lipid sensing and uncoupling. Changes in lipid metabolism are increasingly linked to human disease, which could lead to altered nAChR function (111-113). There is thus a real and pressing need for a greater understanding of nAChR-lipid interactions and their role in nAChR biology.

The ability of the nAChR to uncouple in unfavourable lipid environments may have important implications in the functional role of nAChR and its relationship to human health and disease. For example, Li and Steinbach showed through transfection experiments that although ~15000 α4β2 neuronal-type nAChRs are typically expressed on the surface of HEK293 cells, only ~1000 of these nAChRs gate open in response to agonist – i.e. the vast majority of the nAChRs are functionally uncoupled (114). Similar results were previously reported in 1999 by Fenster et al., who studied α4β2 nAChR expression in *Xenopus* oocytes (115). These studies suggest that the uncoupled conformation may also be common to neuronal nAChRs.

Nicotine exposure upregulates cell-surface nAChRs by awakening previously non-functional, possibly uncoupled, nAChRs, as well as by promoting the trafficking of nAChRs from intracellular compartments to the cell surface (116-118). The former observation leads to the intriguing hypothesis that transitions between uncoupled and coupled (resting, open, and desensitized) conformations could regulate the strength of the synaptic response. In the context of the latter observation, it is important to mention that uncoupled nAChRs in hydrophobically thick PC membranes (similar to the thickness of lipid rafts) undergo a ligand-induced transition to coupled conformations over a minutes-to-hours time frame (89). This result is reminiscent of the time frame of nAChR trafficking from internal membranes to the cell surface. As hydrophobically thicker lipid rafts have been implicated in nAChR trafficking to the cell membrane surface (119-120), it is intriguing to speculate that transitions from uncoupled to coupled conformations may occur as the nAChR associates with lipid rafts during transport to the cell surface.

Finally, the possibility that the ELIC structure may be uncoupled raises an important concern with regards to studies of agonist-induced channel gating using crystallized detergent-solubilized pLGICs. Pore diameter has traditionally been the key factor in assigning a conformation to a pLGIC crystal structure. The constricted diameter of the ELIC pore compared to the structures of other closed pLGICs initially led to great confusion in the interpretation of crystal structures. Understanding how detergent solubilization influences the conformations of crystallized pLGICs is essential to ultimately obtaining mechanistic insight.

5. Research Aims and Organization of Dissertation

The research undertaken for this thesis was aimed primarily at elucidating the mechanisms by which pLGICs adopt an uncoupled conformation, as well as structural features of the uncoupled nAChR.

The work presented in Chapter 2 was undertaken to investigate the role of M4 association with the TMD bundle in coupling/uncoupling. ELIC and GLIC were used as model systems to test the hypothesis that intramembrane aromatics strengthen interactions between M4 and M1/M3, thus decreasing the propensity to uncouple. My results support this hypothesis and suggest that an increased number of aromatic interactions within the transmembrane bundle increases TMD stability, leading to lower lipid sensitivity and more efficient coupling of ligand binding and gating.

Chapter 3 focuses on the biophysical characterization of the uncoupled nAChR, with special emphasis on the structure of the pore region. Specifically, I set out to compare the binding of several channel blockers to the resting, desensitized and uncoupled nAChR. I hypothesized that a constricted channel pore in the uncoupled state, as seen in ELIC, would limit the binding of all channel blockers to the uncoupled PC-nAChR. In agreement with this hypothesis, my data show that although binding fluorescent channel blockers to both resting and desensitized nAChRs could be characterized, no binding was detected to the uncoupled state.

Finally, in Chapter 4, I present data from experiments to further elucidate the structure of the pore region through binding studies. The complex pore pharmacology of the nAChR in the resting and desensitized states is reviewed briefly to aid in the discussion of experimental results.

Chapter 2

Intramembrane Aromatics Influence Lipid Sensitivity

1. Rationale

The ability of the nAChR to undergo conformational transitions is sensitive to its lipid environment, and is likely mediated by the lipid-exposed M4 α-helix in the TMD. The M4-lipid sensor model of uncoupling proposes that lipids modulate the binding of M4 to M1/M3, and that weak binding of M4 leads to ineffective interactions between the ECD and TMD, thereby uncoupling agonist binding from channel gating. Conversely, this model predicts that strengthening M4-M1/M3 interactions should 'lock' M4 in place and reduce the receptor's sensitivity to its lipid environment, as well as promote coupling.

A structural comparison of the M4 α-helix in the nAChR and its prokaryotic homologues GLIC and ELIC reveals that the nAChR has a relative paucity of aromatics at the M4-M1/M3 interface compared to both ELIC, which possesses a cluster near the intracellular side of the TMD, and especially GLIC, which possesses aromatic residues along the length of the M4-M1/M3 interface. As aromatic interactions are known to promote the binding of TMD α-helices (109), we hypothesized that increasing numbers of aromatic interactions between M4 and M1/M3 should increase the stability of the receptor's TMD and decrease its sensitivity to its lipid environment. GLIC, therefore, should be more stable and less lipid-sensitive than either ELIC or the nAChR.

To test this hypothesis, we needed the ability to create mutants and test their activity in different membrane environments. The mammalian nAChR presents a less-than-ideal system in which to do these studies, as it cannot be expressed in bacteria. GLIC and ELIC, however, can both be expressed in *Escheria coli* and purified in relatively large quantities, and are amenable to biophysical studies. These two homologues were therefore used as model systems.

This project was begun by a previous student in the lab, Dr. Casey Carswell, who established purification protocols for ELIC and showed that ELIC is less thermally stable and exhibits a greater sensitivity to its lipid environment than GLIC. In the PC membranes that stabilize the uncoupled nAChR, GLIC function is indistinguishable from its function in asolectin membranes, which consistently stabilize activatable receptors (121). ELIC, however, displays gating function only in asolectin membranes, and not in PC membranes (see Results, ref. 110).

We further hypothesized that if fewer intramembrane aromatics rendered ELIC more lipid-sensitive than GLIC, then engineering additional interacting aromatics at the M4-M1/M3 interface into ELIC should both increase its thermal stability and decrease its propensity to adopt a non-functional conformation in unfavourable PC membranes. My role in the project was to test this hypothesis. I expressed, purified, and reconstituted an ELIC mutant containing three additional M4-M1/M3 interface aromatics (ELIC-3; mutant constructed by Dr. Casey Carswell) into PC membranes, and assessed its biophysical and functional properties relative to those of wildtype ELIC to determine the effects of the added intramembrane aromatics on both thermal stability and lipid sensitivity.

2. Methods

Preparation of ELIC proteoliposomes. MBP-tagged ELIC was expressed in the C41 or C43 strains of E. coli. Cultures were grown in Terrific Broth containing 50μg/ml kanamycin at 37^{o}C to an optical density of ~1.2 units, then induced with 200μM IPTG. Cells were harvested, resuspended in buffer containing 150mM NaCl and 50mM NaH_2PO_4, pH 8.0 (buffer A), and lysed using an Avestin Emulsiflex-C3 homogenizer (Ottawa, Canada). The membrane fraction was solubilised overnight in 1% dodecylmaltoside (DDM) and bound to an amylose affinity resin. ELIC was eluted in 0.02% DDM after cleavage of MBP with herpes simplex 3C protease. Size exclusion to obtain well-formed pentameric receptors was performed on a Superose 6 10/300 gel filtration column (GE Healthcare, Little Chalfont, UK) in buffer containing 150mM NaCl and 10mM NaH_2PO_4, pH 8.0 (buffer B).

Purified ELIC in 0.02% DDM was diluted with lipid (soybean asolectin or phosphatidylcholine) solubilised in 0.625% cholate in buffer B to at least a 1:4 (v/v) ratio to give a 2:1 (w/w) lipid:protein ratio. After gently mixing for at least 15 minutes, the mixture was dialyzed against 2L of buffer B five times at 4°C, with approximately 12 hours between buffer changes. ELIC is slowly incorporated into vesicles and harvested by centrifugation at 41,000 rpm for 2 hours in a 70Ti type rotor (Beckman Coulture, Brea, CA). Samples were stored at -80°C when not in use.

Fourier Transform Infrared Spectroscopy (FTIR). Infrared spectra were recorded on a Digilab (now Agilent Technologies; Santa Clara, CA) FTS7000 spectrometer. Hydrogen/deuterium infrared spectra were collected using a Golden-Gate^{TM} attenuated total internal reflection accessory (SpecAc; Kent, UK). 2-5µl of reconstituted receptor sample were dried under N_2 gas, and 128 scan spectra were recorded at 4 cm^{-1} resolution both before and after rehydration with ^2H_2O, which eliminates ^1H_2O absorptions in the same region as protein peaks of interest. High resolution spectra (2000 scan spectra, 2 cm^{-1} resolution) of receptor exchanged into ^2H_2O buffer for 24 h at 4°C were taken by gently drying approximately 200µg of sample onto a CaF_2 window with a gentle stream of N_2 gas, then rehydration with 8µl of deuterated buffer. These spectra were processed using GRAMS/AI software (Thermo Scientific, Waltham, MA); resolution enhancement was performed on the amide I peak between 1900 and 1300cm^{-1} with γ=7 and a

Bessel smoothing function =70%. Changes in amide I band intensity at 1680 or 1620 cm^{-1} were plotted as a function of temperature to monitor thermal denaturation. The T_d, or temperature at which 50% of the sample was denatured, was calculated by fitting the data in GraphPad Prism (GraphPad Software, Inc., La Jolla, CA) with a Boltzmann sigmoidal, where the fraction of denatured receptor $F_d = y_{initial} + ((y_{final} - y_{initial})/(1 + \exp((T_d - x)/m_b)))$.

Electrophysiology. A two-electrode voltage clamp apparatus (OC-725C oocyte clamp, Holliston, MA) was used for electrophysiological measurements. Mature *Xenopus laevis* oocytes were injected with either 0.2 ng of cRNA or 100-200 ng of membrane-reconstituted receptor and allowed to incubate overnight at 16^{o}C in ND96+ buffer (5mM HEPES, 96mM NaCl, 2mM KCl, 1mM $MgCl_2$, 1mM $CaCl_2$, and 2mM pyruvate). For measurements, oocytes were placed in an RC-1Z oocyte chamber (Harvard Apparatus; Hamden, CT) in buffer containing 150mM NaCl, 0.5mM BaCl2, and 10mM HEPES, pH 7.0. Buffer containing varying concentrations of cysteamine was flowed over the oocyte at ~5ml/min, and currents through the plasma membrane elicited by jumps in ligand concentration were measured with the transmembrane voltage clamped at -40mV.

3. Results

Aromatic additions between M1/M3 and M4 decrease peptide backbone hydrogen exchange. To test the hypothesis that aromatic interactions between M4 and M1/M3 enhance M4 binding to M1/M3 and thus promote tight coupling between the agonist site and channel gate as well as reduce lipid sensitivity, I expressed and purified the ELIC-3 mutant, which contains three additional M4-M1/M3 interface aromatics (Fig. 2.1).

Figure 2.1

TMD of one subunit of an ELIC homology model (based on the structure of GLIC (PDB code 3EAM)) showing aromatic residues (dark grey sticks) at the M4-M1/M3 interface. Boxed area shows residues in ELIC that were mutated to the corresponding aromatic residues from GLIC (right). Mutated residues are shown with transparent spheres.

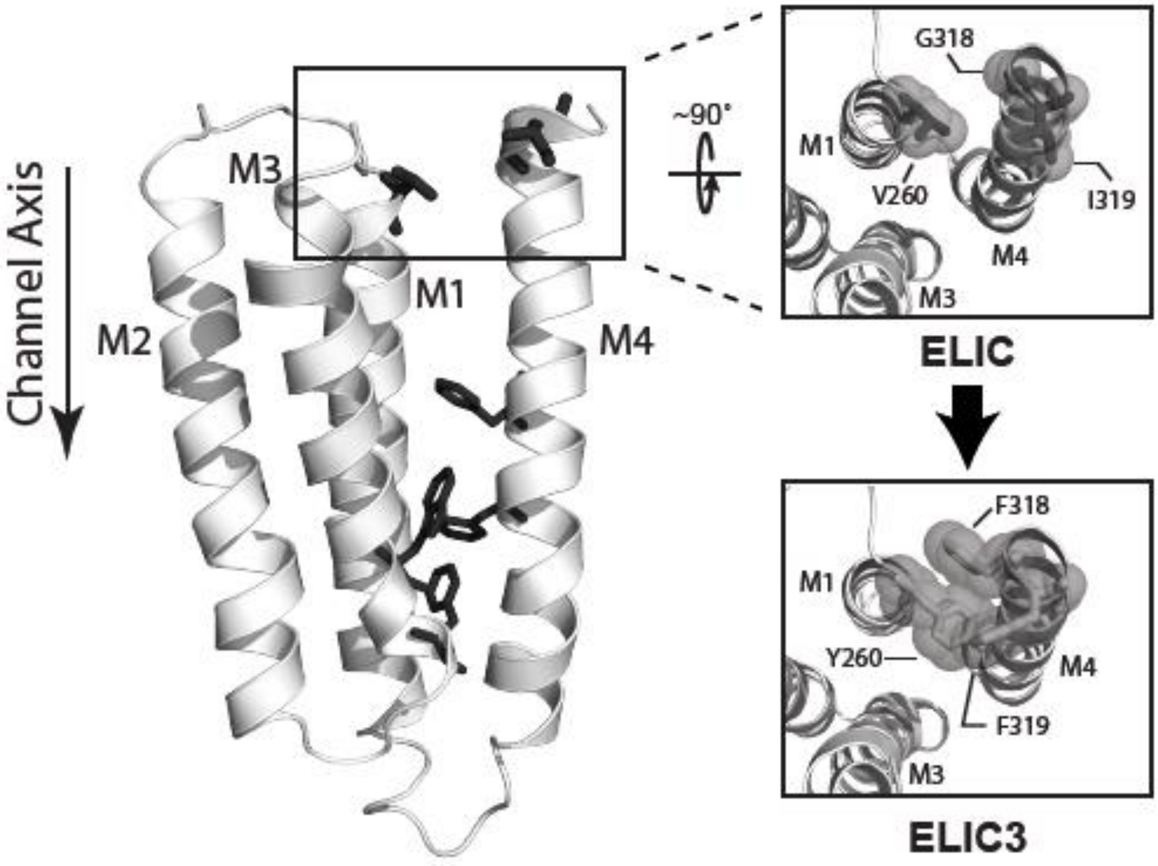
Channel Axis
M3
M2
M1
M4
~90°
G318
M1
V260
I319
M4
M3
ELIC
F318
M1
Y260
M4
F319
M3
ELIC3

This mutant was created by Dr. Casey Carswell and contained the following substitutions: V260Y on M3, G318F on M4, and I319F on M4. These substitutions recapitulate a cluster of aromatic interactions near the ECD that is present in GLIC, but not ELIC. Both receptors also naturally contained a cluster of aromatics near the cytoplasmic side of the transmembrane segments.

I reconstituted ELIC-3 into a PC membrane and examined its secondary structure and thermal stability relative to PC-ELIC using infrared spectroscopy. As water absorption overlaps strongly with protein vibrations, infrared spectra for structural analyses were obtained both after gentle drying under N_2 gas, and then after rehydration in ^2H_2O buffer to assess peptide exchange characteristics. The amide I band, between 1700-1600 cm^{-1}, is primarily due to peptide backbone C=O stretching, and its frequency is sensitive to hydrogen bonding and thus protein secondary structure (Fig. 2.2 A). Upon exposure to deuterated buffer, solvent-exposed α-helical/loop structures (more likely the latter) undergo $N\text{-}^1H/N\text{-}^2H$ exchange and shift their frequency from 1655 cm^{-1} to 1645 cm^{-1}, contributing to a more symmetrical amide I band. The amide II band, centered around 1547 cm^{-1}, is due primarily to $N\text{-}^1H$ bending and drops in intensity upon exposure to deuterated buffer. Its height relative to the adjacent C=O vibration around 1580 cm^{-1} is telling of overall levels of $N\text{-}^1H/N\text{-}^2H$ exchange, or solvent accessibility. Similar changes in spectral shape upon exposure to deuterated buffer have been reported for wildtype ELIC, GLIC, and *Torpedo* and human α4β2 nAChR (94, 121-124).

High fidelity spectra were obtained for samples exchanged into ^2H_2O buffer for 24 hours in order to assess in more detail the secondary structure of ELIC-3. Resolution enhancement of the amide I band reveals two component peaks: the peak maximum near 1655 cm^{-1} corresponds to vibrations of primarily α-helical secondary structures and the peak between 1640-1625 cm^{-1}

Figure 2.2

Infrared spectra of PC-ELIC-3. (A) Spectra recorded after drying from ^1H_2O buffer (black) and subsequent rehydration in ^2H_2O buffer (grey) as in Fig. 2.2.1. (B) Amide I bands (left) both before (grey) and after deconvolution (black) and amide II bands (right) from PC-ELIC (i) and PC-ELIC-3 (ii).

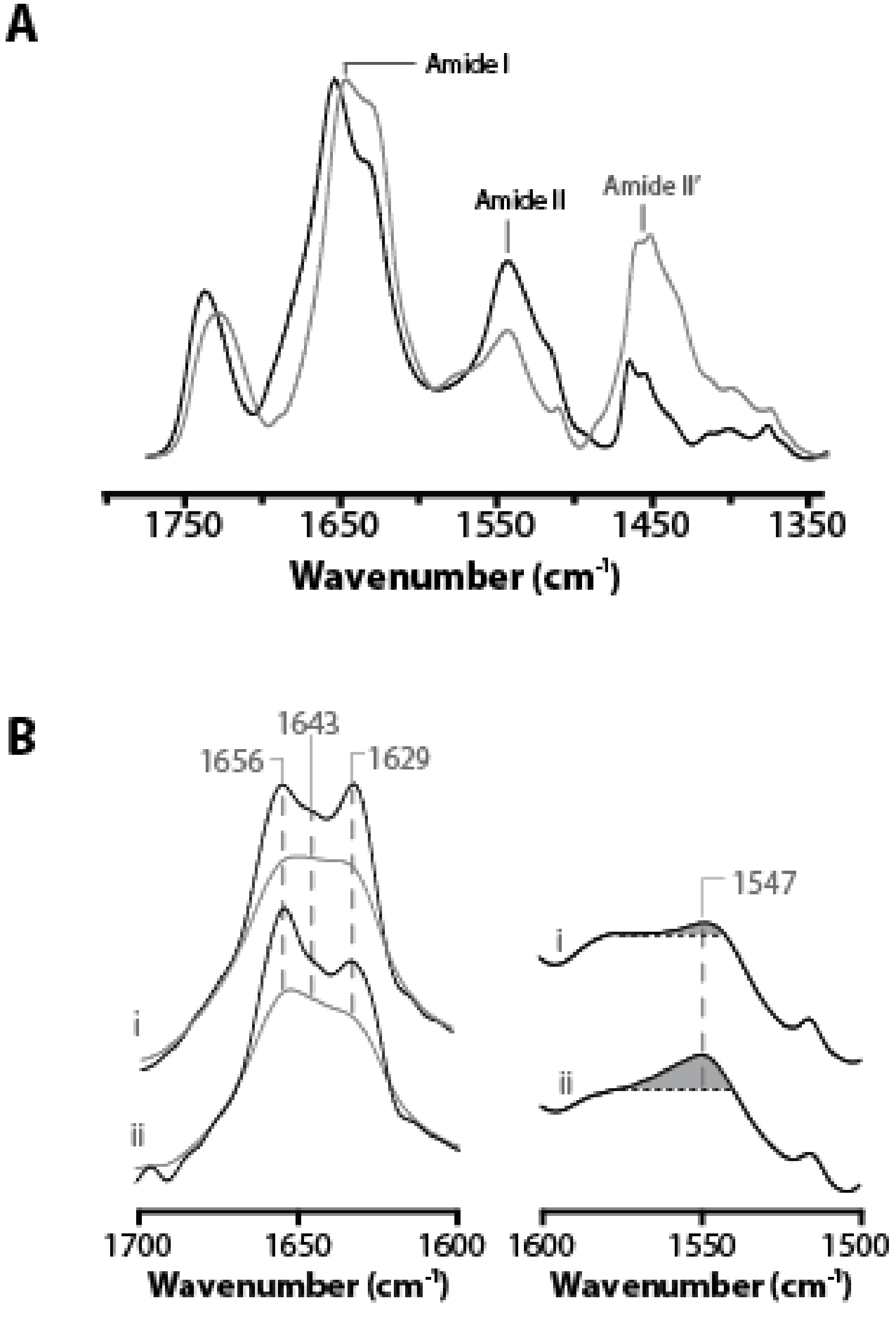
A
Amide I
Amide II
Amide II'
1750
1650
1550
1450
1350
Wavenumber (cm^{-1})
B
1656
1643
1629
i
ii
1700
1650
1600
Wavenumber (cm^{-1})
1547
i
ii
1600
1550
1500
Wavenumber (cm^{-1})

corresponds to β-sheets. The deconvolved amide I band of PC-ELIC-3 suggests an enhanced α-helical/loop character compared to wildtype PC-ELIC (Fig. 2.2B *left*). As the M4 of the wildype ELIC structure is partially unwound and the final five residues are poorly resolved by X-ray diffraction, it is plausible that the additional aromatic interactions promote a more structured M4 α-helix that interacts tightly with M1/M3. Additionally, PC-ELIC-3 demonstrated noticeably higher intensity at the amide II band than PC-ELIC, (Fig. 2.2B, *right*), suggesting less extensive N-^{1}H/N-^{2}H exchange. ELIC therefore likely contains a population of solvent-accessible α-helical/loop structures that became shielded from solvent upon the addition of three aromatics.

Aromatics increase TMD stability. The thermal stability (resistance to heat denaturation) of PC-ELIC-3 was assessed by measuring amide I intensity as a function of increasing temperature. Receptor unfolding is accompanied by characteristic changes in the FTIR spectra, most notably the appearance of a new peak around 1620 cm^{-1} and a reduction in amide II intensity as the protein unfolds and more backbone peptide hydrogens become exposed to solvent (Fig. 2.3). To quantify the degree of denaturation, the intensity at 1620 cm^{-1} was monitored and plotted as a function of temperature. This was fitted with a Boltzmann sigmoidal function to obtain a T_d, or the temperature at which 50% of receptors have become denatured (Fig. 2.4).

Previous thermal denaturation experiments had yielded a T_d of 59.7 ± 3.5 ^oC (n = 4) for aso-ELIC and 65.1 ± 2.2 ^oC for PC-ELIC (n = 4; data from Dr. Casey Carswell, see ref. 110). In comparison, although the PC-ELIC-3 spectra showed decreasing amide II intensity with increasing temperature, this was not accompanied by changes in amide I shape indicative of complete denaturation (see also Fig. 2.3.C and Fig. 2.4). These data suggest that over our accessible temperature range (maximum 78^{o}C), PC-ELIC-3 only partially denatures. It is likely that the engineered aromatic interactions resulted in a more structured M4 α-helix that interacts more

Figure 2.3

Thermal denaturation ELIC and ELIC-3. (Left panel) Stacked plots showing changes in spectral shape as a function of temperature and (right) an overlay of the receptor sample at 36^{o}C (black line) and at 76 or 78^{o}C (grey line) for aso-ELIC (A), PC-ELIC (B), and PC-ELIC-3 (C). Data for wildtype ELIC (A and B) were collected by Dr. Casey Carswell.

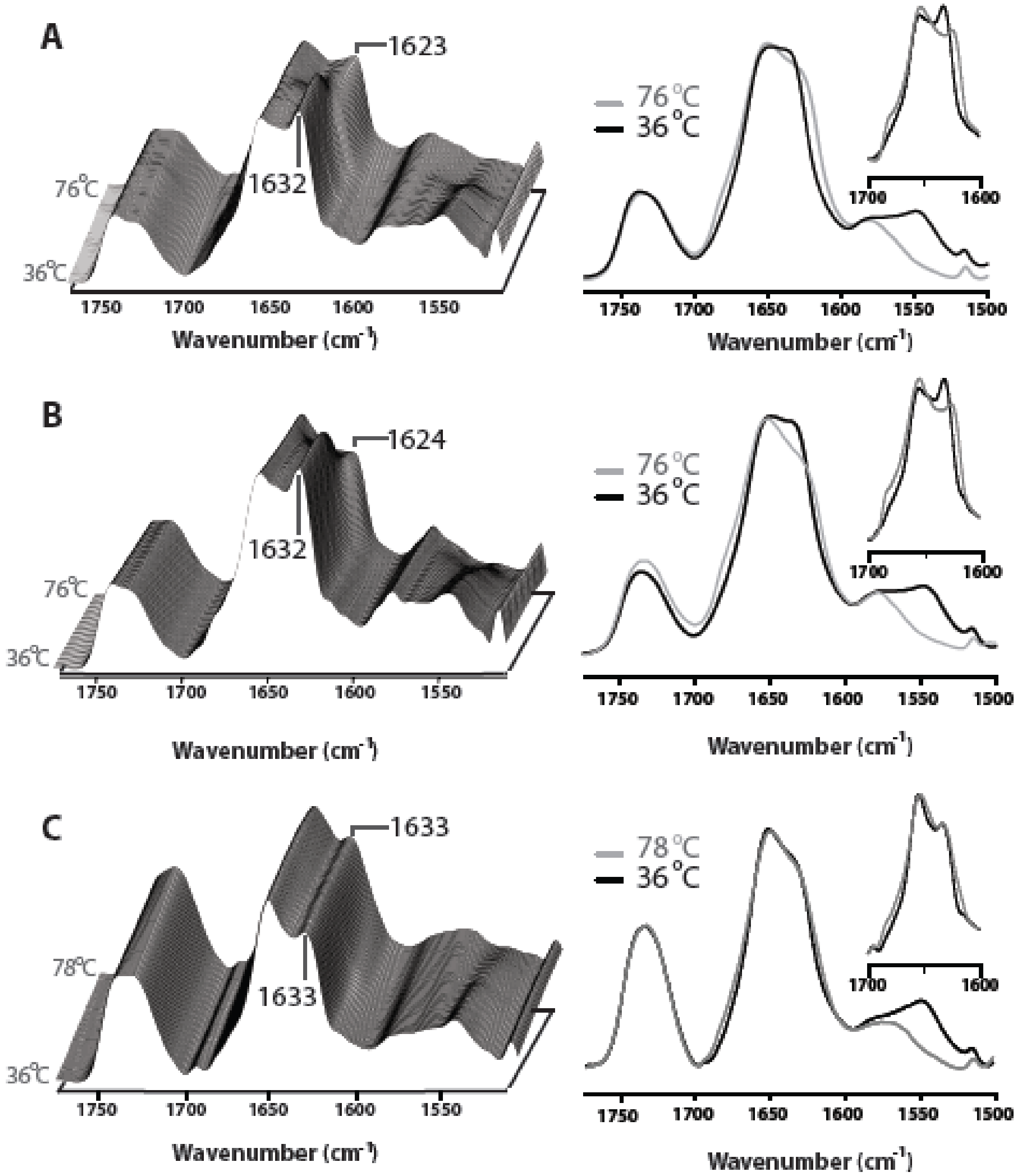
A
1623
1632
76°C
36°C
1750
1700
1650
1600
1550
Wavenumber (cm-1)
76°C
36°C
1700
1600
1750
1700
1650
1600
1550
1500
Wavenumber (cm-1)
B
1624
1632
76°C
36°C
1750
1700
1650
1600
1550
Wavenumber (cm-1)
76°C
36°C
1700
1600
1750
1700
1650
1600
1550
1500
Wavenumber (cm-1)
C
1633
1633
78°C
36°C
1750
1700
1650
1600
1550
Wavenumber (cm-1)
78°C
36°C
1700
1600
1750
1700
1650
1600
1550
1500
Wavenumber (cm-1)

Figure 2.4

Thermal denaturation curves plotting amide I intensity at 1620 cm^{-1} as a function of temperature. Representative curves are shown for aso-ELIC (solid circles), PC-ELIC (empty squares), and PC-ELIC-3 (solid upward triangles). As noted in the text, although the PC-ELIC-3 amide II intensity drops with increasing temperature, there is nearly no change in amide I band shape. Data for aso-ELIC and PC-ELIC have been fit with a Boltzmann sigmoidal function to obtain a T_d.

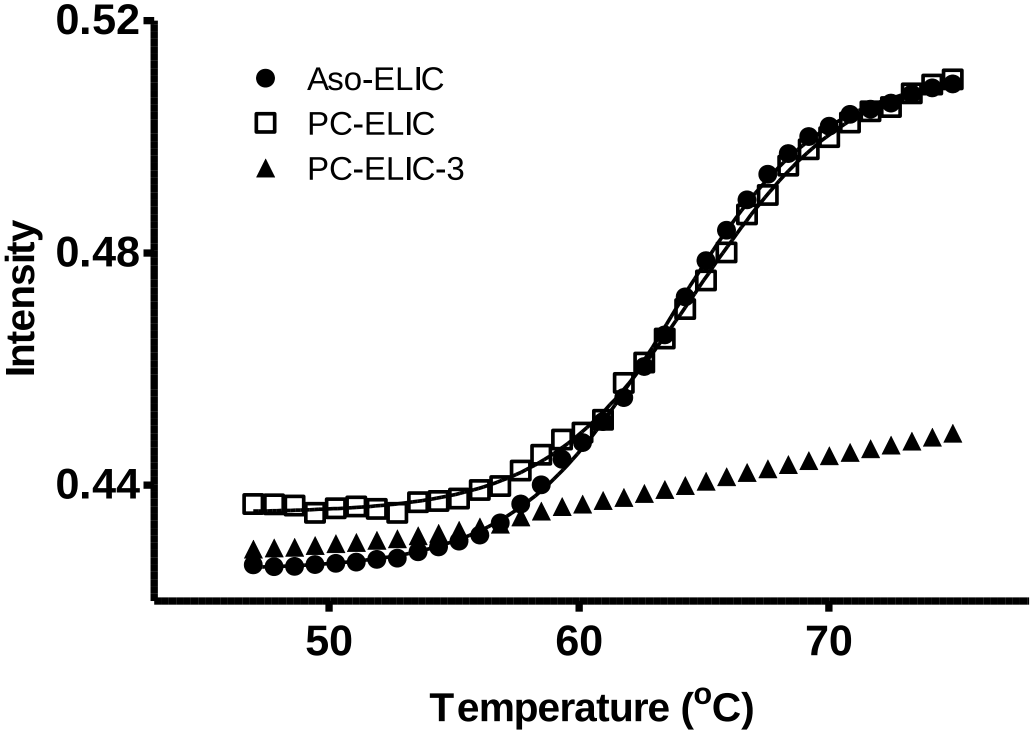
0.52
0.48
0.44
Intensity
50
60
70
Temperature (^{o}C)
● Aso-ELIC
☐ PC-ELIC
▲ PC-ELIC-3

tightly with M1/M3, leading to a more stable TMD that does not unfold even at high temperatures.

Aromatic additions between M1/M3 and M4 promote coupling in ELIC. I next assessed gating of the ELIC-3 mutant using two-electrode voltage clamp electrophysiology. Previous work using this technique has shown that the injection of either aso-nAChR or PC-nAChR into *Xenopus laevis* oocytes leads to the appearance of agonist binding sites on the cell surface, but agonist application leads to measurable current across the membrane only in oocytes injected with aso-nAChR (121). These results are consistent with PC-nAChR adopting a functionally uncoupled conformation.

As a control, I injected wildtype ELIC cRNA into oocytes, which led predictably to the appearance of dose-dependent, cysteamine-induced currents across the plasma membrane (EC_{50} = 0.94 ± 0.16 mM, n=23; Fig. 2.5). Oocytes injected with ELIC-3 cRNA also gave rise to a measurable dose-response curve (EC_{50} = 0.18 ± 0.02mM, n=9). Notably, the dose-response curve of oocytes injected with ELIC-3 cRNA was left-shifted with respect to that of oocytes injected with wildtype ELIC cRNA, indicating an increased response to cysteamine in ELIC-3. As ELIC-3 carries mutations only within the TMD, distant from the agonist binding site, it is unlikely that the aromatic substitutions have changed the affinity of the receptor for cysteamine. Instead, this change observed in EC_{50} likely reflects tighter coupling between the agonist site and the channel gate, so that agonist binding translates more efficiently into gating.

I next assessed the gating behaviour of ELIC-3 reconstituted into PC membranes. Oocytes injected with wildtype PC-ELIC have been previously shown to be non-responsive to cysteamine, suggesting that PC-ELIC is functionally uncoupled (data from Dr. Casey Carswell, see 106). My

Figure 2.5

Cysteamine dose-response curves of oocytes injected with cRNA for wildtype ELIC (solid downward triangles; n = 9), cRNA for the ELIC-3 mutant (open circles; n = 9), and PC-ELIC-3 (grey circles; n = 7). Inset: peak current measured for oocytes injected with reconstituted PC-ELIC or PC-ELIC-3. Error bars show SEM.

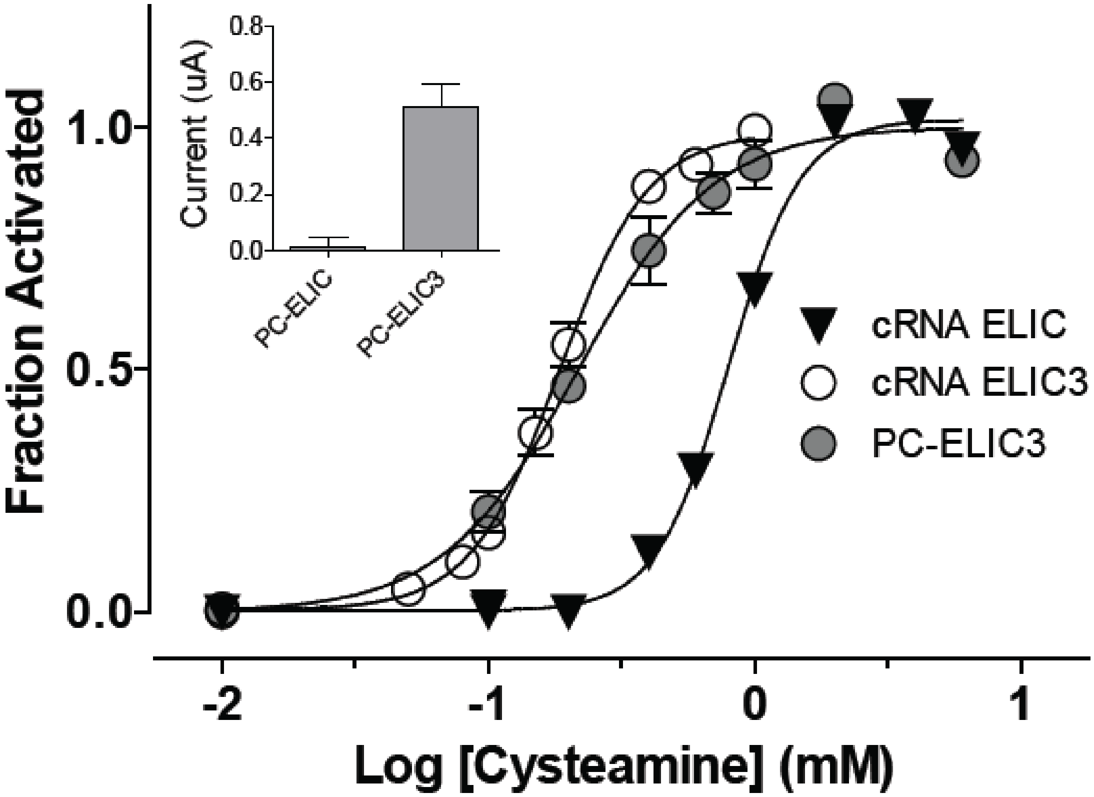
Fraction Activated
1.0
0.5
0.0
-2
-1
0
1
Log [Cysteamine] (mM)
cRNA ELIC
cRNA ELIC3
PC-ELIC3
Current (uA)
0.8
0.6
0.4
0.2
0.0
PC-ELIC
PC-ELIC3

own control data (Fig. 2.5 inset) supports this conclusion. PC-ELIC-3 injected into oocytes, however, gave rise to dose-dependent currents across the oocyte membrane, yielding a dose-response curve that is also left-shifted compared to that of wildtype ELIC cRNA (Fig. 2.5). Strikingly, the dose-response curve of PC-ELIC-3 (EC_{50} = 0.18 ± 0.04mM, n=7) is not significantly different from that of ELIC-3 cRNA, indicating that ELIC-3 has similar functionality in both the PC membrane and the oocyte membrane. Note that receptors retain the lipids into which they were reconstituted after injection into oocytes (125). Together, my data indicate that the added aromatic interactions enhance M1/M3 interactions with M4, which promotes TMD stability, tighter coupling between agonist-binding and gating, and decreases ELIC's lipid sensitivity and thus its propensity to adopt an uncoupled-like conformation in unfavourable lipid environments.

3. Discussion

In our current model of pLGIC uncoupling, the most peripheral α-helix in the TMD, M4, plays a vital role in lipid sensing and mediating lipid effects on receptor function. M4 also directly impacts upon the receptor's gating ability, as the interaction between the M4 C-terminal segment and the Cys-loop in the ECD is implicated in the allosteric pathway leading from the agonist binding site to the channel gate (35, 100). This M4 lipid sensor model proposes that lipids affect receptor function by altering the relative positioning of M4 to M1/M3, thereby changing the strength of M4's association with M1/M3 and with the Cys-loop. Based on this model, we made the following predictions: 1) tight M4-M1/M3 interactions will increase the stability of the TMD, 2) M4 association with M1/M3 will allow for strong interactions between the M4 C-terminus and the Cys-loop, leading to more efficient coupling, and 2) tight M4-M1/M3 interactions will reduce M4's ability to sense membrane composition.

Previous biophysical and functional studies performed by Dr. Casey Carswell and Jon Labriola, another former student in the lab, confirmed that the stability of nAChR, GLIC, and ELIC TMDs correlated well with the number of interacting aromatics at their M4-M1/M3 interfaces. All three receptors retained their ability to undergo agonist-induced channel gating in complex soybean asolectin membranes which stabilize activatable nAChR, but exhibited different lipid sensitivities in PC membranes lacking anionic lipids and cholesterol (110, 121). Whereas PC-nAChR and PC-ELIC adopted functionally uncoupled conformations, PC-GLIC retained its ion flux capabilities and behaved no differently from aso-GLIC.

These results suggest that the nAChR's extraordinary lipid sensitivity is a result of having no potential aromatic interactions at the M4-M1/M3 interface, leading to weak interactions along the length of the transmembrane segment. The nAChR M4 is likely capable of a relatively wide range of motion, and thus requires the presence of activating lipids to ensure proper contacts between M4-M1/M3 and between the M4 C-terminal and Cys-loop for coupling. Both ELIC and GLIC possess aromatic interactions at the M4-M1/M3 interface and can be purified as activatable receptors in the absence of lipid, suggesting decreased lipid sensitivity relative to the nAChR. In particular, the aromatic interactions along the length of the GLIC M4 ensure strong contacts with M1/M3. Molecular dynamics simulations of GLIC with the extracellular cluster of aromatics removed shows a consistent tilting-away of the M4 C-terminus from the transmembrane bundle (126). ELIC lacks this cluster of aromatics and is more sensitive to lipid-dependent uncoupling in PC membranes, further supporting a role for the strength of the M4-M1/M3 interaction in a pLGIC's lipid sensitivity.

Engineering aromatic residues into ELIC to mimic the complex network between M4 and M1/M3 found in GLIC altered its secondary structure and biophysical characteristics. ELIC-3 exhibited an increased α-helical/loop character relative to wildtype ELIC. This is likely a result of increased ordering of the M4 C-terminus, which in wildtype ELIC is relatively unconstrained (this segment is unresolved in the crystal structure of ELIC). ELIC-3 additionally undergoes less extensive N-^{1}H/N-^{2}H exchange than wildtype ELIC and has a higher thermal denaturation temperature. Taken together, these observations suggest that enhancing the M4-M1/M3 interaction increases the stability of the TMD. This is supported also by the observation that the thermal denaturation temperature correlates well with the number of aromatic interactions between M4 and M1/M3 in GLIC, ELIC, and the nAChR (see ref. 110).

Functionally, the added aromatic interactions restored ELIC's ability to gate open in the minimal PC membranes. The similar dose-response curves obtained from ELIC-3 cRNA and PC-ELIC-3 suggest that the added aromatic interactions render the receptor almost completely insensitive to the differences in lipid composition between the oocyte membrane and the PC membrane, similar to what was seen in GLIC (121). ELIC-3 is additionally more sensitive to agonist without any change in agonist affinity, likely because enhancing M4 C-terminus interactions with the Cys-loop promotes more efficient coupling of ligand binding and channel gating. This raises an intriguing possibility that it is the positioning of aromatic interactions along the length of the M4-M1/M3 interface, rather than their total number, that is important for the enhancing effect they have on coupling. If enhancing only the M4 C-terminus/Cys-loop interaction is sufficient for improving coupling, then we expect that the extracellular cluster of aromatics should be more important for coupling than the intracellular cluster. In fact, an alanine scan of the M4 α-helix in GLIC shows that large loss-of-function occurs upon mutation of the aromatic residues near the M4 C-terminus, but no change in function upon mutation of the aromatic residues near the intracellular membrane (127). Studies of the coupling mechanism show only a small role for the M4 C-terminus/Cys-loop interaction in the propagation of ligand binding to gating (36), suggesting that this interaction has a more structural role in anchoring the ECD to the TMD. Intriguingly, an alanine scan of the ELIC M4 shows large gains-of-function upon mutation of aromatics in the intracellular cluster (127). In the absence of an extracellular cluster that tethers the M4 C-terminus in a favourable position for interaction with the Cys-loop, bulky aromatics may negatively affect the packing of the TMD α-helices.

4. Conclusions

The work undertaken in this chapter provides insight into the mechanisms of lipid-dependent uncoupling. Consistent with our working model of the uncoupled state, we found that the M4 α-helix plays an important role in the ability of pLGICs to sense their lipid environment, and that its interactions with the adjacent M1 and M3 α-helices have a profound impact on the receptor's propensity to uncouple in unfavourable lipid environments. Specifically, tight association of M4 with M1/M3 promotes TMD structural stability and enhances coupling between the ECD and TMD, reflected in the gain-of-function observed when additional aromatic interactions were engineered into ELIC. Aromatic interactions drive the tight association of TMD α-helices, and our experiments provide evidence to suggest that increasing the extent of the intrasubunit aromatic network promotes association of M4 with M1/M3. In the context of the lipid-dependent uncoupling model, it is likely that activating lipids necessary for coupling play a similar role as intramembrane aromatics by stabilizing an orientation of M4 that allows appropriate contacts to be made with the ECD Cys-loop, and that the absence of these lipids causes uncoupling by allowing the movement of M4 away from the receptor core.

Chapter 3

Alterations to Pore Conformation in Uncoupling

1. Preface

This manuscript was submitted to the journal Biochimica et Biophysica Acta – Biomembranes in June, 2016 and was accepted for publication in November, 2016. The paper characterizes the binding of two fluorescent pore-binding probes, ethidium and crystal violet, to reconstituted nAChR in resting, desensitized, and uncoupled conformations using fluorescence spectroscopy. Here, I show that the nAChR pore adopts a distinct conformation in the uncoupled state from resting or desensitized nAChR and has low binding affinity for both ethidium and crystal violet.

Frederique Comeau collected a small portion of the ethidium data with nAChR reconstituted into membranes containing a mix of phosphatidylcholine, phosphatidic acid, and cholesterol in a 3:1:1 mol:mol ratio (PC/PA/Chol-nAChR). His contributions are noted in the figure captions where they appear. I collected all other data presented in this manuscript, and I wrote this manuscript in collaboration with my supervisor.

2. Rationale

The ability of the nicotinic acetylcholine receptor (nAChR) to undergo agonist-induced conformational transitions is sensitive to its membrane environment (128-129). Increasing levels of anionic lipids and/or cholesterol in a reconstituted phosphocholine (PC) membrane stabilize an increasing proportion of nAChRs in an agonist-responsive conformation (84, 96). In PC membranes lacking these activating lipids, the nAChR adopts an uncoupled conformation that retains native-liked fold and binds agonist with resting state-like affinity, but does not gate open upon ligand-binding; in this conformation, agonist binding is “uncoupled” from channel gating (94). Lipid-dependent uncoupling is also accompanied by the solvent-exposure of peptide backbone hydrogens that are buried from solvent in the resting and desensitized states (94-95).

The nAChR exhibits two main functional domains, a predominantly β-sheet (β1-β10) extracellular agonist-binding domain (ECD) and an α-helical (M1-M4) transmembrane channel-gating domain (TMD). These two domains meet at an interface, with non-covalently interacting loops from both domains playing a key role in translating agonist binding into channel-gating (34, 130-131). Both the enhanced backbone solvent exposure and the uncoupling of binding-to-gating may result from ineffective interactions at the ECD/TMD interface (94). Lipids could influence ECD/TMD interactions via the TMD α-helix, M4 (100-102), which is on the periphery of each subunit and is thus exposed to the lipid environment (132, 10). M4 also extends beyond the lipid bilayer to interact with the functionally important Cys-loop (β6-β7 loop) at the ECD/TMD interface. One model suggests that lipids modulate coupling between the agonist site and channel gate by altering M4/Cys-loop interactions, thus influencing the Cys-loop conformation (94, 126-127).

The prokaryotic homolog ELIC shares a common topology with the nAChR (10, 13), but its crystal structures exhibit several features consistent with those proposed for the uncoupled state (Fig. 3.1). First, the final five residues at the M4 C-terminus are not resolved, suggesting weak, if any, interactions between the M4 C-terminus and the β6-β7 loop. Second, there are few direct contacts between the β1-β2/β6-β7 loops and the M2-M3 linker, suggesting weak ECD/TMD interactions (18). Finally, no changes in the orientation of the pore-lining M2 α-helices are observed between structures crystallized in the presence versus absence of agonist, suggesting a

Figure 3.1.

Structural comparison of the nAChR and ELIC highlighting potential features of the uncoupled state. (A) The *Torpedo* nAChR structure (PDB ID: 2BG9) showing a single subunit in cartoon format. (B) The ECD-TMD coupling interface (roughly the dashed box in (A)) of a single subunit for the nAChR (top) and ELIC (bottom; PDB ID: 2VL0). The β6-β7 loop is in green, the M2-M3 linker in blue, the M4 C-terminus in orange, and the β1-β2 loop in red. In the nAChR, residues αV132 and αF135 of the β6-β7 loop and residues αP272 and αI274 of the M2-M3 linker are shown as spheres, as are the corresponding residues (D114 and R116 of the β6-β7 loop and P252 and Y256 of the M2-M3 linker) in ELIC. The interacting residues αF136 on the β6-β7 loop (F120 in ELIC) and αQ434 on the post-M4 segment (no equivalent in ELIC structure) are shown in sticks. (C) A side view showing M2 and M3 from two nonadjacent subunits (left), with the gating residues αL251 and αV255 in the nAChR and L238 and F245 in ELIC highlighted as yellow spheres. The right panel shows a bird's-eye view of the pore-forming M2 α-helices from all subunits, illustrating the constricted diameter of the channel pore in ELIC.

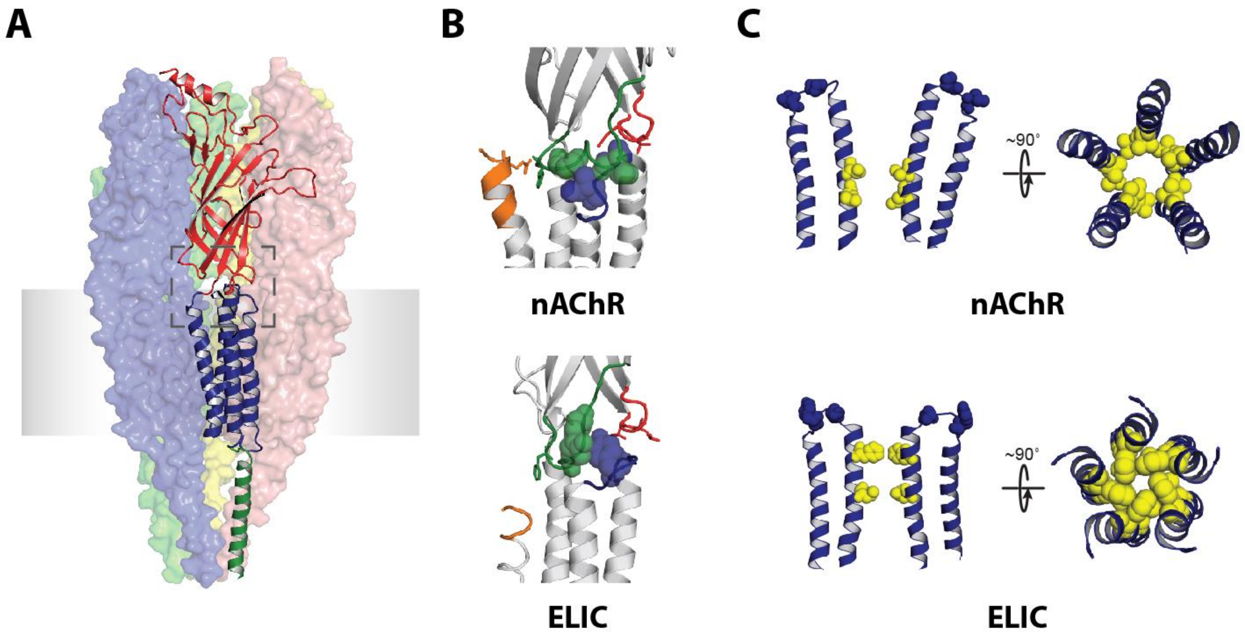
A
B
C
~90°
nAChR
nAChR
~90°
ELIC
ELIC

functional uncoupling of binding and gating (133, 108). Intriguingly, the channel pore of crystallized ELIC is constricted relative to that of other closed pLGICs, raising the possibility that a constricted or “collapsed” pore may be another structural feature of the uncoupled state (Fig. 3.1 C).

Both the ECD and TMD of the uncoupled PC-nAChR bind agonists and non-competitive antagonists, respectively, with lower affinity than the desensitized nAChR (94, 134). As the resting nAChR also binds both agonists and antagonists with relatively low affinity, the simplest interpretation is that each domain adopts a resting-state-like structure. The ELIC structure, however, raises the possibility that at least the TMD adopts a conformation distinct from both the resting and desensitized conformations. In fact, a constricted pore could explain the apparently weak pore-binding of functional probes, such as ethidium bromide and 3-trifluoromethyl-3-(m-[^{125}I]iodophenyl) diazirine (TID), to the uncoupled PC-nAChR (94, 99) (see Discussion).

To probe the conformations of the individual functional domains, we characterize here the binding of acetylcholine (ACh) and two fluorescent channel blockers, ethidium and crystal violet (CrV), to the uncoupled PC-nAChR. We confirm that the ECD binds acetylcholine with an affinity similar to that of the resting state. Although the binding of both ethidium and CrV were characterized for resting and desensitized nAChRs, no binding of either probe was detected to the uncoupled nAChR. Our data show that the TMD of the uncoupled PC-nAChR adopts a distinct conformation with channel blocker pharmacologies consistent with a constricted channel pore. The implications of a constricted channel pore in the uncoupled state are discussed in the context of current models of pentameric ligand-gated ion channel (pLGIC) gating.

3. Methods

Materials. Frozen *Torpedo California* electroplax tissue was obtained from Aquatic Research Consultants (San Pedro, CA). 1-palmitoyl-2-oleoyl-*sn*-glycero-3-phosphocholine (PC), 1-palmitoyl-2-oleoyl-*sn*-glycero-3-phosphatidic acid (PA), and cholesterol (Chol) were from Avanti Polar Lipids, Inc. (Alabaster, AL). Soybean asolectin (L-α-phosphatidylcholine, type II-S), carbamylcholine chloride (Carb), proadifen hydrochloride, dibucaine hydrochloride, ethidium bromide, crystal violet (CrV), and sodium cholate were from Sigma (St. Louis, MO). α-bungarotoxin (α-BTX) was from Tocris Biosciences. [^{3}H]-Acetylcholine iodide (76 mCi/mmol) (^{3}H-ACh) was from Perkin Elmer Life Sciences (Waltham, MA).

Preparation of reconstituted nAChR. Crude membranes from *T. californica* electroplax tissue were solubilised in 1% cholate and then applied to a bromoacetylcholine column as described elsewhere (94). The bound nAChR was washed extensively with lipids solubilized in the same cholate buffer, and then eluted with 10 mM Carb. The pooled eluate was dialyzed extensively to form proteo-liposomes at a molar lipid-to-protein ratio of roughly 500:1.

Fourier transform infrared spectroscopy. Infrared spectra were recorded, after exposure of each nAChR membrane to ^2H_2O for 72 hours at 4°C, on a Digilab (now Agilent Technologies; Santa Clara, CA) FTS7000 spectrometer. Spectra were processed using GRAMS/AI software (Thermo Scientific, Wlatham, MA), with resolution enhancement performed between 1900 and 1300 cm^{-1} with γ=7 and a Bessel smoothing function set at 70%.

Equilibrium ^{3}H-ACh binding. nAChR membranes (roughly 45 nM and 150 nM ACh sites for aso-nAChR and PC-nAChR, respectively) were incubated with the indicated concentrations of ^{3}H-ACh for a minimum of 75 minutes at 4 °C. Bound versus free ^{3}H-ACh were then separated from each other by filtration under vacuum through 25mm GF/F glass fibre filter paper (Whatman). Specific binding is the difference between total binding and non-specific binding, the latter observed in the presence of a 20-fold molar excess of α-BTX. Filter papers (bound ^{3}H-ACh) and filtrate (free ^{3}H-ACh) were quantified by liquid scintillation counting in Ecolite(+)^{TM} (MP Biochemicals, Santa Ana, CA). The binding isotherms were fit using Prism, with a one-site specific binding function (Y=Bmax*X(Kd + X), where Y is specific binding and X is the concentration of ^{3}H-ACh).

Fluorescence spectroscopy. Spectra were acquired at 22.5^{o}C on a Cary Eclipse fluorescence spectrometer (Agilent Technologies). Except where noted, data was collected with excitation/emission wavelengths set to 530 nm/590 nm and excitation/emission slits at ±5/20 nm for ethidium (except where noted). For CrV, the excitation/emission wavelengths and excitation/emission slit widths were 590/630 nm and ±10/20 nm, respectively. Non-specific ethidium or CrV binding was determined in the presence of 20 μM proadifen. Resting state samples were stabilized by pre-incubation for at least 30min with α-BTX at 10- or 20-fold the molar concentration of nAChR.

4. Results

The uncoupled nAChR in PC membranes. The nAChR reconstituted into membranes composed of soybean asolectin (aso-nAChR), PC/PA/Chol (3:1:1 mol:mol:mol) (PC/PA/Chol-nAChR) and PC (PC-nAChR) exhibits similar structural and biophysical properties (Fig. 3.2). The nAChR in each membrane also binds agonist. Only aso-nAChR and PC/PA/Chol-nAChR, however, respond to agonist by undergoing conformational transitions. Specifically, addition of

Figure 3.2.

Structure and function of the membrane-reconstituted nAChR. (A, left) Infrared spectra showing the amide I band of aso-nAChR (i) and PC-nAChR (ii) both before (gray line) and after resolution enhancement (black). Non-deconvolved amide II bands are shown on the right. The amide II band intensity at 1547 cm^{-1} reflects unexchanged peptide N-^{1}H. The relative intensity of the band can be visually quantified by comparison with that of the overlapping side chain carboxyl stretching vibration near 1580 cm^{-1} (dashed line). Spectra were recorded after 72 hours exposure to ^2H_2O at 4 °C. (B) Kinetics of N-^{1}H/N-^{2}H exchange of aso-nAChR (black circles) and PC-nAChR (open squares). The amide II/amide I band intensity ratio is plotted as a function of time after exposure to ^2H_2O. All spectral data is the average of at least 3 sets of scans. (C) Kinetic ethidium binding experiments show an agonist-induced fluorescence increase due to enhanced ethidium binding to the channel pore, and then displacement by dibucaine in (i) aso-nAChR and (ii) PC-nAChR. Time points indicate addition of 0.3 μM ethidium, 100nM nAChR, 500μM Carb, and 500μM dibucaine (Dib). (au) refers to arbitrary units. Lower panel shows a schematic for the fluorescence experiments: ethidium binding to the channel pore leads to a ~15-fold increase in fluorescence intensity (95). (D) Equilibrium binding of [^{3}H]ACh to aso-nAChR (black circles, n=3) and PC-nAChR (open squares, n=4). Inset: Scatchard analysis of aso-nAChR (left) suggests single site, one affinity. PC-nAChR binding data (right) reveals two distinct binding sites.

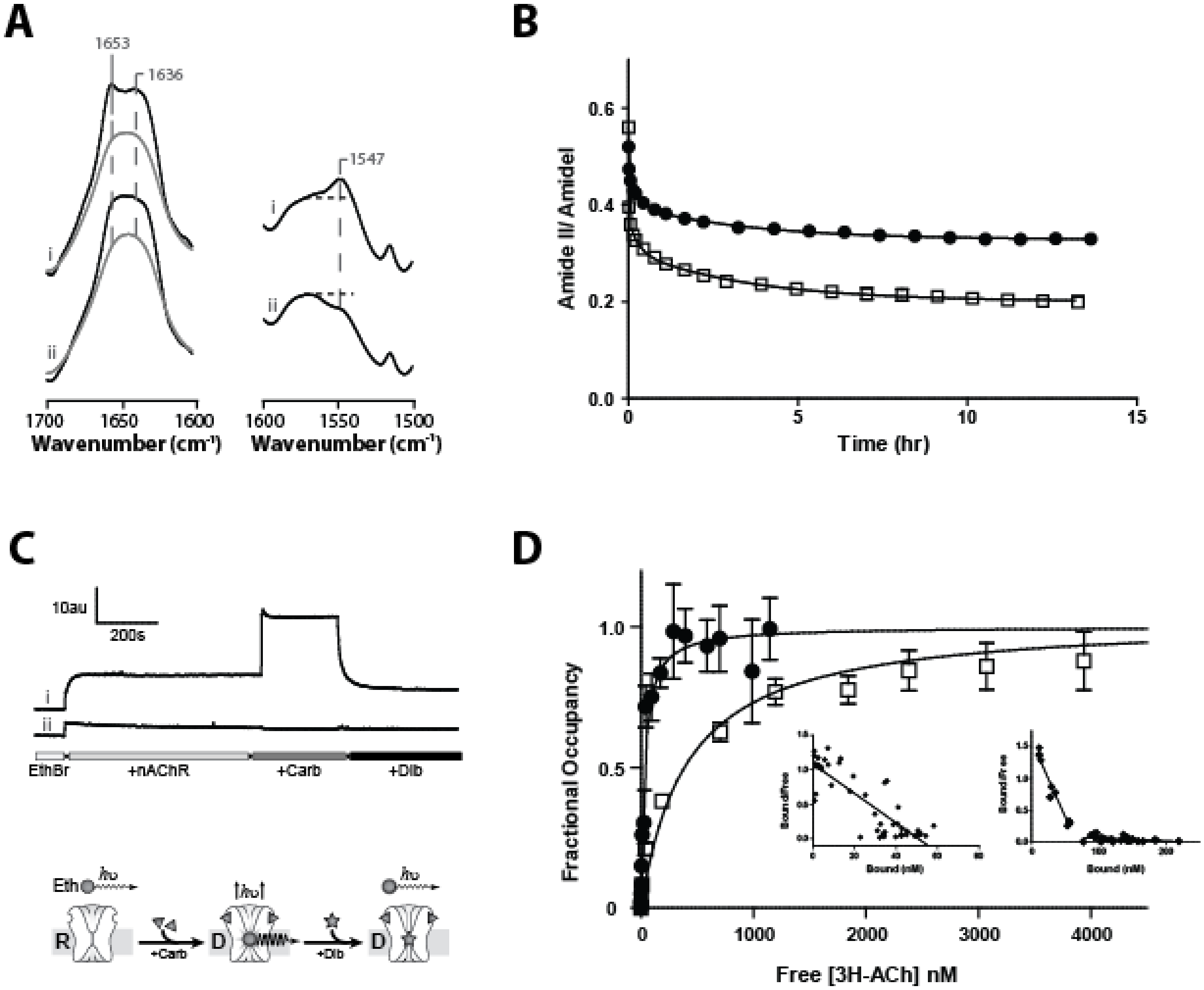
A
1653
1636
1547
i
ii
i
ii
1700
1650
1600
Wavenumber (cm⁻¹)
1600
1550
1500
Wavenumber (cm⁻¹)
B
Amide II/ AmideI
0.0
0.2
0.4
0.6
0
5
10
15
Time (hr)
C
10au
200s
i
ii
EthBr
+nAChR
+Carb
+Dib
Eth
hυ
R
+Carb
D
hυ
+Dib
D
hυ
D
Fractional Occupancy
0
0.5
1.0
0
1000
2000
3000
4000
Free [3H-ACh] nM
Bound/Free
Bound (nM)
Bound/Free
Bound (nM)

the agonist, Carb, to a solution containing ethidium bromide and either aso-nAChR or PC/PA/Chol-nAChR (data not shown, see ref. 94) leads to rapid ethidium binding as the nAChR transitions from the low-affinity resting to open and then high-affinity desensitized (Kd ~1 mM and ~0.3 μM, respectively; 99) states (Fig. 3.2 C). In contrast, no binding is observed when Carb is added to a solution of ethidium and PC-nAChR. PC-nAChR is stabilized primarily in an uncoupled conformation that does not transition on the seconds to minutes time scale to the high-affinity ethidium-binding desensitized state.

The different functional capacities of the nAChR in these three membranes are further illustrated in ^{3}H-ACh binding experiments (Fig. 3.2 D). ^{3}H-ACh binding to aso-nAChR and PC/PA/Chol-nAChR (data not shown, see 94) yield equilibrium dissociation constants (K_{eq}) in the 30 to 60 nM range, which is between the values expected for resting (K_d = 800 nM) and desensitized (K_d = 2nM) nAChRs (98). In both cases, the equilibrium binding constants are closer to that of the desensitized state because the resting-to-desensitized equilibrium shifts toward the desensitized conformation with increasing ACh binding. In contrast, the uncoupled PC-nAChR binds ACh with an affinity (K_d = 2.4 μM), slightly lower than that of the resting state (Table 3.1), and does not transition to the high affinity binding desensitized conformation. Note that PC-nAChR does not appreciably transition on the minutes time scale to resting, open or desensitized (i.e. "coupled") conformations because the activation energy between uncoupled and coupled conformations in PC membranes is insurmountably high. Reconstitution of the nAChR into thicker phosphatidylcholine membranes promotes ligand-induced transitions from uncoupled to coupled conformations, but on the tens of minutes-to-hours time-scale (89). Scatchard analysis of ACh binding reveals a small component (~10% of total sites) of high affinity ^{3}H-ACh binding (K_d = 42 nM) to PC-nAChR, as observed previously (90). This could be due to a population of receptors

Table 3.1. Scatchard analysis of ^{3}H-ACh equilibrium binding to reconstituted nAChR.

Sample	**High Affinity Site**[1]		**Low Affinity Site**		**n**
	K_d (nM)	**Proportion**	**K_d (μM)**	**Proportion**	
Aso-nAChR	47 ± 3.4	~100%	--	--	3
PC-nAChR	42 ± 3.4	~12.5%	2.4 ± 900	~87.5%	4

[1] Binding determined using Scatchard analysis.

that exist in coupled resting or desensitized conformations in the absence of agonist, or that transition from uncoupled to desensitized states over the longer time course (≥75 minutes) of the ^{3}H-ACh binding experiments.

Note also that the structure of the nAChR in the different reconstituted membranes was evaluated using infrared spectroscopy. Aso-nAChR, PC/PA/Chol-nAChR (data not shown, see 94) and PC-nAChR exhibit similar secondary structure-sensitive amide I band shapes (left panel of Fig. 3.2 A). In each case, spectral deconvolution reveals two prominent amide I component bands near 1655 cm^{-1} (α-helix) and 1635 cm^{-1} (β-sheet), suggestive of the expected mixed α-helix/β-sheet secondary structure. Infrared spectra are typically recorded in ^2H_2O buffer to avoid overlap between the amide I band and the absorption of ^1H_2O. Immersion in ^2H_2O leads to the exchange of peptide N-^{1}H to N-^{2}H, which is accompanied by a shift in frequency of the amide II vibration from near 1547 cm^{-1} down to near 1450 cm^{-1}. The weaker residual amide II vibration indicates that PC-nAChR undergoes more extensive peptide hydrogen exchange than aso-nAChR or PC/PA/Chol-nAChR (right panel of Fig. 3.2 A). Peptide N-^{1}H to N-^{2}H exchange also leads to ~10 cm^{-1} downshift in frequency of the α-helical amide I component band, leading to a slightly reduced intensity near 1655 cm^{-1} in spectra of PC-nAChR (95). The differential peptide N-^{1}H to N-^{2}H exchange kinetics can be monitored by following the decrease in amide II band intensity as a function of time after exposure of the nAChR to ^2H_2O (Fig. 3.2 B). Curve fitting the peptide N-^{1}H/N-^{2}H kinetic exchange curves suggests that a population of exchange resistant and thus solvent buried peptide backbone hydrogens in the resting and desensitized conformations becomes exposed to solvent in the uncoupled state (94).

No detectable binding of ethidium to the pore of the uncoupled nAChR. We next set out to characterize the binding of ethidium to the nAChR in the resting, desensitized and uncoupled conformations, in order to ascertain whether the TMD adopts a conformation similar to, or distinct from, the TMD in the resting and desensitized states. Ethidium binding was first measured for both aso-nAChR and PC/PA/Chol-nAChR in the absence and/or presence of Carb (Fig. 3.3). In the absence of Carb, binding is best described by a sigmoidal curve with an EC50 of 5.5 ± 0.69 µM and a Hill slope of 1.4 ± 0.06 µM (n = 6) (Table 3.2), consistent with previous measurements obtained using native nAChR membranes (EC_{50} = 6.8 µM) (99). As with ACh binding, this value is between the measured Kd for resting and desensitized nAChRs in native membranes (K_d ~ 0.3 µM and ~1 mM for desensitized and resting, respectively), but is closer to that of the desensitized conformation as ethidium binding shifts the resting-to-desensitized equilibrium towards the desensitized state.

In the presence of Carb, ethidium binding to both aso-nAChR and PC/PA/Chol-nAChR is best described by single site non-cooperative binding with measured K_d values of 0.55 ± 0.08 µM (n = 4) and 0.85 ± 0.13 µM (n = 9), respectively (Table 3.2), consistent with similar titrations performed with native membranes (K_d = 0.25 µM for the desensitized nAChR (99)). In contrast to the binding experiments performed in the presence or absence of Carb, no binding of ethidium was observed to PC/PA/Chol-nAChR pre-incubated with α-BTX to stabilize the resting conformation (n = 3). Similarly, no binding was observed to the uncoupled PC-nAChR (n = 3). The lack of ethidium binding under these conditions shows that both the resting and uncoupled conformations have binding affinities that are weaker than the binding affinities for the desensitized state, consistent with the reported K_d for ethidium binding to the resting nAChR in native membranes (K_d ~ 1 mM). Note that the B_{max} value for ethidium binding to PC/PA/Chol- nAChR in the absence of Carb is slightly greater than the Bmax value for binding to the same membranes in the presence of Carb due to additional ethidium binding to the agonist site. Agonist- site binding is also observed

Figure 3.3.

Ethidium binding to membrane-reconstituted nAChR. Specific ethidium binding is plotted for PC/PA/Chol-nAChR pre-incubated with 500µM Carb (desensitized, black squares, n=9) and in the absence of agonist (open upside-down triangles, n=6). Binding was analyzed using a one-site specific binding function with Hill slope in GraphPad Prism ($Y=B_{max}*X^{\wedge}H/(K_d{}^{\wedge}H + X^{\wedge}H)$). No binding was detected for PC/PA/Chol-nAChR pre-incubated with a 10-fold molar excess of α-BTX (resting, closed circles, n=3) or PC-nAChR (uncoupled, open squares, n=3). Error bars showing ±SEM are present, but are smaller than the data points.

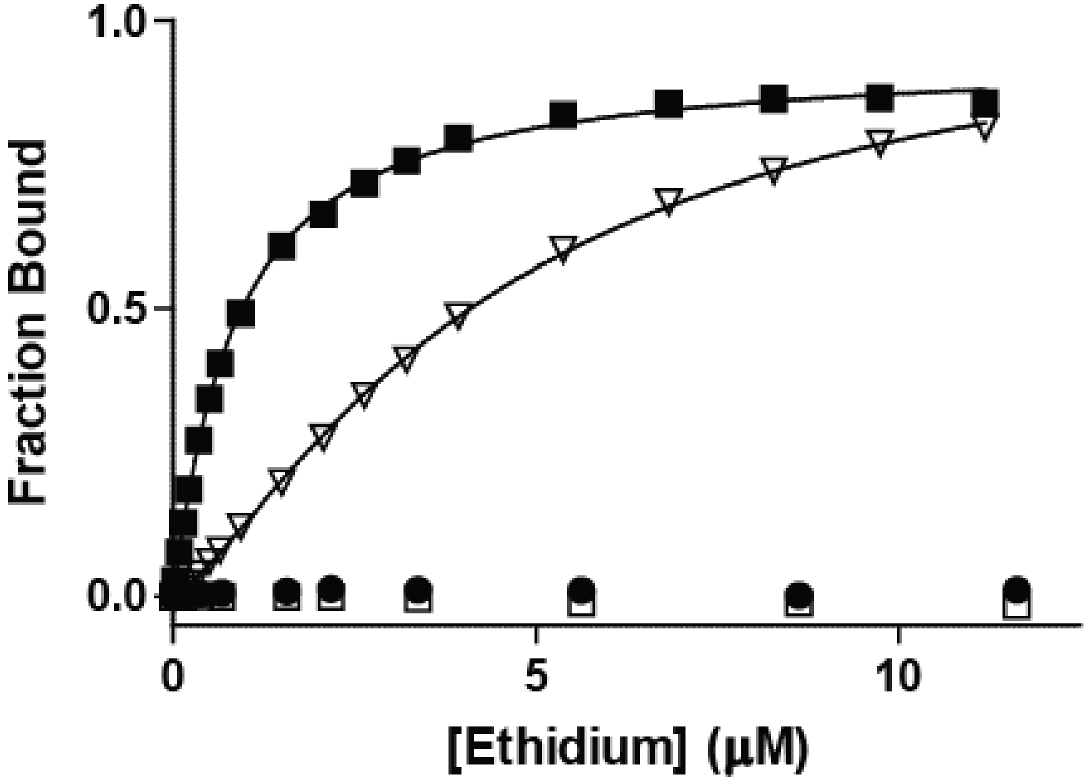
1.0
0.5
0.0
Fraction Bound
0
5
10
[Ethidium] (μM)

Table 3.2. Binding of ethidium bromide and crystal violet to reconstituted nAChR.

Fluorescent Compound	Sample	K_D or EC_{50} (μM)[1]	Hill Slope	Bmax	N
Ethidium Bromide	PC/PA/Chol +Carb	0.85 ± 0.13	1.03 ± 0.04	122.2 ± 8.4	9
	PC/PA/Chol -Carb	5.45 ± 0.69	1.38 ± 0.06	134.8 ± 7.7	6
	PC/PA/Chol +BTX	--	--	--	3
	Asolectin +Carb	0.55 ± 0.08	1.12 ± 0.13	101.4 ± 8.3	4
	PC-nAChR	--	--	--	3
	Native-nAChR +Carb*	0.36			
	Native-nAChR -Carb*	11			
	Native-nAChR +BTX*	~1000			
Crystal Violet	PC/PA/Chol +Carb	0.077 ± 0.008	0.993 ± 0.10	29.90 ± 1.04	4
	Asolectin +Carb	0.049 ± 0.003	1.02 ± 0.06	22.94 ±0.41	7
	Asolectin +BTX	0.25 ± 0.011	0.915 ± 0.04	22.01 ± 0.53	7
	PC-nAChR	--	--	--	5

[1] Binding affinities determined by curve fitting with a one-site specific binding function with Hill slope as in Figure 3.3.

in the kinetic ethidium binding experiments discussed below (Fig. 3.4).

We titrated the nAChR to higher concentrations to compare the relative affinities for the resting and uncoupled conformations, but significant auto-quenching prevented an analysis of the binding data even when acquisition parameters minimized the fluorescence signal. Ethidium binding to the resting nAChR has been previously performed using competition binding experiments with ^{3}H-phencyclidine (99) or its analog, ^{3}H-tenocyclidine (^{3}H-TCP). We considered using a similar approach to characterize binding to both resting and uncoupled nAChRs in reconstituted membranes, but no binding of ^{3}H-TCP to PC-nAChR could be detected (Michael Blanton, personal communications). While the lack of ^{3}H-tenocyclidine binding to the uncoupled nAChR is itself indicative of an altered pore conformation in the uncoupled versus the resting conformation, it suggested that ethidium/^{3}H-TCP competition experiments with PC-nAChR would not be fruitful.

Alternatively, we explored the binding of ethidium to resting and uncoupled nAChRs via kinetic ethidium binding experiments similar to those shown in Fig. 3.2 C. At the lowest concentration tested ($0.5K_d = 0.43$ μM), mixing ethidium with either aso-nAChR or PC/PA/Chol-nAChR leads to ethidium binding to pre-existing desensitized nAChRs, while Carb-addition leads to additional and rapid ethidium binding as nAChRs shift from resting to open and then desensitized conformations (Fig. 3.4 A). Note that at a $0.5K_d$ concentration, ethidium only binds to a small fraction of the total number of Carb-stabilized desensitized nAChRs, so the total fluorescent signal is relatively low. At $35K_d$ (30 μM) concentrations, ethidium binding saturates and shifts the resting-to-desensitized equilibrium in favor of the desensitized state prior to Carb addition, leading to a more intense fluorescence signal. As noted above, Carb addition reduces slightly ethidium fluorescence by competing with ethidium binding to the agonist site.

Figure 3.4.

Kinetic ethidium binding experiments to desensitized, resting, and uncoupled nAChRs. (A) Roughly 100nM aso- or PC/PA/Chol-nAChR pre-incubated in the absence of ligand (activatable resting that converts to desensitized) or presence of α-BTX (resting) or PC-nAChR (uncoupled) were mixed with either 0.4 μM (light gray), 4 μM (medium gray) or 30 μM (black) ethidium. 500 μM Carb and 20 μM proadifen were added at the indicated times. Data were acquired with excitation/emission wavelengths at 530/590nm and slit widths of 5/20nm. (B) Similar kinetic binding experiments performed at 30 μM (gray), 100 μM (medium gray) and 250 μM (black) concentrations of ethidium, but acquired with slit widths of 1.5/20nm. At the indicated times, 500 μM Carb and 20 μM proadifen were added, although two aliquots of proadifen were added to ensure that there was complete displacement of ethidium from the pore binding site. Note that for presentation purposes, the lowest concentration (30 μM) has been placed at the top and the highest concentration (250μM) at the bottom. All kinetic traces are the average of at least 3 runs. (C) Bar graphs quantify the proadifen-displaceable ethidium fluorescence in (B) at each concentration. (au) refers to arbitrary units. Error bars are ± SEM.

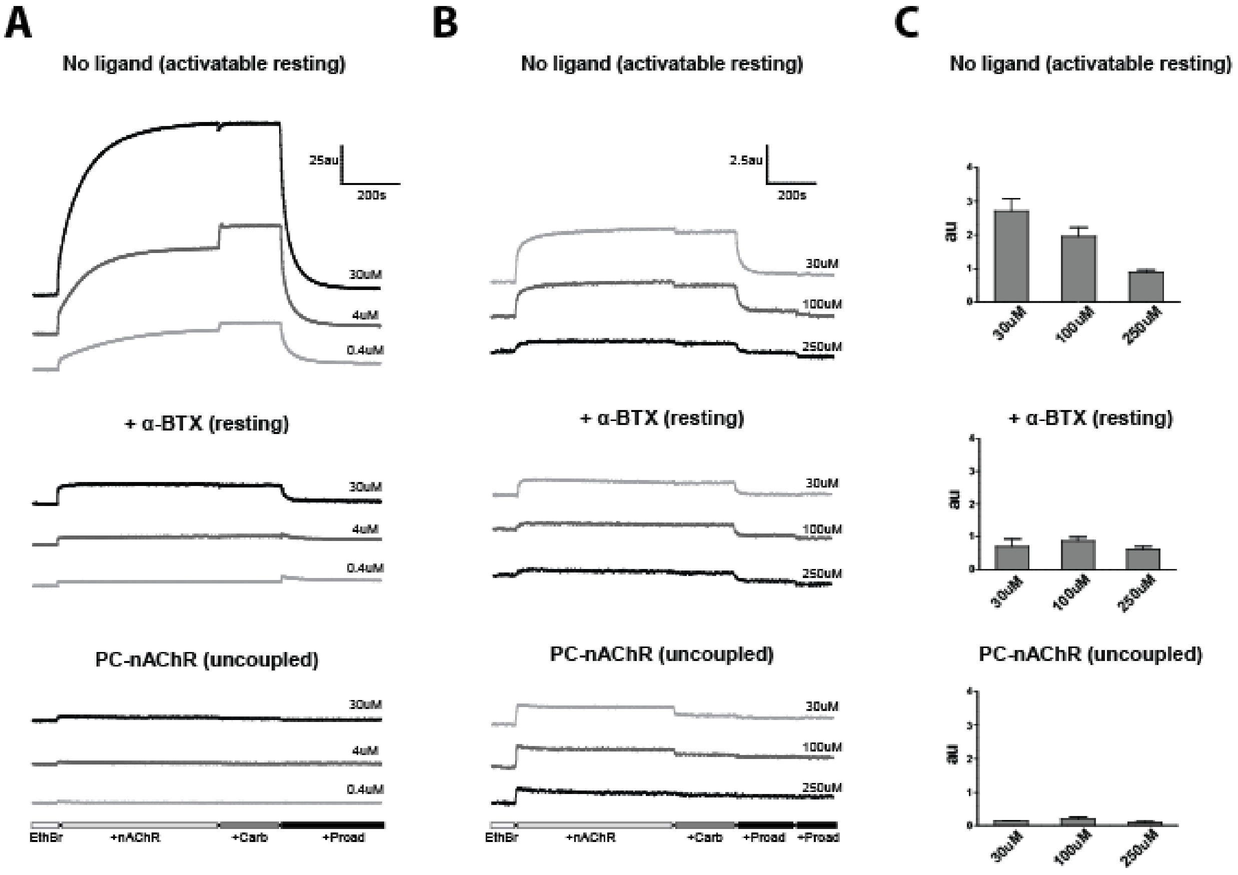
A
B
C
No ligand (activatable resting)
25au
200s
30uM
4uM
0.4uM
+ α-BTX (resting)
PC-nAChR (uncoupled)
EthBr
+nAChR
+Carb
+Proad
2.5au
100uM
250uM
au
0
1
2
3
4

We next performed similar kinetic experiments with the nAChR stabilized in the resting (+α-BTX) and uncoupled (PC-nAChR) states. No proadifen displaceable and thus pore-specific binding of ethidium was observed to resting nAChRs at the $0.5K_d$ (0.43 μM) and $5K_d$ (4.25 μM) concentrations, consistent with the ethidium binding isotherms (Fig. 3.3). A small component of specific pore binding ethidium fluorescence, however, was detected at 30 μM ethidium, showing that the kinetic experiments can detect ethidium binding to the resting state. In contrast, no ethidium binding to the uncoupled PC-nAChR was observed at any of the tested concentrations, suggesting that the affinity for the uncoupled state is lower than the affinity for the resting conformation.

Ethidium binding to resting, desensitized and uncoupled nAChRs was explored further using similar kinetic experiments performed at even higher ethidium concentrations (30, 100, and 250 μM), but using smaller excitation slit widths to minimize the excitation of ethidium and thus auto-quenching (Fig. 3.4 B and 3.4 C). Each increment in ethidium concentration led to increased auto-quenching thus reducing the absolute fluorescence intensity. Regardless, specific proadifen-displaceable ethidium binding to the channel pore was observed at all three ethidium concentrations with both resting and desensitized nAChRs. It is notable that the magnitude of the pore-bound ethidium fluorescence in the resting nAChR approaches that of pore bound ethidium in the desensitized state at the higher ethidium concentrations. Again, no ethidium binding was detected for the uncoupled PC-nAChR at any of the ethidium concentrations up to 250 μM. Thus, while we were not able to define the affinity constants for ethidium binding to resting or uncoupled nAChRs, our data show unequivocally that ethidium binds with a lower affinity to the uncoupled versus the resting state.

No detectable binding of CrV to the pore of the uncoupled PC-nAChR. CrV is another fluorescent probe that binds to the channel pore in a conformationally selective manner, but its binding affinity is 7- to 30-fold higher than that of ethidium. We first probed binding of CrV to desensitized (+Carb) and resting (+α-BTX) nAChRs in reconstituted membranes. Saturable CrV binding to the desensitized nAChR yielded K_d values of 56.0 ± 15.5 nM (n=5) and 99.4 ± 15.5 nM (n=5) for PC/PA/Chol-nAChR and aso-nAChR, respectively (Fig. 3.5 and Table 3.2); these values are consistent with literature binding affinities (10 nM to 80 nM) (135-136). Note that both the high partition coefficient of CrV into lipid membranes and its strong propensity to interact with glass and plastic surfaces make it difficult to accurately determine free CrV concentrations in binding experiments. Although we used a detergent standard curve to estimate our free [CrV] (135, see Appendix A), our binding affinities differ slightly from those reported by others. The lack of precision in experimental K_d values for CrV binding, however, does not impact on our ability to accurately compare CrV binding to resting versus uncoupled nAChRs in parallel binding experiments.

Unlike with ethidium, we detect saturable binding to the resting nAChR stabilized by α-BTX. Binding was characterized by a K_d = 0.25 ± 0.01 μM for the resting aso-nAChR (see Appendix B**).** This value is higher than the K_{eq} value recorded by Lurtz & Pedersen (100 nM (135)) for CrV binding in the absence of added ligand (i.e. not in the presence of either Carb or α-BTX) where an equilibrium exists between resting and desensitized conformations, but initially favors the resting state. On the other hand, our value is lower than that reported by Fernandez Nievas et al. (~370 nM (137)), and Arias et al. (270 nM (136)). Our data is best compared to the data of Lurtz & Pedersen, as neither of the latter two authors use a detergent standard curve to estimate the free concentration of CrV. As expected, the K_{eq} value reported by Lurtz & Pedersen is in

Figure 3.5.

Binding of crystal violet to the membrane-reconstituted nAChR. The binding of CrV to 50 nM desensitized (pre-incubated with 500 μM Carb) (black squares, n=4) and resting (pre-incubated with 100 μM α-BTX) (closed circles, n=7) aso-nAChR fit with a one-site specific binding function with Hill slope (as in Figure 3). No binding was detected to the uncoupled PC-nAChR (open squares, n=5). Error bars are ± SEM.

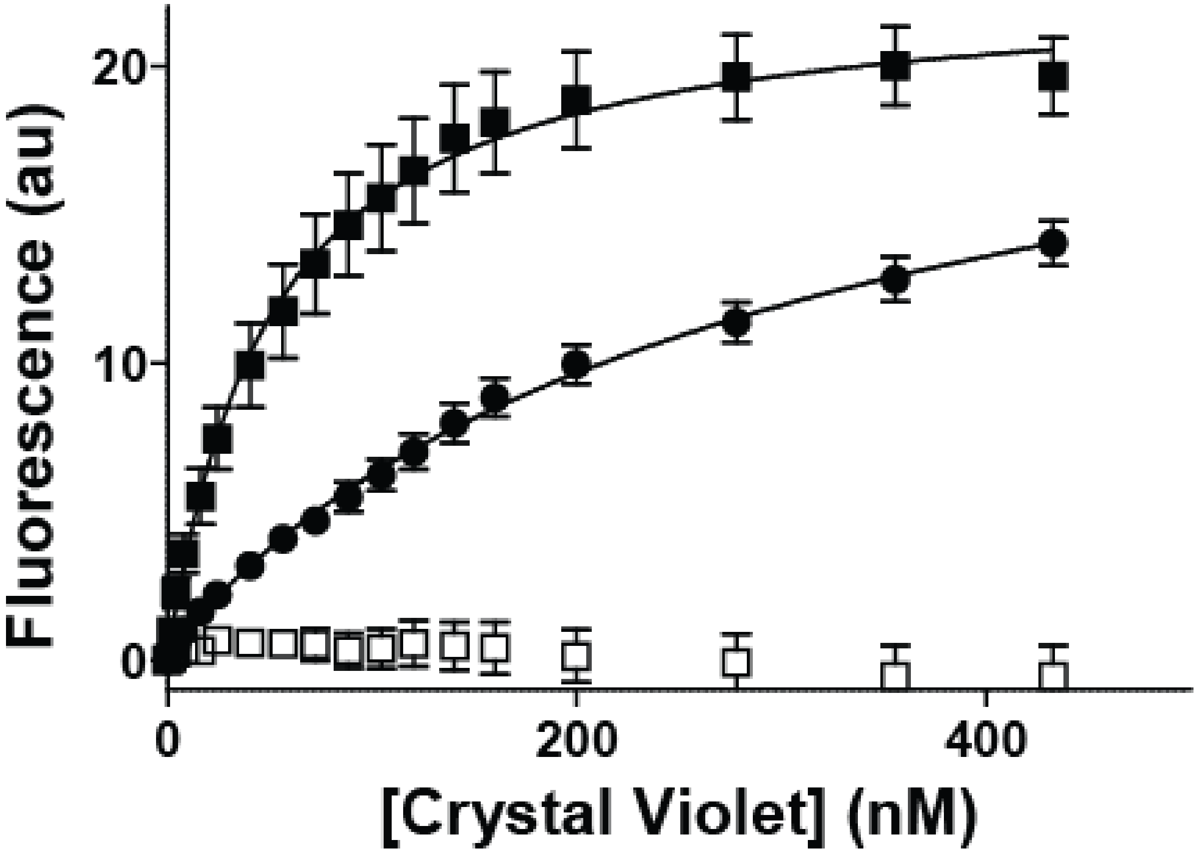
Fluorescence (au)
20
10
0
0
200
400
[Crystal Violet] (nM)

between that of our K_d values for the resting and desensitized states.

We considered the possibility that high CrV concentrations compete allosterically with α-BTX to shift the conformational equilibrium in favor of the desensitized state, and thus that our observed CrV binding to the resting state is actually due to a small population of nAChRs that shift into the desensitized state at high CrV concentrations. Several observations, however, suggest that this is not the case. First, if the CrV binding curve leads to a conformational switch from resting to desensitized states, then we would expect a sigmoidal binding curve. Such a sigmoidal binding curve is observed by Lurtz & Pedersen (135) upon titration of native nAChR membranes with CrV in the absence of added ligand (Carb or α-BTX), although they still fit this data assuming single site non-cooperative binding. Second, parallel binding experiments performed using the same reconstituted membranes in the presence of Carb (desensitized) versus α-BTX (resting) yield similar B_{max} values (Table 3.2) – a finding inconsistent with exclusive binding to only a *small* population of nAChRs that shift into the desensitized state. Finally, we recorded fluorescence spectra using nAChR membranes incubated with up to 600 fold molar excess of α-BTX to further stabilize the resting conformation and still detected a large component of CrV binding (data not shown). These findings support our assertion that the detected CrV binding in the presence of α-BTX is to the resting nAChR.

We performed parallel binding experiments to test whether CrV binds to the uncoupled PC-nAChR. At concentrations similar to those that saturate binding to the resting nAChR, we did not detect any CrV binding to the uncoupled state. These findings show clearly that the affinity of CrV for the uncoupled nAChR is well below that of both the resting and desensitized conformations. The absence of ethidium, CrV, and ^{3}H-TCP binding to the uncoupled nAChR show that the uncoupled TMD adopts a conformation distinct from the TMD conformation in the resting and desensitized states. The data indirectly supports the assertion that a constricted pore conformation is a characteristic of the uncoupled conformation.

5. Discussion

Although it has been known for decades that PC-nAChR adopts a conformation that is not responsive to agonist (74, 78), it was originally thought that the lack of response was due to the stabilization of a desensitized conformation. The subunit-labeling pattern of PC-nAChR with the hydrophobic photo-activatable chemical probe, ^{125}I-TID is similar to that of PC-PA/Chol-nAChR in the presence of Carb, thus suggesting a desensitized state (see below) (90, 138). The hypothesis that lipids modulate the resting-to-desensitized equilibrium is reasonable given that there is a natural equilibrium between these conformations in native membranes (roughly 80:20 resting:desensitized (98, 139)) - the energy difference between the two conformations is thus relatively small. In fact, a large proportion of desensitized nAChRs are favored in PC membranes containing phosphatidylserine (140). PC-nAChR, however, does not exhibit the high affinity binding for agonists expected of the desensitized state (94, 134). PC-nAChR also adopts a conformation that undergoes more extensive peptide N-^{1}H/N-^{2}H exchange than either the resting or desensitized nAChRs (94-95).

The uncoupled nAChR binds both agonists and channel-binding non-competitive antagonists with a lower affinity than the desensitized nAChR, consistent with both domains adopting resting state-like conformations. In this report, we characterized the binding of ACh and two fluorescent channel blockers, ethidium and CrV, to the uncoupled PC-nAChR in order to assess whether the ECD and TMD adopt conformations similar to the resting state. We show that the binding affinity of the uncoupled PC-nAChR for ACh is similar to that for the resting nAChR in native membranes (2.4 μM vs 0.8 μM, respectively) (98). In contrast, although we were able to characterize the binding of both ethidium and CrV to resting (+α-BTX) and desensitized (+Carb) conformations in two different "functional" membranes (asolectin and PC/PA/Chol), no binding of either ligand could be detected to the uncoupled PC-nAChR. The affinity of both ethidium and CrV for the pore of the uncoupled PC-nAChR is thus much lower than the affinities for either the resting or desensitized conformations. Our data thus provide definitive evidence that the channel pore of PC-nAChR adopts a conformation distinct from that of the resting and desensitized conformations. Furthermore, no binding of another channel pore blocker, ^{3}H-TCP, was detected in preliminary binding experiments (M. Blanton, personal communication). While binding affinities cannot be interpreted in terms of 3D structure, the absence of binding of all three probes could result from a constriction of the channel pore that restricts access to the non-competitive channel blocker site(s). A constricted channel pore is observed in crystal structures of the prokaryotic pLGIC ELIC (13), which coincidentally does not exhibit a change in pore diameter when crystallized with or without bound agonist (133, 108). A constricted channel pore may thus be a characteristic of the uncoupled conformation.

An altered conformation of the channel pore could explain the apparent discrepancy between ligand binding studies and the ^{125}I-TID photo-affinity labeling experiments noted above. Although ^{125}I-TID partitions into the lipid bilayer and weakly labels residues at the lipid-protein interface (132), it reacts strongly with pore-lining residues in the resting state, leading to relatively intense labeling of the γ and α subunits (91, 138). In contrast, ^{125}I-TID labeling of desensitized nAChRs is relatively weak, with a subunit-stoichiometric labelling pattern – i.e. labeling of the α, β, γ and δ subunits occurs with an intensity of roughly 2:1:1:1. The uncoupled PC-nAChR also exhibits relatively weak labeling with a 2:1:1:1 subunit labeling stoichiometry, thus suggesting a desensitized conformation. Alternatively, the labeling pattern of PC-nAChR could simply reflect an altered pore conformation that prevents pore binding of ^{125}I-TID, leaving only weak stoichiometric labeling at the lipid-protein interface. Unfortunately, we were unable to directly test this hypothesis because ^{125}I-TID is no longer commercially available, thus precluding the mapping of ^{125}I-TID labeling sites on the uncoupled nAChR. Although we synthesized non-radioactive TID for binding studies using calorimetric approaches, TID binding to nAChR membranes exhibits multiple components, (one additional component likely being the binding to the lipid bilayer itself) from which it is impossible to extract useful binding data (data not shown).

Originally, the crystal structure of ELIC in the absence of agonist suggested that the closed channel results from steric block of the pore (13), as opposed to the hydrophobic gate proposed for the nAChR (141). The pore diameter of another prokaryotic homolog, GLIC, in the open state is much larger than that of ELIC (142, 12), thus potentially highlighting gating motions between the two conformations. The pore diameter of GLIC, however, is similar to that of the closed nAChR, initially raising the question as to which pore diameters correspond to closed and/or open conformations. Subsequent crystal structures of GLIC in both closed and locally closed conformations (143, 30), as well as structures of other pLGICs (14-17, 31, 144) now confirm that gating results from more subtle movements of the pore lining α-helices than the conformational differences observed between ELIC and GLIC. Extrapolation of our data provides additional evidence that the crystallized ELIC is stabilized in a non-responsive uncoupled conformation, from which gating insight cannot be obtained.

The altered pore conformation in the uncoupled state suggests that effective ECD/TMD interactions are required for the pore-lining α-helices to adopt an orientation that is “poised” for channel gating, with agonist binding then triggering additional movements of the pore-lining α-helices to gate open the channel pore. Consistent with this finding, chimeras formed between the acetylcholine binding protein and the α7-nAChR TMD suggest that effective ECD/TMD interactions are required for the ECD to adopt an activatable resting-like conformation. The acetylcholine binding protein, however, likely adopts a desensitized conformation in the absence of effective ECD/TMD interactions (38). Studies with other chimeras are required to further explore how interactions at the ECD/TMD interface influence the conformations of both the ECD and TMD.

Elucidating the nature of the conformational changes associated with lipid-dependent uncoupling is essential for understanding lipid-nAChR interactions. Functionally uncoupled conformations are also observed when neuronal nAChRs are expressed in heterologous systems, and may play a role in nicotine addiction (114, 116). Thicker PC membranes promote transitions from uncoupled to coupled conformations. Transitions from uncoupled to coupled conformations could occur as the nAChR traffics from thinner internal to the thicker plasma membranes (89). Further efforts are required to test whether uncoupling plays a role in nAChR physiology.

Chapter 4

Pore pharmacology of membrane reconstituted nAChR

1. Rationale

As an extension of the work presented in the previous chapter, I had planned to characterize the binding of a variety of non-fluorescent non-competitive antagonists (NCAs) to the uncoupled PC-nAChR and both the resting and desensitized aso-nAChR. Local anesthetics are classical nAChR pore-blockers, and several classes of antidepressants have been found to occupy NCA sites in the nAChR pore (Fig. 4.1) (145-148). The constricted pore hypothesis predicts that they, like ethidium and CrV, will bind more weakly, if at all, to the uncoupled nAChR. The initial goal of the work was to characterize the binding of a variety of pore blockers to the resting, desensitized and uncoupled nAChR to indirectly test the constricted uncoupled pore hypothesis.

Because most channel blockers are not fluorescent and are not commercially available in a radiolabeled form, I had planned to directly measure their binding to the nAChR pore using isothermal titration calorimetry (ITC), which measures heat change upon binding. Calorimetric studies, however, require large sample quantities. To partially circumvent this limitation, I decided to first characterize binding to the desensitized and resting nAChR through competition binding experiments with ethidium bromide and crystal violet. Surprisingly, the initial competition studies revealed unexpected complexity in the interactions between the various channel blockers and the resting and desensitized conformations. These data are presented here in the context of what is currently known about nAChR pore pharmacology.

I was additionally able to characterize binding of the local anesthetic tetracaine to aso-nAChR stabilized in the resting conformation by α-BTX using ITC. ITC studies with reconstituted PC-nAChR, however, generated large amounts of noise that made it impossible to quantify binding and thus impossible for me to ultimately complete this aspect of my project.

Figure 4.1

Noncompetitive angatonists of the nAChR. The binding of ethidium and CrV was characterized in Chapter 3. Tetracaine, proadifen, dibucaine, procaine, and adiphenine are local anesthetics, and bupropion is an antidepressant. TID has previously been used as a hydrophobic probe.

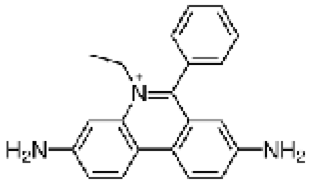

Ethidium

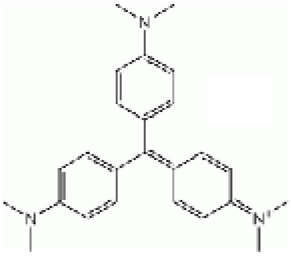

Crystal Violet

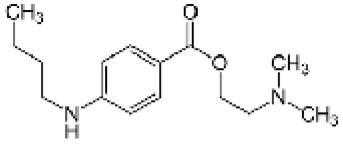

Tetracaine

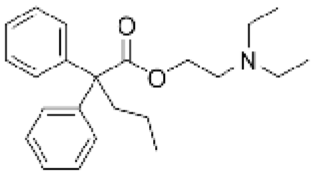

Proadifen

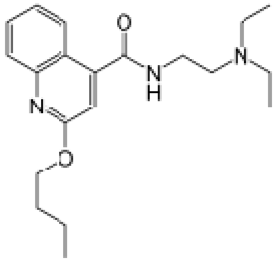

Dibucaine

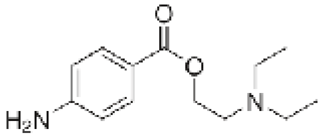

Procaine

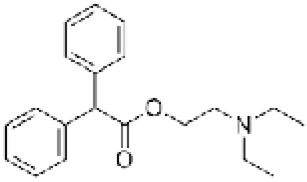

Adiphenine

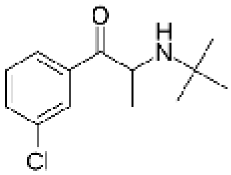

Bupropion

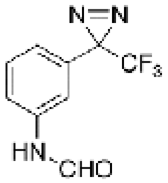

TID

2. METHODS

Preparation of reconstituted nAChR. The nAChR was affinity purified on a bromoacetylcholine column as described elsewhere (94). Briefly, crude membranes from *T. californica* electroplax tissue were solubilised in dialysis buffer (100 mM NaCl, 10 mM Tris-HCl, 0.1 mM EDTA, 0.02% (w/v) NaN_3, pH 7.6) for 1 hr at 4^oC, then centrifuged for 30 min at 87, 000g. The supernatant was applied to the bromoacetylcholine column. The bound nAChR was then washed with three column volumes each of 1.0% cholate dialysis buffer with: 1) 1.3 mM, 2) 3.2 mM, and 3) 1.05 mM lipid. The receptor was eluted with 10mM carbamylcholine in 250 mM NaCl, 0.1 mM EDTA, 0.02% (w/v) NaN_3, 10 mM Tris-HCL buffer, pH 7.6, with 1.05 mM lipid and 1.0% cholate. Fractions were pooled to achieve a final $A_{280} = 1.0$, yielding a lipid/protein ratio of ~500:1 (mol/mol). The pooled eluate was dialyzed against 5x 2L of fresh dialysis buffer, then pelleted by centrifugation. Samples were stored at -80^oC when not in use.

*Fluorescence spectroscopy***.** Spectra were acquired at 22.5^oC on a Cary Eclipse fluorescence spectrometer (Agilent Technologies). Resting and desensitized samples were stabilized by preincubating 20 nM (for CrV experiments) or 50 nM aso-nAChR (for ethidium experiments) with a 20-fold molar excess α-BTX or 1 mM carbamylcholine, respectively, for at least 30 min. Desensitized or resting samples were mixed with 0.3 μM ethidium or 80 nM or 240 nM CrV until stable fluorescence was achieved. Nonfluorescent NCAs were then titrated into the mix up to the concentrations indicated. Measurements were made in quartz glass fluorescence cuvettes (10 mm light path; Hellma (Canada)) with Ringer buffer solution (250 mM NaCl, 5 mM KCl, 2 mM $MgCl_2$, 5 mM Na_2HPO_4, 0.02% w/v NaN_3, pH 7.0). Data were collected with excitation/emission wavelengths set to 530 nm/590 nm and excitation/emission slits at ±5/20nm for ethidium and 590 nm/630 nm with slits ±10/20 nm for CrV.

For competition experiments between CrV and ethidium, CrV was titrated into 50 nM aso-nAChR, 1 mM carb, and 0.35 μM ethidium in Ringer buffer. Excitation/emission wavelengths were 490/700 nm and slits were ±10/20 nm. Where possible, data was fitted with a one-site competition function (logEC50 = log (10^log K_i*(1+HotNM/HotK_dNM)); Y = Bottom + (Top-Bottom)/(1+10^(X-LogEC50))) or a two-site competition function (logEC50Lo = log (10^log K_iLo*(1+HotNM/HotKdNMLo)); logEC50Hi = log (10^log K_iHi*(1+HotNM/ HotK_dNMHi))). K_i's reported are obtained from EC_{50} values by Cheng-Prusoff correction.

Isothermal calorimetry. ITC experiments were performed in the Gariepy lab (Sunnybrook Research Institute, Toronto, ON) with the help of Dr. Marzena Cydzik on a MicroCal iTC200 system (GE Healthcare, Little Chalfont, UK). Traces were obtained using 10 μM or 20 μM aso-nAChR in the presence of an equivalent molar concentration of α-BTX or excess Carb between 20^{o}C and 30^{o}C. Stirring speed was set to 750 rpm.

3. RESULTS

Local anesthetics occupy more than one pore site. I first tested the ability of several local anesthetics to displace ethidium, whose binding has been well characterized in both native and reconstituted membranes, from the pore of the desensitized nAChR. Briefly, local anesthetic was titrated into samples of aso-nAChR equilibrated with both 1 mM Carb and 0.3 μM ethidium (~K_d for the desensitized conformation). The addition of anesthetic displaces ethidium into solution, reducing the measurable fluorescence intensity.

I chose to initially test the binding of five local anesthetics (tetracaine, proadifen, dibucaine, procaine, and adiphenine) that are readily available and in use clinically. In each case, titration of the local anesthetic into a solution containing the desensitized nAChR and ethidium led to a displacement curve that could be well fit with a one-site competition binding function (Fig. 4.2). Of the compounds tested, the binding of tetracaine and proadifen have previously been characterized for the desensitized nAChR in native membranes. Both tetracaine and proadifen displaced ethidium with K_i's similar to their previously measured K_d's (47 ± 0.3 μM versus 30 μM and 1 ± 0.4 μM versus 3.2 μM, respectively; Table 4.1) (149-153). Tetracaine and proadifen therefore compete with ethidium for the same site in the pore. Given the similar binding pattern observed for all the local anesthetics, dibucaine, procaine, and adiphenine likely do the same. This finding additionally shows that the pharmacological properties of nAChR are comparable in native and reconstituted asolectin membranes, so that the binding affinities measured here for dibucaine, procaine, and adiphenine are likely similar to those for native-nAChR.

The ethidium experiments suggested that I would be able to indirectly measure affinities for unlabeled pore-blockers using competition binding. However, ethidium binds resting nAChR with very low affinity and cannot be used to assess binding to the resting pore. I therefore continued the competition studies using CrV as the bound ligand. As established in Chapter 3, CrV binds both the desensitized and resting nAChR with nanomolar affinity.

I first examined the binding of the same local anesthetics to the desensitized nAChR expecting to see similar K_i's and binding patterns as for the competition experiments with ethidium. Strikingly, however, the local anesthetics showed dramatically different behaviour in competition with CrV from both a qualitative and quantitative perspective. Note that at high concentrations of titrant (>1 mM), analysis of fluorescence data is complicated by off-target effects such as interactions with the lipid membrane, binding to non-pore sites, etc. The following analyses therefore focus on the trends observed at more relevant concentrations.

Figure 4.2

Competition binding of local anesthetics to desensitized nAChR against ethidium bromide. Tetracaine (solid circles), proadifen (solid upward triangles), dibucaine (empty downward triangles), procaine (solid diamonds), and adiphenine (open squares) were titrated into solutions of 50nM aso-nAChR, 1mM carbamylcholine, and 0.35 μM ethidium. Data was fit with a one-site competition binding function.

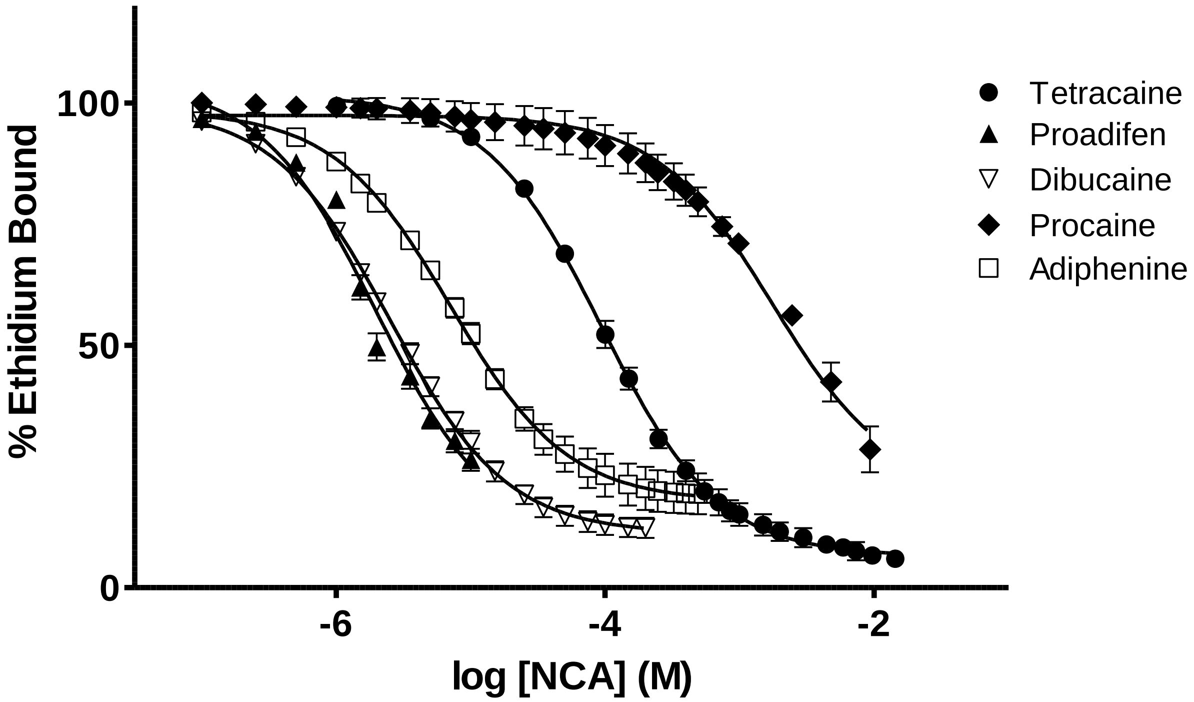
% Ethidium Bound
100
50
0
-6
-4
-2
log [NCA] (M)
● Tetracaine
▲ Proadifen
▽ Dibucaine
◆ Procaine
□ Adiphenine

As in the competition experiments with ethidium, the local anesthetics tetracaine, proadifen and procaine all displaced CrV in a binding curve shapes consistent with one-site competition (Fig. 4.3). However, the competition curves were all right-shifted about 10-fold compared to the ethidium data (Table 4.1), suggesting an allosteric inhibitory mechanism. The observed right-shift in K_i is also true for adiphenine, though confounding factors at high adiphenine concentrations made it impossible to fit the data well. These data show that binding of the local anesthetics to the 'ethidium' site in the pore does not directly displace CrV, and suggest that an additional binding site(s) is involved. This finding is surprising given that both ethidium and CrV competitively displace the pore blocker, phencyclidine (99, 135). One possible interpretation is that the CrV binding site does not completely overlap with the ethidium site in the desensitized nAChR pore and that the local anesthetics actually bind to two distinct sites – a high affinity site that overlaps the ethidium site, and a lower affinity site where binding ultimately leads to CrV displacement (either competitively or allosterically). Another possibility is that the local anesthetics bind to the ethidium site with high affinity, but alter the pore conformation to displace CrV. In the latter scenario, the measured K_i will depend on both binding affinity and the efficiency of the coupling between binding and allosteric transitions – thus accounting for the higher Ki values observed in the CrV competition experiments.

Significantly, dibucaine displacement of CrV fluorescence results in a biphasic curve, which was fitted with a two-site competition function. The dibucaine displacement data suggest that local anesthetics bind to two sites on the nAChR – one with relatively high affinity ($K_i = 1.4 \pm 0.3$ μM) and one with relatively low affinity ($K_i = 940 \pm 60$ μM). Given that previous binding data for CrV are all suggestive of simple one-site binding, the biphasic competition data likely reflects allosteric inhibition of CrV by dibucaine. If dibucaine competes directly with CrV,

Figure 4.3

Competition binding of local anesthetics to desensitized nAChR against CrV. Tetracaine (solid circles), proadifen (solid upward triangles), and procaine (solid diamonds) displaced CrV from desensitized nAChR in a pattern consistent with one-site competition binding. Dibucaine binding (empty downward triangles) was fit with a two-site competition function. Adiphenine is shown as (open squares). Titrations were performed with 20nM aso-nAChR, 1mM carbamylcholine, and 80 nM CrV.

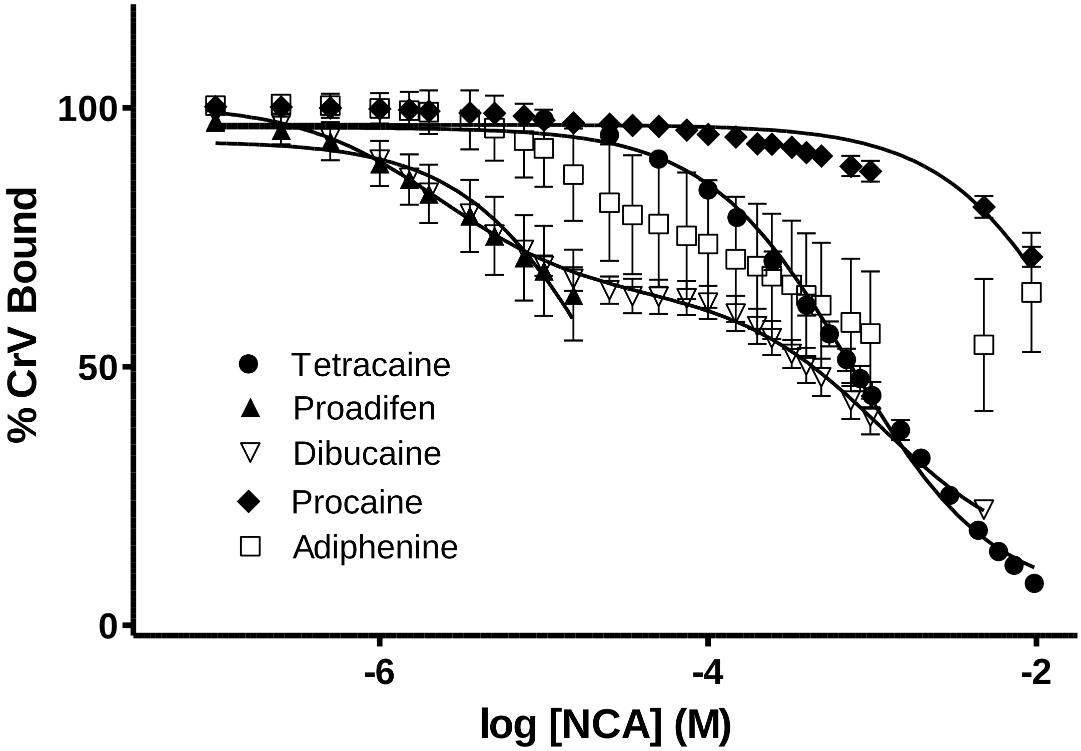
% CrV Bound
100
50
0
-6
-4
-2
log [NCA] (M)
● Tetracaine
▲ Proadifen
▽ Dibucaine
◆ Procaine
□ Adiphenine

Table 1. Competition binding of NCAs to desensitized and resting nAChR.

Compound	K_i (µM)			$K_d/K_{eq}/IC_{50}$ (µM)	
	EtBr – D	**CrV – D**	**CrV – R**	**Literature D**	**Literature R**
Tetracaine (150)	47 ± 0.3	440 ± 18	--	30	0.5
Bupropion (66, 152)	8.3 ± 0.4	180 ± 21	--	1-10[a]	3-20[a]
Proadifen (151, 153)	1 ± 0.4	13 ± 3	107 ± 800	3	20[b]
Dibucaine (154)	1.3 ± 0.1	1.4 ± 0.3; 940 ± 60	3.8 ± 2 (mM)	60[c]	60[c]
Procaine (153)	880 ± 150	11.5 ± 0.17 (mM)	4 ± 1.5 (mM)	5 mM	1 mM[b]
Adiphenine (154)	3.5 ± 0.33	--	--	5[c]	5[c]
TID (155-156)	--	--	--	~4	~4

[a] Reported values are IC_{50}'s

[b] Measured to unliganded nAChR, as opposed to stabilized by α-BTX

[c] Value reported is a K_{eq} value

*Binding determined through fit with one- or two-site competitive binding function.

however, the data would require that each of these sites overlaps with a distinct binding site for CrV, and that CrV must therefore also occupy two distinct sites. One possibility is that CrV binds to two nearby sites in the desensitized nAChR pore each with a similar affinity. In this interpretation, dibucaine is uniquely positioned such that binding at the high affinity site overlaps one CrV site, and binding at the low affinity site overlaps the other.

I next carried out competition experiments with the local anesthetics by titrating them into samples of aso-nAChR stabilized in the resting conformation with α-BTX and equilibrated with 240 nM CrV (K_d for the resting state). These experiments reveal another layer of complexity in the binding behaviour of pore-blocking compounds, which is not entirely unexpected as the binding sites of many compounds are known to be conformation-dependent (see Discussion). Previous studies have concluded that all local anesthetics used in these competition studies are able to inhibit ion flux or compete with a pore-bound compound in the resting conformation, and are thus able to bind to the resting nAChR pore. Interestingly, none of the competition binding experiments with the local anesthetics detected displacement of CrV from the resting conformation near the expected K_d values for the resting conformation (Fig. 4.4, Table 4.1). For example, tetracaine, which preferentially binds the resting conformation with high affinity (K_d ~0.5 μM) (150), only begins to displace CrV from the resting nAChR pore at around 100 μM. These data suggest that, like in the desensitized conformation, local anesthetics bind an additional low-affinity pore site in the resting conformation that overlaps the CrV site.

Notably, the addition of increasing amounts of adiphenine leads to changing effects on CrV fluorescence. Disregarding non-regular behaviour at high concentrations of adiphenine, the initial increase in CrV fluorescence may be due to interactions of adiphenine with CrV in solution or allosteric effects upon adiphenine binding to the nAChR that enhance CrV binding or fluorescence.

Figure 4.4

Competition binding of local anesthetics to resting nAChR against CrV. Proadifen (solid upward triangles), dibucaine (empty downward triangles), and procaine (solid diamonds) displaced CrV from resting nAChR in a pattern consistent with one-site competition binding. Tetracaine (solid circles) and adiphenine (open squares) displaced CrV, but could not be well fit. Titrations were performed with 20nM aso-nAChR, 1mM carbamylcholine, and 240 nM CrV

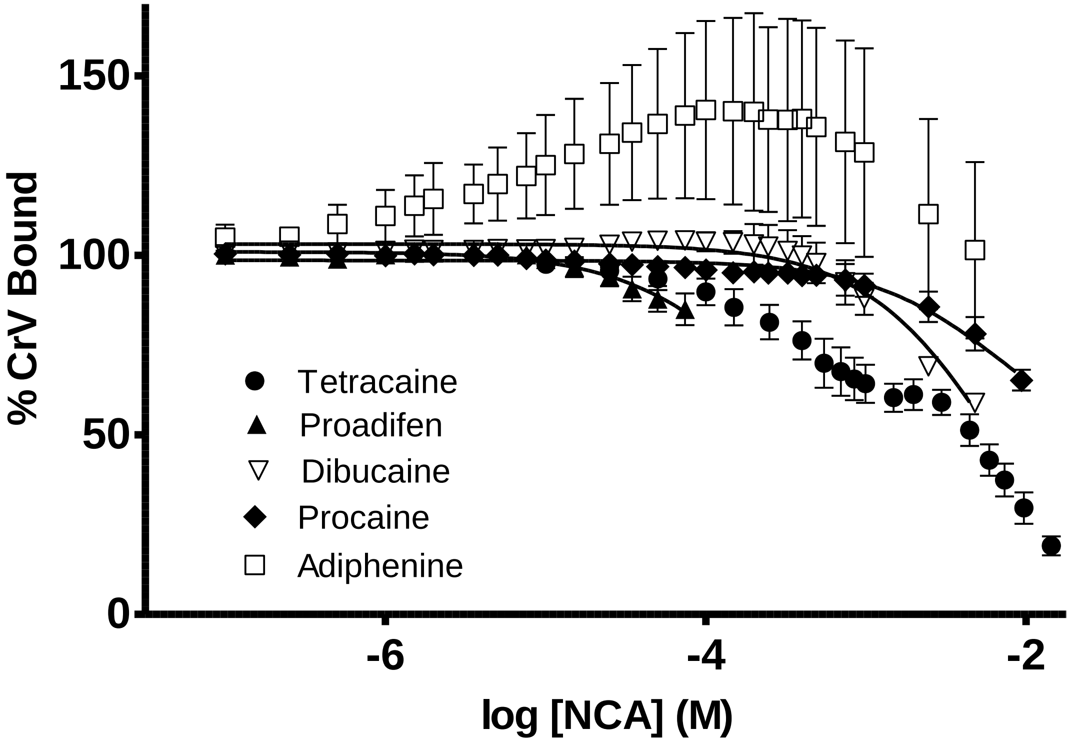

150
100
50
0
% CrV Bound
-6
-4
-2
log [NCA] (M)
● Tetracaine
▲ Proadifen
▽ Dibucaine
◆ Procaine
□ Adiphenine

It is unlikely that the increase in CrV fluorescence is due to stabilization of the desensitized state, since the aso-nAChR sample has been pre-equilibrated with α-BTX to stabilize the resting state, and adiphenine has been shown to decrease the receptor's affinity for ligand (154).

Displacement of ethidium and CrV by an antidepressant. The nAChR is also known to bind several classes of antidepressant drugs in its pore, including serotonin selective reuptake inhibitors, tricyclic antidepressants, and others (146-147, 157). Here, I tested the binding of bupropion, a norepinephrine selective reuptake inhibitor whose binding site in the nAChR pore has been elucidated through photoaffinity labeling studies and whose binding affinities have been previously characterized.

I first tested the ability of bupropion to competitively displace both ethidium and CrV from the desensitized nAChR. In these experiments, bupropion exhibited binding characteristics similar to those observed for the local anesthetics. Specifically, bupropion displaced ethidium from the desensitized pore with a $K_i = 8.3 \pm 0.4$ μM, similar to its measured binding affinity of 1-10 μM (Fig. 4.5, Table 4.1) (66, 152), while buproprion displaced CrV binding with a K_i that is roughly 20-fold higher than its K_I for ethidium displacement. Consistent with the local anesthetic data, the bupropion competition curves suggest that ethidium and CrV bind to distinct, although likely overlapping sites, and that bupropion binds to two sites in the pore – a higher affinity site that overlaps with the site for ethidium and a lower affinity site that overlaps with the site for CrV.

In contrast to the local anesthetic competition curves, however, bupropion was unable to displace CrV binding to the resting nAChR. Previous studies have shown that bupropion binds to the pore of the resting-nAChR and competes with ^{3}H-TCP with a $K_i \sim 5\mu M$ (158). These data therefore indicate that bupropion binds a site in the resting nAChR that neither overlaps nor is

Figure 4.5

Competition binding of buproprion. Bupropion displacement of ethidium from desensitized nAChR (solid circles) and of CrV to desensitized nAChR (open circles) were fit with one-site competition functions. Displacement of CrV from resting nAChR (solid diamonds) was negligible.

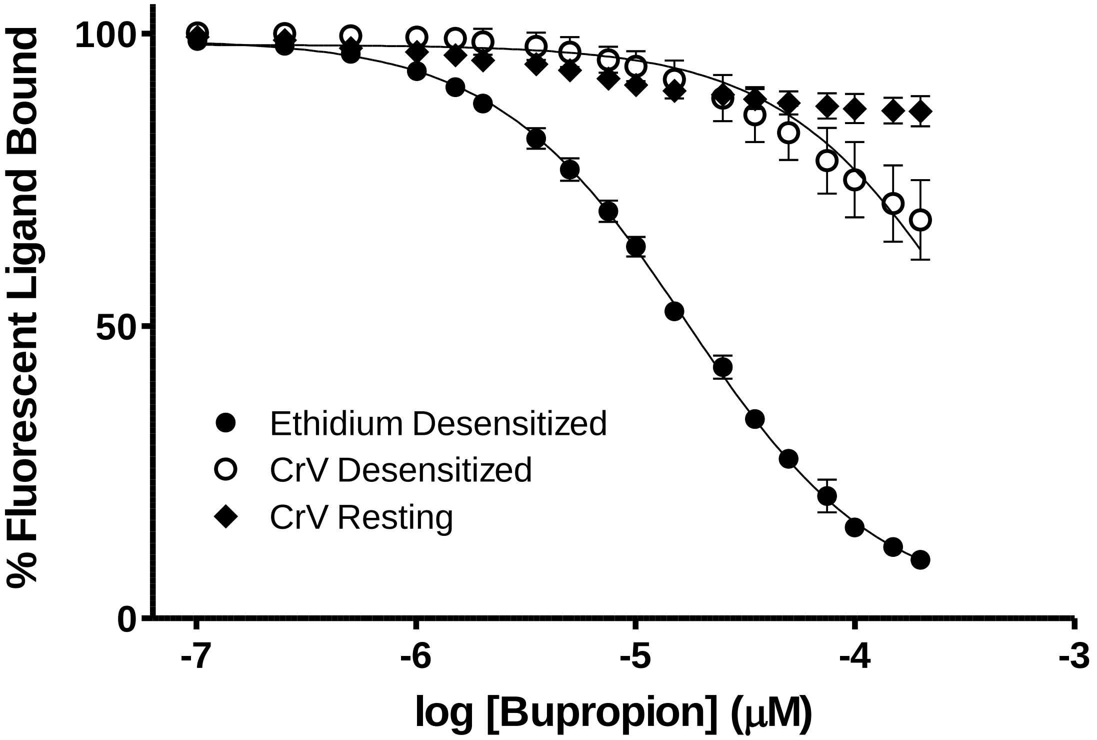

% Fluorescent Ligand Bound
100
50
0
-7
-6
-5
-4
-3
log [Bupropion] (μM)
● Ethidium Desensitized
○ CrV Desensitized
◆ CrV Resting

allosterically linked to the CrV site. In light of data showing that CrV is able to compete with ^{3}H-PCP in the resting state (135), the simplest interpretation of these results is that PCP/TCP binds a site in between the bupropion and CrV sites with significant overlap with both.

TID does not compete for either the ethidium or the CrV binding sites. The small hydrophobic probe ^{125}I-TID has previously been used to photoaffinity label lipid exposed residues of the nAChR. TID is also known to bind to the desensitized and resting pores with similar affinity ($K_d \sim 4$ μM), and photolabeling studies have mapped the pore-residues that contribute to its binding site in both resting and desensitized conformations (155-156). In the context of the constricted pore hypothesis discussed in Chapter 3 and the role played by ^{125}I-TID in elucidating the conformation of the uncoupled PC-nAChR, an initial important goal was to compare the binding affinity of TID for the resting and desensitized conformations to that for the uncoupled conformation.

In contrast to the competition binding experiments observed with both the local anesthetics and the anti-depressant, bupropion, no displacement of ethidium was observed at TID concentrations up to 100 μM, a concentration close to 100-fold above the measured Kd for ethidium binding to the desensitized pore (Fig. 4.6). Furthermore, even higher TID concentrations led to minimal ethidium displacement. The data show clearly that TID does not compete for the ethidium site. TID was additionally unable to compete with CrV binding in either the desensitized or resting conformations.

Ethidium and CrV bind desensitized nAChR at different but overlapping loci. Ethidium and CrV are both able to competitively displace ^{3}H-PCP or its close analogue ^{3}H-TCP, and so have been presumed to share the same binding site (99, 135). However, the data I have presented thus

Figure 4.6

Competition binding of TID. TID caused an initial increase in ethidium fluorescence in the desensitized conformation (closed circles), and then decrease at higher concentrations. Increasing TID concentrations has little effect on CrV fluorescence both in the desensitized (open circles) and resting conformations (solid diamonds).

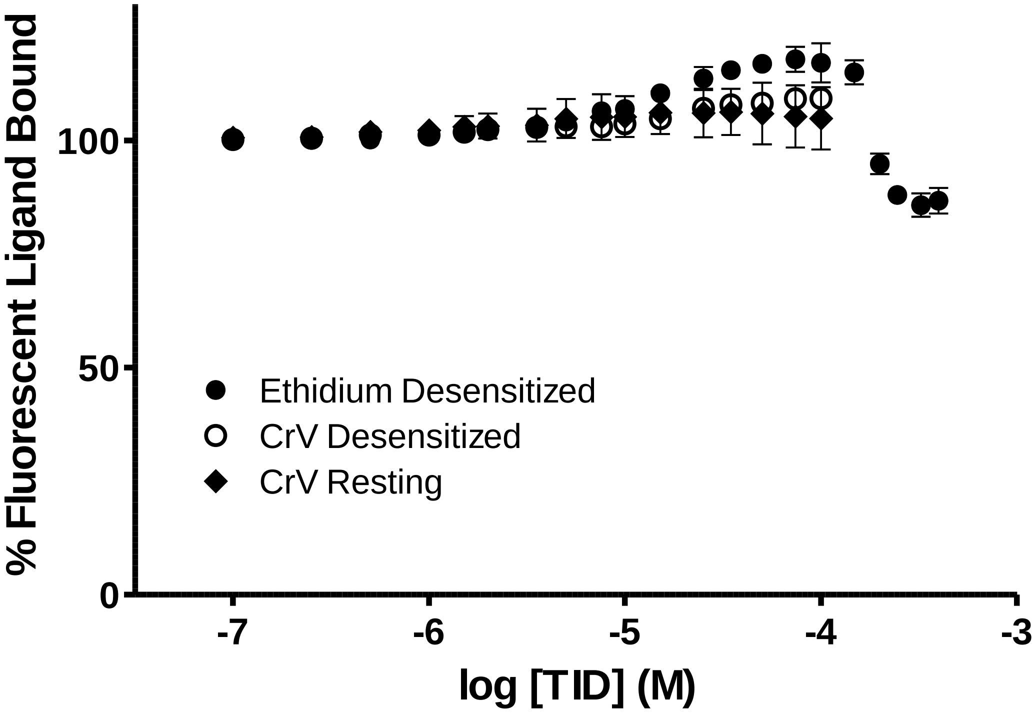
% Fluorescent Ligand Bound
100
50
0
-7
-6
-5
-4
-3
log [TID] (M)
● Ethidium Desensitized
○ CrV Desensitized
◆ CrV Resting

far suggest that they bind different sites in the pore. To definitively test whether ethidium and CrV share a binding site, I examined whether CrV could directly compete with ethidium for binding to the channel pore. Note that both ethidium and CrV are fluorescent compounds, which complicates the analysis of binding studies using fluorescence as a reporter. I designed my experiment as follows to circumvent potential problems arising from overlapping fluorescence signals. First, because ethidium fluoresces more strongly both in solution and when bound to the nAChR than CrV in solution or bound to the nAChR, I used the more weakly fluorescent compound, CrV, to displace bound ethidium. I next chose excitation and emission wavelengths (490 nm and 700 nm, respectively) that maximized the fluorescence of bound ethidium and minimized the fluorescence of both free and bound CrV. With these excitation/emission wavelengths, strong fluorescence due to bound ethidium (the excitation and emission maxima for bound ethidium are 530 nm and 600 nm, respectively (99)) could be detected. In contrast, little or no fluorescence due to CrV either bound or in solution could be detected (CrV excitation and emission maxima are 600 nm and 630 nm, respectively (135)). The excitation/emission wavelengths were chosen after the performance of a screening test, which showed that 490/700 nm gave the highest ratio of fluorescence intensity from bound ethidium versus free or bound CrV (>> 10:1). In other words, the addition of CrV under these conditions contributes negligible fluorescence intensity, thus allowing me to test for the CrV-induced displacement of bound ethidium.

To measure competitive binding, I incubated aso-nAChR with roughly 0.3 μM ethidium in the presence of Carb to stabilize the desensitized state. I then added increasing amounts of CrV and measured the ability of the CrV to displace bound ethidium by quantifying decreasing ethidium fluorescence. At concentrations of CrV up to 100 nM – a concentration just above the measured K_d for CrV binding to the desensitized nAChR pore (K_d = 80 nM), there was no detectable change in ethidium fluorescence (Fig. 4.7). In fact, even after addition of CrV up to concentrations of 10 μM (100-fold higher than the Kd), only a small drop in ethidium fluorescence of ~20% was observed. The data suggest strongly that while both the ethidium and CrV sites overlap with the binding site for phencyclidine (99, 135), the two sites are distinct.

Calorimetric measurement of NCA binding to nAChR. As noted above, my initial goal was to compare the binding of a number of channel blockers to the nAChR in the resting, desensitized and uncoupled conformations. I characterized binding to the resting and desensitized nAChR using the competition studies with ethidium and CrV, as described above. In parallel, I attempted to measure binding of these same compounds to the uncoupled PC-nAChR using ITC. As a positive control, I first attempted to characterize the binding of tetracaine to the resting aso-nAChR (incubated with α-BTX). The addition of tetracaine led to binding isotherms that returned K_d's in the range of 0.5 – 2.5 μM (n = 6), similar to the previously reported K_d = 0.5 μM (Fig. 4.8) (150). This is much higher-affinity binding than what was seen in the competition experiments with CrV, suggesting that these two sets of experiments measure binding to two different sites. Notably, the ITC experiments reported number of sites (N) nearing 1 for the interaction, suggesting one-site pore binding. This is to be expected, as tetracaine was only titrated into the ITC experiments up to a maximal concentration of ~100 μM, below the Ki for interaction at the low affinity site (see Fig. 4.4). Note that in the figure, the heat of binding, ΔH, is quantified as the area under the injection peak and decreases with each consecutive injection, indicating saturation of binding. The similar K_d's obtained by ITC and as previously reported in the literature suggest that ITC is a valid technique for the study of binding to reconstituted nAChR samples.

I also focused considerable effort on characterizing the binding of TID to nAChR using ITC because TID photoffinity labeling experiments played a crucial role in the initial

Figure 4.7

Competition binding of CrV to desensitized nAChR against ethidium bromide. Crystal violet was titrated into 50nM aso-nAChR, 1mM carb, and 0.35uM EtBr. The Kd of CrV in the D state is 80nM, which corresponds on this log scale to -7.1. Conditions were excitation at 490nm, emission at 700nm, and slits at 10 and 20nm.

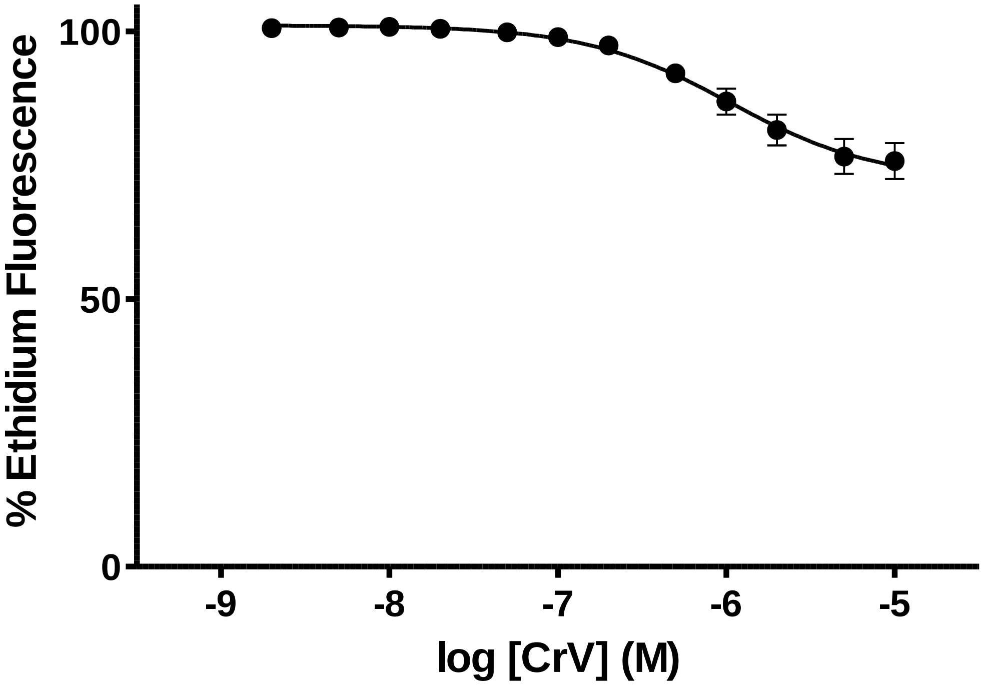
% Ethidium Fluorescence
100
50
0
-9
-8
-7
-6
-5
log [CrV] (M)

Figure 4.8

Tetracaine binding to resting state nAChR. *Top*: A raw ITC trace with corrected baseline. Downward peaks represent exothermic heats of binding upon injection of a small amount of tetracaine. *Bottom*: Binding isotherm derived from integration of the area under the injection peaks. The fit, measured as K_a, and number of sites N are reported in the inset.

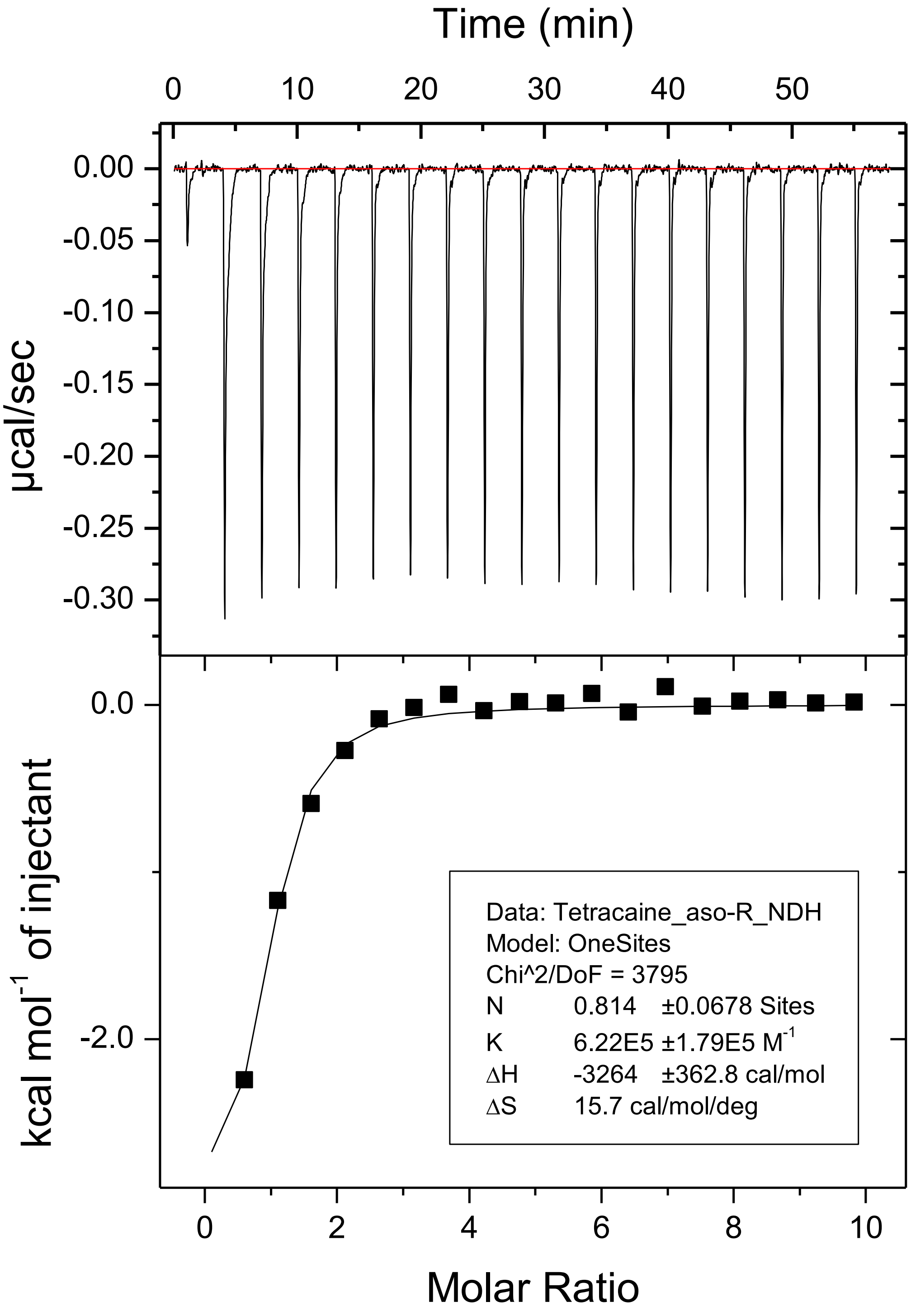
Time (min)
0
10
20
30
40
50
0.00
-0.05
-0.10
-0.15
-0.20
-0.25
-0.30
µcal/sec
0.0
-2.0
kcal mol^{-1} of injectant
Data: Tetracaine_aso-R_NDH
Model: OneSites
Chi^2/DoF = 3795
N 0.814 ±0.0678 Sites
K 6.22E5 ±1.79E5 M^{-1}
ΔH -3264 ±362.8 cal/mol
ΔS 15.7 cal/mol/deg
0
2
4
6
8
10
Molar Ratio

characterization of the uncoupled nAChR (see Chapter 3). Specifically, the photolabeling pattern of the uncoupled PC-nAChR is distinct from that of the resting state, and is similar to that of the desensitized nAChR even though PC-nAChR does not exhibit the high ethidium and ACh binding affinities expected of the desensitized nAChR (84). Weaker labeling in the desensitized state may correspond to labeling primarily of residues at the lipid-protein interface, as opposed to residues in the channel pore. We hypothesized that the channel pore in the uncoupled PC-nAChR is constricted, thus leading to only labeling of the periphery of the protein as in the desensitized state.

To test this hypothesis, I needed to determine whether I could detect binding of TID to the pore of the uncoupled PC-nAChR. Unfortunately, control binding experiments of TID to resting aso-nAChR stabilized with α-BTX revealed multi-component peaks, likely due to binding events to the pore, residues at the lipid-protein interface, as well as TID partitioning into the lipid membrane (Fig. 4.9). It was not possible to isolate and quantify the component of each peak due to pore-binding, so assessment of TID binding to the nAChR pore was ultimately not possible.

I next attempted to assess the binding of NCAs to the uncoupled nAChR, as low affinity binding would still provide support for the constricted pore hypothesis. However, PC-nAChR samples generated large amounts of noise in the baseline, making injection peaks difficult to identify. Data from binding to PC-nAChR could not be quantified to yield binding isotherms, and I was thus unable to complete this portion of my project.

4. DISCUSSION

In the context of the constricted pore hypothesis discussed in Chapter 3, I initially set out to compare the binding affinity of pore-blocking compounds to the uncoupled conformation

Figure 4.9

TID binding to resting aso-nAChR. A raw ITC trace of TID injection into a sample of aso-nAChR incubated with α-BTX. Upward peaks represent endothermic events, and downward peaks exothermic events. Each peak corresponds to one injection.

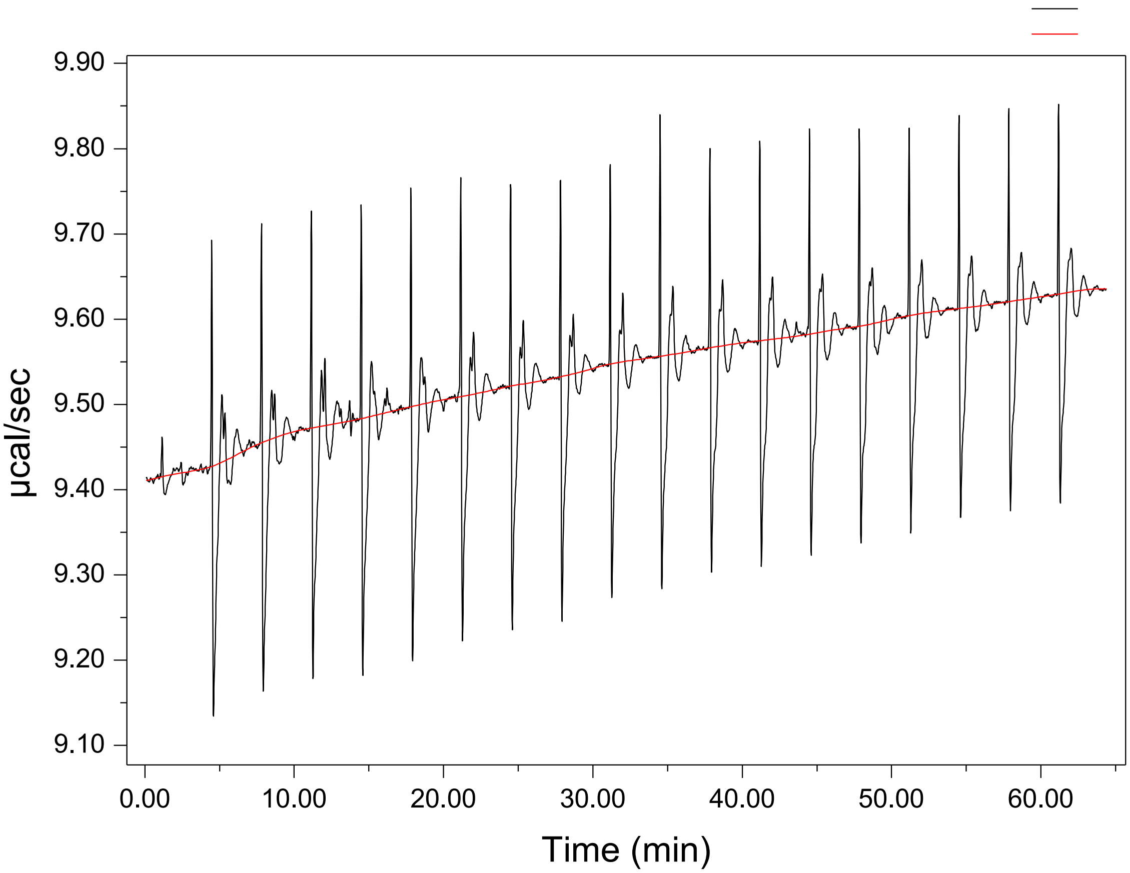
9.90
9.80
9.70
9.60
9.50
9.40
9.30
9.20
9.10
µcal/sec
0.00
10.00
20.00
30.00
40.00
50.00
60.00
Time (min)

relative to the desensitized and resting conformations using ITC. I was able to characterize the binding of tetracaine to resting aso-nAChR using this technique in preliminary experiments. Previous work from other labs have used ITC to characterize binding to detergent-solubilized pLGICs, but this is the first report of ITC being used to successfully measure the binding of a ligand to a membrane-reconstituted pLGIC (159). Despite this success, however, PC-nAChR was not amenable to binding studies using ITC. PC-nAChR generated significant noise in the absence of added ligand and even stirring, compared to a clean baseline from aso-nAChR. As anionic lipids and cholesterol have been shown to increase the ordering of lipid membranes (84), it is likely that the PC membrane lacking these lipids is more disordered and undergoes random movements of individual lipid molecules that result in small amounts of heat being continuously generated.

In parallel, I also characterized the binding of a number of NCAs to the nAChR pore using competition with both ethidium and CrV. NCA binding to the nAChR pore is generally framed in the context of its ability to compete with two classes of pore-blockers: the dissociative anesthetics phencyclidine (PCP) and its close analogue tenocyclidine (TCP), and barbiturates. The PCP and barbiturate loci overlap in the desensitized conformation, but not the resting conformation.

In desensitized nAChR, PCP competes directly with the ethidium analogue ^{3}H-ethidium diazide, which labels residues at positions 9’ and 10’ on the α subunit M2, as well as unidentified residues on the M1 and M2 of the δ subunit (Fig. 4.10) (160). A recent photolabeling study using the barbiturate analogue 5-allyl-1-methyl-5-(*m*-trifluoromethyldiazirinylphenyl)barbituric acid (^{3}H-*R*-*m*TFD-MPAB) covalently labels pore-lining residues from 2’ to 17’, with residues 6’ to 13’ being most strongly labeled (161). The labeled residues encompass the PCP site, which is consistent with competition studies that show barbiturates are able to displace ^{3}H-TCP from the desensitized nAChR pore (145).

Figure 4.10

Model of NCA binding sites in the nAChR pore. Binding sites of PCP/ethidium/high affinity local anesthetics (red), barbiturates (blue), tetracaine (grey), TID (yellow), and bupropion (purple) are depicted against the *Torpedo* nAChR TMD (PDB code 2BG9) in both the desensitized (A) and resting (B) conformations. Putative location of CrV/low affinity local anesthetic binding site shown in (green). One subunit has been omitted, and one subunit is shown as a cartoon for clarity; Dashed lines and numbering to the right indicate the level of pore-lining residues in M2.

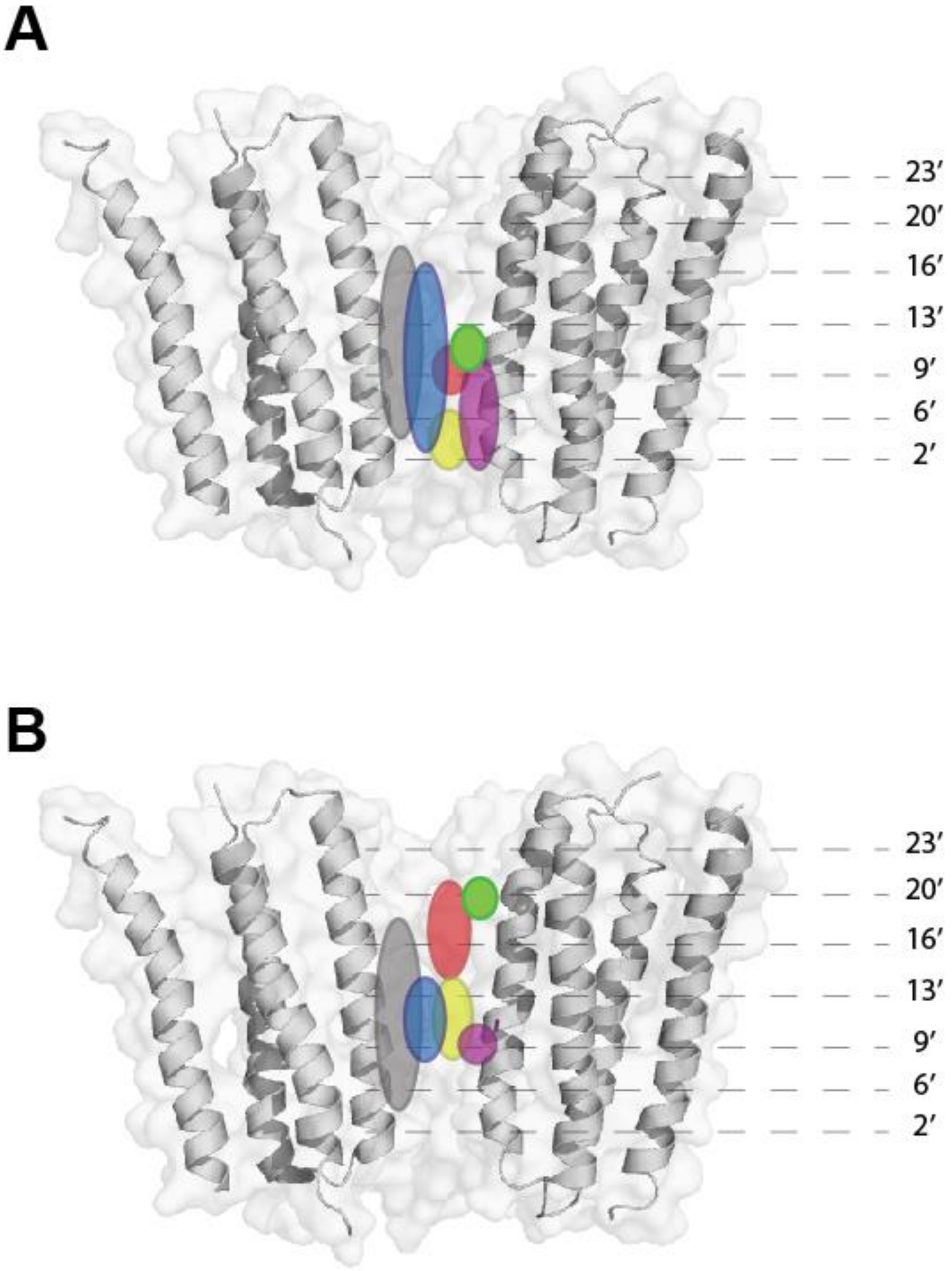
A
23′
20′
16′
13′
9′
6′
2′
B
23′
20′
16′
13′
9′
6′
2′

In contrast to the desensitized state, barbiturate binding to the resting nAChR does not overlap with the PCP site. Barbiturates efficiently inhibit the binding of ^{125}I-TID, which labels residues at the 9’ to 13’ positions, indicating that they bind at an overlapping site (145, 155). PCP, however, allosterically potentiates ^{125}I-TID binding (162), and competition studies between ^{3}H-TCP and the barbiturate amobarbital show no direct competition (163). Subsequent studies by Arias et al. using a series of adamantine derivatives to inhibit ^{3}H-TCP binding revealed that the PCP binding site in the resting nAChR pore imposed few structural restrictions on binding, leading them to propose that PCP binds above the level of 13’, near to the 20’ position where the pore vestibule is widest (164). This is supported by molecular modeling with closed, unliganded nAChR (presumed resting conformation), which suggests that CrV, which competes with PCP in the resting conformation, also bind near 20’ (136).

Early binding experiments in the 1980s and 1990s demonstrated that ethidium and CrV both compete with ^{3}H-PCP/^{3}H-TCP with K_i’s nearing their K_d’s for both desensitized and resting conformations (99, 135). The simplest interpretation of this data is that both ethidium and CrV bind at sites that overlap with the binding site for PCP. If this is the case, then we would expect that the compounds that competitively displaced ethidium would also displace CrV with similar efficacy. Contrary to this, my data show that for every compound that displayed competitive binding with ethidium, much higher concentrations were necessary to displace an equivalent proportion of CrV fluorescence. My data show that there are at least two pore sites for the binding of local anesthetics and bupropion, and that ethidium and CrV binding overlap with the high and low affinity sites, respectively. The lack of direct competition binding between ethidium and CrV further supports the idea that they do not compete for the same site in the desensitized nAChR pore. These conflicting results with the ^{3}H-PCP/^{3}H-TCP binding data can be reconciled by the interpretation that ethidium and CrV bind nearby loci in the pore, and that the PCP locus bridges these sites with enough overlap to compete with both compounds.

As the nAChR pore binds many classes of compounds, I also measured the binding of bupropion as a representative antidepressant. Photolabeling studies using bupropion (±)-2-(*N-tert*-butylamino)-3′-[^{125}I]-iodo-4′-azidopropiophenone (SADU-3-72) show that it binds between residues 2’ to 9’ in the desensitized state and labels 9’ in the resting state (152). My competition studies are consistent with these data – bupropion and ethidium compete for binding at the 9’ site in the desensitized conformation, and in the resting conformation, bupropion binds at a site distant from the 20’ site proposed for CrV, resulting in no displacement of CrV fluorescence.

Of the other compounds tested in this chapter, TID and tetracaine were of particular interest to me. As previously discussed, the constricted pore hypothesis presented in Chapter 3 was proposed in part because reduced labeling of pore residues in the uncoupled conformation could be explained by hindered access to the TID site due to pore constriction. ^{125}I-TID photolabels residues at the level of 2’ and 6’, toward the cytoplasmic side of the TMD, in the desensitized conformation (155), explaining its non-competitive interaction with both ethidium and CrV. As noted, in the resting conformation, TID binds between 9’ and 13’, also distant from the putative CrV site near 20’ and explaining the lack of competitive binding between the two compounds.

Previous studies have shown that TID binding is inhibited by both barbiturates and the local anesthetic tetracaine (165). Studies with ^{3}H-tetracaine have labeled residues at the level of 5’, 9’, 13’, and possibly even 16’/17’ on all muscle type subunits, covering a broad section of the pore that bridges both the PCP and barbiturate sites.(149-150) This unusually large binding locus explains its ability to compete with TID, ethidium, and CrV.

Finally, an aspect of pore pharmacology in the nAChR that is rarely discussed is the possibility that pore-blocking NCAs may also be able to bind at non-pore sites. $GABA_A$ receptors bind anesthetics at an intrasubunit TMD site (60), and the prokaryotic homologue ELIC has been crystallized with a local anesthetic, lidocaine, bound at an analogous site (73). Preliminary docking simulations with CrV and PCP have also suggested that these pore-blocking compounds may bind in the cavity formed by the 4 TMD α-helices (data not shown). Binding at an intrasubunit site may cause changes to M2 conformation that could allosterically affect the pore-binding of another NCA, and may contribute to the observed complexity of nAChR pore pharmacology.

5. CONCLUSION

Pore pharmacology of the nAChR is of great interest both from a pharmaceutical perspective and from a mechanistic perspective. In the absence of direct methods of visualization, the data so far on pore structure has been gleaned largely from binding/labeling studies. Together, the data paint a picture of complex pore pharmacology involving multiple overlapping binding sites in the nAChR pore. Although binding is usually discussed in the context of a few classical pore-blocking compounds or classes of compounds, these competition studies reveal nuances in the binding sites of individual drugs that contribute to our overall understanding of pore structure in different conformations of the nAChR.

Chapter 5

General Conclusion

The nAChR is implicated in a great number of neurological diseases, and there is interest in characterizing its structure, function, and pharmacology both for the development of therapeutics and because data from the nAChR can be extrapolated to some extent to other mammalian pLGICs. A key and poorly-understood factor in nAChR biology is the role that lipids in its environment play in modulating its function, including lipid-dependent uncoupling. Based on previous work on uncoupling, a structural/mechanistic model has been proposed. The primary aim of the work presented in this dissertation was to test this model and characterize in greater detail the structure of the uncoupled conformation of the nAChR. More broadly, we hoped that this work would contribute to our understanding of lipid-nAChR interactions.

1. M4 Acts as a Lipid Sensor

One key component of the lipid-dependent model of uncoupling is the ability of the nAChR to sense its surrounding lipids and to undergo conformational transitions in response to changing lipid environments. The uncoupling model proposes that the key structure for lipid-sensing is the lipid-exposed M4 α-helix, which lies at the nAChR-lipid interface. During uncoupling, it has been proposed that M4 tends to interact more with surrounding lipids, as opposed to the adjacent TMD helices, M1 and M3. Weak M4-M1/M3 interactions may lead to ineffective interactions between the M4 C-terminus and the Cys-loop, thus ultimately leading to an increased separation between the ECD and TMD. This model predicts that tight association of M4 with the TMD bundle should increase coupling and conversely decrease the nAChR's sensitivity to lipids. Intramembrane aromatic interactions, which are known to energetically drive the association of α-helices in the

TMD, should therefore promote tightness of M4 association and thereby decrease propensity to uncouple.

Electrophysiology data from the wildtype prokaryotic homologue ELIC and ELIC with three aromatic residues introduced to enhance M4-M1/M3 interactions (ELIC-3) shows that aromatics at the M4-M1/M3 interface promote coupling between the agonist site and channel gate. Additionally, the increased aromatic interactions in ELIC-3 decrease lipid sensitivity and restored gating when ELIC is reconstituted into PC membranes. FTIR data for reconstituted ELIC and ELIC-3, in comparison with GLIC and the nAChR, reveal a trend for increasing thermal stability and decreasing solvent-exposure with increasing numbers of aromatic interactions between M4 and M1/M3. Aromatic interactions between the TMD α-helices generally increase TMD stability. These data are in line with the lipid-dependent model of uncoupling and definitively implicate the M4 α-helix as a key determinant in pLGIC lipid sensing.

2. nAChR Pore Conformations

The crystal structures of the prokaryotic homologue ELIC bear great resemblance to the conformational changes proposed for the lipid-dependent uncoupling conformation. The inability of agonist to induce conformational change in the pore of crystallized ELIC provides additional evidence that crystallized ELIC adopts a non-functional and possibly uncoupled conformation. Notably, the channel pore of ELIC is severely constricted relative to that of other closed pLGICs. Pore collapse may be a structural feature of uncoupling. To test this idea, I characterized the binding of various NCAs to the pore of the nAChR in the desensitized, resting, and uncoupled conformations. If the channel pore is collapsed in the uncoupled conformation, then NCA binding affinity should be reduced relative to what is observed for the desensitized and resting nAChR, or even eliminated.

Binding studies with the fluorescent compounds ethidium bromide and crystal violet revealed binding to both desensitized and resting conformations. Both compounds stabilize the desensitized conformation, and showed higher affinity binding to desensitized nAChR as opposed to resting nAChR. At concentrations of both fluorescent compounds that approach saturation of the resting conformation, no specific pore binding of either compound could be detected to uncoupled nAChR. This is consistent with the hypothesis that the channel is collapsed or constricted in the uncoupled conformation.

Further studies to investigate the binding of NCAs to the uncoupled nAChR pore were not met with great success, but I was able to characterize in greater detail the pore pharmacology of resting and desensitized nAChR through competition studies between NCAs and both ethidium and CrV. My data reveal a complex network of overlapping binding sites in the nAChR pore and resolves in greater detail the sites and interactions of several compounds. Much more extensive characterization is needed to gain a clear picture of how pharmaceuticals interact with the structural transitions that occur upon conformational change.

3. Final Remarks

Great advances have been made in recent years in our understanding of pLGIC structure and function, due largely to crystal structures having been obtained for several prokaryotic and mammalian pLGICs both in unliganded and liganded states. Global conformational changes that accompany gating have been largely elucidated, and the mechanisms by which ligand binding is translated to channel function are now well-understood. Lipid interactions with pLGICs and the mechanisms by which they influence pLGIC function, however, remain relatively clouded in mystery. Investigating the ability of the plasma membrane composition to modulate the function of the nAChR is especially significant given the topological and functional similarities the nAChR bears to other members of the Cys-loop family, which include the $GABA_A$ receptor, 5-$HT3_A$ receptor, glycine receptor, and glutamate-gated chloride channels. Furthermore, the lipid-modulation of the nAChR and other members of the pLGIC superfamily may play a yet-uninvestigated role in health and disease. As research increasingly correlates human disease states with altered lipid metabolism, lipid-dependent modulation of pLGICs may gain new significance in understanding and treating neurological disease.

References

1. Bertrand, D. (2002) Neuronal nicotinic acetylcholine receptors and epilepsy. *Epilepsy Curr.* 2(6), 191-193.
2. Dineley, K.T., Pandya, A.A., and Yakel, J.L. (2015) Nicotinic ACh receptors as therapeutic targets in CNS disorders. *Trends Pharmacol Sci.* 36(2), 96-108.
3. Posadas, I., López-Hernández, B., and Ceña, V. (2013) Nicotinic receptors in neurodegeneration. *Curr Neuropharmacol.* 11(3), 298-314.
4. Martin, L.F. and Freedman, R. (2007) Schizophrenia and the alpha7 nicotinic acetylcholine receptor. *Int Rev Neurobiol.* 78, 225-46.
5. Schaaf, C.P. (2014) Nicotinic acetylcholine receptors in human genetic disease. *Genetics in Medicine.* 16, 649-656.
6. Changeux, J.P., Podleski, T.R., and Wofsy, L. (1967) Affinity labeling of the acetylcholine-receptor. *PNAS.* 58, 2063-2070.
7. Wessler, I.K. and Kirkpatrick, C.J. (2001) The non-neuronal cholinergic system: an emerging drug target in the airways. *Pulm Pharmacol Ther.* 14(6), 423-434.
8. Dani, J.A. and Bertrand, D. (2007) Nicotinic acetylcholine receptors and nicotinic cholinergic mechanisms of the central nervous system. *Annu Rev Pharmacol Toxicol.* 47, 699-729.
9. Gotti, C., Moretti, M., Zanardi, A., Gaimarri, A., Champtiaux, N., Changeux, J.-P., Whiteaker, P., Marks, M.J., Clementi F., and Zoli, M. (2005) Heterogeneity and selective targeting of neuronal nicotinic acetylcholine receptor (nAChR) subtypes expressed on retinal afferents of the superior colliculus and lateral geniculate nucleus: identification of a new native nAChR subtype α3β2 (α5 or β3) enriched in retinocollicular afferents. *Mol Pharmacol.* 68(4), 1162-1171.
10. Unwin, N. (2005) Refined structure of the nicotinic acetylcholine receptor at 4Å resolution. *J Mol Biol.* 346(4), 967-89.
11. Brejc, K., Dijk, W.J., Klaassen R.V., Schuurmans, M., van Der Oost, J., Smit, A.B., and Sixma, T.K. (2001) Crystal structure of an ACh-binding protein reveals the ligand-binding domain of nicotinic receptors. *Nature*. 411(6835), 269-76.
12. Bocquet, N., Nury, H., Baaden, M., Le Poupon, C., Changeux, J.P., Delarue, M., and Corringer, P.J. (2009) X-ray structure of a pentameric ligand-gated ion channel in an apparently open conformation. *Nature*. 457(7225), 111-114.
13. Hilf, R.J. and Dutzler. R. (2008) X-ray structure of a prokaryotic pentameric ligand-gated ion channel. *Nature.* 452(7185), 375-379.
14. Du, J., Lu, W., Wu, S.P., Cheng, Y.F., and Gouaux, E. (2015) Glycine receptor mechanism elucidated by electron cryo-microscopy. *Nature*. 526, 224-229.
15. Hibbs, R.E. and Gouaux, E. (2011) Principles of activation and permeating in an anion-selective Cys-loop receptor. *Nature.* 474, 54-60.
16. Hassaine, G., Deluz, C., Grasso, L., Wyss, R., Tol, M.B., Hovius, R., Graff, A., Stahlberg, H., Tomizaki, I. Desmyter, A., Moreau, C., Li, X.D., Poitevin, F., Vogel, H., and Nury, H. (2014) X-ray structure of the mouse serotonin 5-HT3 receptor. *Nature*. 514, 276-281.
17. Miller, P.S. and Aricescu, A.R. (2014) Crystal structure of a human GABAa receptor. *Nature.* 512, 270.
18. daCosta, C.J.B. and Baenziger, J.E. (2013) Gating of pentameric ligand-gated ion channels: structural insights and ambiguities. *Structure*. 21, 1271-1283.

19. Kracun, S., Harkness, P.C., Gibb, A.J., and Millar, N.S. (2008) Influence of the M3-M4 intracellular domain upon nicotinic acetylcholine receptor assembly, targeting and function. *Br Pharmacol.* 153(7), 1474-1484.
20. Celie, P.H., van Rossum-Fikkert, S.E., van Dijk, W.J., Brejc, K., Smit A.B., and Sixma, T.K. (2004) Nicotine and carbamylcholine binding to nicotinic acetylcholine receptors as studied in AChBP crystal structures. *Neuron*. 41(6), 907-914.
21. Huang, X., Chen, H., Michelsen, K., Schneider, S., and Shaffter, P.L. (2015) Crystal structure of human glycine receptor-α3 bound to antagonist strychnine. *Nature.* 526(7572), 277-280.
22. Dennis, M., Giraudat, J., Kotzyba-Hibert, F., Goeldner, M.., Hirth, C., Chang, J.Y., Lazure, C., Chretien, M., and Changeux, J.P. (1988) Amino acids of the *Torpedo marmorata* acetylcholine receptor alpha subunit labeled by a photoaffinity ligand for the acetylcholine binding site. *Biochemistry*. 27, 2346-2357.
23. Galzi, J.L., Revah, F., Black, D., Goeldner, M., Hirth, C., and Changeux, J.P. (1990) Identification of a novel amino acid alpha-tyrosine 93 within the cholinergic ligands binding sites of the acetylcholine receptor by photoaffinity labeling. Additional evidence for a three-loop model of the cholinergic ligands-binding sites. *J Biol Chem.* 265, 10430-10437.
24. Middleton, R.E. and Cohen, J.B. (1991) Mapping of the acetylcholine binding site of the nicotinic acetylcholine receptor: [3H]nicotine as an agonist photoaffinity label. *Biochemistry*. 30, 6987-6997.
25. Gao, F., Bren, N., Burghardt, T.P., Hansen, S., Henchman, R.H., Taylor, P., McCammon, J.A., and Sine, S.M. (2005) Agonist-medited conformational changes in acetylcholine-binding protein revealed by simulation and intrinsic tryptophan fluorescence. *J Biol Chem.* 280, 8443-8451.
26. Corringer, P.J., Galzi, J.L., Eisele, J.L., Bertrand, S., Changeux, J.P., and Bertrand, D. (1995) Identification of a new component of the agonist binding site of the nicotinic alpha 7 homooligomeric receptor. *J Biol Chem.* 270, 11749-11752.
27. Czajkowski, C., Kaufmann, C., and Karlin, A. (1993) Negatively charged amino acid residues in the nicotinic receptor delta subunit that contribute to the binding of acetylcholine. *PNAS.* 90, 6285-6289. .
28. Unwin, N., Miyazawa, A., Li, J., and Fujiyoshi, Y. (2002) Activation of the nicotinic acetylcholine receptor involves a switch in conformation of the alpha subunits. *J Mol Biol.* 319(5), 1165-1176.
29. Sauguet, L., Poitevin, F., Murail, S., Van Renterghem, C., Moraga-Cid, G., Malherbe, L., Thompson A.W., Koehl, P., Corringer, P.J., Baaden, M., and Delarue, M. (2013) Structural basis for ion permeation mechanism in pentameric ligand-gated ion channels. *EMBO J.* 32(5), 728-741.
30. Sauguet, L., Shahsavar, A., Poitevin, F., Huon, C., Menny, A., Nemecz, A., Haouz, A., Changeux, J.P., Corringer, P.J., and Delarue, M. (2014) Crystal structures of a pentameric ligand-gated ion channel provide a mechanism for activation. *PNAS.* 111(3), 966-971.
31. Althoff, T., Hibbs, R.E., Banerjee, S., and Gouaux, E. (2014) X-ray structures of GluCl in apo states reveal a gating mechanism of Cys-loop receptors. *Nature.* 512(7514), 333-337.
32. Nemecz, A., Prevost, M.S., Menny, A., and Corring, P.J. (2016) Emerging molecular mechanisms of signal transduction in pentameric ligand-gated ion channels. *Cell*. 90, 452-470.

33. Shan, Q., Haddrill, J.L., and Lynch, J.W. (2001) Invermectin, an unconventional agonist of the glycine receptor chloride channel. *J Biol Chem.* 276(16), 12556-64.
34. Lee, W.Y. and Sine, S.M. (2005) Principal pathway coupling agonist binding to channel gating in nicotinic receptor. *Nature.* 438, 243-247.
35. Shen, X.M., Ohno, K., Tsujino, A., Brengman, J.M., Gingold, M., Sine, S.M., and Engel A.G. (2003) Mutation causing severe myasthenia reveals functional asymmetry of AChR signature cystine loops in agonist binding and gating. *J Clin Invest.* 111(4), 497-505.
36. Sine, S.M., Shen, X.M., Wang, H.L., Ohno, K., Lee, W.Y., Tsujino, A., Brengmann, J., Bren, N., Vajsar, J., and Engel, A.G. (2002) Naturally occurring mutations at the acetylcholine receptor binding site independently alter ACh binding and channel gating. *J Gen Physiol*. 120(4), 483-96.
37. Nury, H., Bocquet, N., Le Poupon, C., Raynal, B., Haouz, A., Corringer, P.J., and Delarue, M. (2010) Crystal structure of the extracellular domain of a bacterial ligand-gated ion channel. *J Mol Biol.* 395(5), 1114-1127.
38. Bouzat, C., Gumilar, G., Spitzmaul, G., Wang, H.L., Rayes, D., Hansen, S.B., Taylor, P., and Sine, S.M. (2004) Coupling of agonist binding to channel gating in an ACh-binding protein linked to an ion channel. *Nature.* 430(7002), 896-900.
39. Eiselé, J.L., Bertrand, S., Galzi, J.L., Devillers-Thiéry, A., Changeux, J.P., and Bertrand, D. (1993) Chimaeric nicotinic-serotonergic receptor combines distinct ligand binding and channel specificities. *Nature*. 366, 479-483.
40. Grutter, T., Prado de Carvalho, L., Virginie, D., Taly, A., Fischer, M., and Changeux, J.P. (2005) A chimera encoding the fusion of an acetylcholine binding protein to an ion channel is stabilized in a state close to the desensitized form of ligand-gated ion channels. *C R Biol.* 328, 223-234.
41. Schmandt, N., Velisetty, P., Chalamalasetti, S.V., Stein, R.A., Bonner, R., Talley, L., Parker, M.D., Mchaourab, H.S., Yee, V.C., Lodowski, D.T., and Chakrapani, S. (2015) A chimeric prokaryotic pentameric ligand-gated channel reveals distinct pathways of activation. *J Gen Physiol.* 146, 323-340.
42. Tillman, T.S., Seyoum, E., Mowrey, D.D., Xu, Y., and Tang, P. (2014) ELIC-a7 nicotinic acetylcholine receptor (a7 nAChR) chimeras reveal a prominent role of the extracellular-transmembrane domain interface in allosteric modulation. *J Biol Chem.* 289, 13851-13857.
43. Changeux, J.P. (2013) 50 years of allosteric interactions: the twists and turns of the models. *Nat Rev Cell Mol Bio.* 14, 819-829.
44. Burzomato, V., Beato, M., Groot-Kormelink, P.J., Colquhoun, D., and Sivilotti, L. (2004) Single-channel behavior of heteromeric α1β glycine receptors: an attempt to detect a conformational change before the channel opens. *J Neurosci.* 24(48), 10924-10940.
45. Boyd, N.D. and Cohen, J.B. (1980) Kinetics of binding of [3H]acetylcholine to Torpedo postsynaptic membranes: association and dissociation rate constants by rapid mixing and ultrafiltration. *Biochemistry*. 19(23), 5323-8.
46. Franco-Obregon, A. Jr. and Lansman, J.B. (1995) Spontaneous opening of the acetylcholine receptor channel in developing muscle cells from normal and dystrophic mice. *J Neurosci Res.* 42(4), 452-8.
47. Giniatullin, R., Nistri, A., and Yakel, J.L. (2005) Desensitizaion of nicotinic ACh receptors: shaping cholinergic signaling. *Cell Trends Neurosci.* 28(7), 371-378.
48. Suto, M.J. & Zacharias, N. (2004) Neuronal nicotinic acetylcholine receptors as drug targets. *Expert Opin Ther Targets.* 8(2), 61-64.

49. D’hoedt, D. & Bertrand, D. (2009) Nicotinic acetylcholine receptors: an overview on drug discovery. *Expert Opin Ther Targets.* 13(4), 395-411.
50. Bertrand, D. and Gopalakrishnan, M. (2007) Allosteric modulation of nicotinic acetylcholine receptors. *Biochemistry Pharmacol.* 74(8), 1155-1163.
51. Seo, S., Henry, J.T., Lewis, A.H., Wang, N., and Levandoski, M.M. (2009) The positive allosteric modulator morantel binds at noncanonical subunit interfaces of neuronal nicotinic acetylcholine receptors. *J Neurosci.* 29(27), 8734-8742.
52. Gronlien, J.H., Hakerud, M., Ween, H., Thorin-Hagene, K., Briggs, C.A., Gopalakrishnan, M., and Malysz, J. (2007) Distinct profiles of alpha7 nAChR positive allosteric modulation revealed by structurally diverse chemotypes. *Mol Pharmacol.* 72(3), 715-724.
53. Hurst, R.S., Hajos, M., Raggenbass, M., Wall, T.M., Higdon, N.R., Lawson, J.A., Rutherford-Root, K.L., Berkenpas, M.B., Hoffmann, W.E., Piotrowski, D.W., Groppi, V.E., Allaman, G., Ogier, R., Bertrand, S., Bertrand, D., and Arneric, S.P. (2005) A novel positive allosteric modulator of the alpha7 neuronal nicotinic acetylcholine receptor: in vitro and in vivo characterization. *J Neurosci.* 25(17), 4396-405.
54. Young, G.T., Zwart, R., Walker, A.S., Sher, E., and Millar, N.S. (2008) Potentiation of alpha7 nicotinic acetylcholine receptors via an allosteric transmembrane site. *PNAS.* 105(38), 14686-91.
55. Krause, R.M., Buisson, B., Bertrand, S., Corringer, P.J., Galzi, J.L., Changeux, J.P., and Bertrand, D. (1998) Ivermectin: a positive allosteric effector of the alpha7 neuronal nicotinic acetylcholine receptor. *Mol Pharmacol.* 53(2), 283-294.
56. Arias, H.R. and Bouzat, C.B. (2006) Modulation of nicotinic acetylcholine receptors by noncompetitive antagonists. *Biological and Biophysical Aspects of Ligand-Gated Ion Channel Receptor Superfamilies.* Arias, H.R. (Ed.) Research Signpost, Kerala, India, 61-107.
57. Hansen, S.B. and Taylor P. (2007) Galanthamine and non-competitive inhibitor binding to ACh-binding protein: evidence for a binding site on non-alpha-subunit interfaces of heteromeric neuronal nicotinic receptors. *J Mol Biol.* 369(4), 895-901.
58. Hosie, A.M., Wilkins, M.E., da Silva, H.M., and Smart, T.G. (2006) Endogenous neurosteroids regulate GABAA receptors through two discrete transmembrane sites. *Nature.* 444(7118), 486-489.
59. Bertrand, D., Bertrand, S., Cassar, S., Gubbins, E., Li, J., and Gopalakrishnan, M. (2008) Positive allosteric modulation of the a7 nicotinic acetylcholine receptor: ligand interactions with distinct binding sites and evidence for a prominent role of the M2-M3 segment. *Mol Pharmacol.* 74, 1407-1416.
60. Collins, T. and Millar, N.S. (2010) Nicotinic acetylcholine receptor transmembrane mutations convert ivermectin from a positive to a negative allosteric modulator. *Mol Pharmacol.* 78(2), 198-204.
61. Mihic, S.J., Ye, Q., Wick, M.J., Koltchine, V.V., Krasowski, M.D., Finn, S.E., Mascia, M.P., Valenzuela, C.F., Hanson, K.K., Breenblatt, E.P., Harris, R.A., and Harrison, N.L. (1997) Sites of alcohol and volatile anaesthetic action on GABA(A) and glycine receptors. *Nature.* 389(6649), 385-389.
62. Ye, Q., Koltchine, V.V., Mihic, S.J., Mascia, M.P., Wick, M.J., Finn, S.E., Harrison, N.L., and Harris, R.A. (1998) Enhancement of glycine receptor function by ethanol is inversely correlated with molecular volume at position alpha267. *J Biol Chem.* 273(6), 3314-3319.

63. Chiara, D.C., Gill, J.F., Chen, Q., Tillman, T., Dailey, W.P., Eckenhoff, R.G., Xu, Y., Tang, P., and Cohen, J.B. (2014) Photoaffinity labeling the propofol binding site in GLIC. *Biochemistry*. 53(1), 135-42.
64. Brannigan, G., Hénin, J., Law, R., Eckenhoff, R., and Klein, M.L. (2008) Embedded cholesterol in the nicotinic acetylcholine receptor. *PNAS*. 105(38), 14418-14423.
65. Arias, H.R. and Bhumireddy, P. (2005) Anesthetics as chemical tools to study the structure and function of nicotinic acetylcholine receptors. *Curr Protein Pept Sci.* 6, 451-472.
66. Arias, H.R., Gumilar, F., Rosenberg, A., Targowska-Duda, K.M., Feuerbach, D., Jozwiak, K., Moaddel, R., Wainer, I.W., and Bouzat, C. (2009) Interaction of bupropion with muscle-type nicotinic acetylcholine receptors in different conformational states. *Biochemistry*. 48, 4506-4518.
67. Spitzmaul, G., Gumilar, F., Dilger, J.P., and Bouzat, C. (2009) The local anaesthetics proadifen and adiphenine inhibit nicotinic receptors by different molecular mechanisms. *Br J Pharmacol.* 157, 804-817.
68. Gumilar, F., Arias, H.R., Spitzmaul, G., and Bouzat, C. (2003) Molecular mechanism of inhibition of nicotinic acetylcholine receptors by tricyclic antidepressants. *Neuropharmacol.* 45, 964-976.
69. Lape, R., Krashia, P., Colquhoun, D., and Sivilotti, L.G. (2009) Agonist and blocking actions of choline and tetramethylammonium on human muscle acetylcholine receptors. *J Physiol.* 587(21), 5045-5072.
70. Akk, G., and Steinbach, J.H. (2003) Activation and block of mouse muscle-type nicotinic receptors by tetraethylammonium. *J Physiol.* 551(1), 155-168.
71. Khodakhah, K., Melishchuk, A., and Armstrong, C.M. (1997) Killing K Channels with TEA+. *PNAS.* 94, 13335-13338.
72. Gonzales-Gutierrez, G. and Grosman, C. (2015) The atypical cation-conduction and gating properties of ELIC underscore the marked functional versatility of the pentameric ligand-gated ion-channel fold. *J Gen Physiol.* 146(1), 15-36.
73. Lindstrom, J., Anholt, R., Einarson, B., Engel, A., Osame, M., and Montal, M. (1980) Purification of acetylcholine receptors, reconstitution into lipid vesicles, and study of agonist-induced cation channel regulation. *J Biol Chem.* 255(17), 8340-8350.
74. Criado, M., Eibl, H., and Barrantes, F.J. (1984) Functional properties of the acetylcholine receptor incorporated in model lipid membranes. Differential effects of chain length and head group of phospholipids on receptor affinity states and receptor-mediated ion translocation. *J Biol Chem.* 259(14), 9188-9198.
75. Huganir, R.L., Schell, M.A., and Racker, E. (1979) Reconstitution of the purified acetylcholine receptor from Torpedo californica. *FEBS Lett.* 108(1), 155-160.
76. Epstein, M. and Racker E. (1978) Reconstitution of carbamylcholine-dependent sodium ion flux and desensitization of the acetylcholine receptor from Torpedo californica. *J Biol Chem.* 253(19), 6660-6662.
77. Jones, O.T., Eubanks, J.H., Earnest, J.P., and McNamee, M.G. (1988) A minimum number of lipids are required to support the functional properties of the nicotinic acetylcholine receptor. *Biochemistry.* 27(10), 3733-3742.
78. Fong, T.M. and McNamee, M.G. (1986) Correlation between acetylcholine receptor function and structural properties of membranes. *Biochemistry*. 25, 830-840.

79. Ochoa, E.L., Dalziel, A.W., and McNamee, M.G. (1983) Reconstitution of acetylcholine receptor function in lipid vesicles of defined composition. *Biochim Biophys Acta.* 727, 151-162.
80. Sunshine, C. and McNamee, M.G. (1992) Lipid modulation of nicotinic acetylcholine receptor function: the role of neutral and negatively charged lipids. *Biochim Biophys Acta*. 1108, 240-246.
81. Addona, G.H., Sandermann, H. Jr., Kloczewiak, M.A., Hussaine, S.S., and Miller, K.W. (1998) Where does cholesterol act during activation of the nicotinic acetylcholine receptor? *Biochim Biophys Acta.* 1370, 299-309.
82. Schiebler, W. and Hucho, F. (1978) Membranes rich in acetylcholine receptor: characterization and reconstitution to excitable membranes from exogenous lipids. *Eur J Biochem.* 85, 55-63.
83. Popot, J.L., Demel, R.A., Sobel, A., Van Deenen, L.L., and Changeux, J.P. (1978) Interaction of the acetylcholine (nicotinic) receptor protein from Torpedo marmorata electric organ with monolayers of pure lipids. *Eur J Biochem.* 85, 27-42.
84. Baenziger, J.E., Morris, M.L., Darsaut, T.E., and Ryan, S.E. (2000) Effect of membrane lipid composition on the conformational equilibria of the nicotinic acetylcholine receptor. *J Biol Chem*. 275, 777-784.
85. Marsh, D. and Barrantes, F.J. (1978) Immobilized lipid in acetylcholine receptor-rich membranes from Torpedo marmorata. *PNAS.* 75, 4329-4333.
86. Ellena, J.F. Blazing, M.A., and McNamee, M.G. (1983) Lipid-protein interactions in reconstituted membranes containing acetylcholine receptor. *Biochemistry*. 22, 5523-5535.
87. Jones, O.T. and McNamee, M.G. (1988) Annular and non-annular binding sites for cholesterol associated with the nicotinic acetylcholine receptor. *Biochemistry.* 27, 2364-2374.
88. Sunshine, C. and McNamee, M.G. (1994) Lipid modulation of nicotinic acetylcholine function: the role of membrane lipid composition and fluidity. *Biochim Biophys Acta.* 1191, 59-64.
89. daCosta, C.J., Dey, L., Therien, J.P.D., and Baenziger, J.E. (2013) A distinct mechanism for activating uncoupled nicotinic acetylcholine receptors. *Nat Chem Biol.* 9, 701-707.
90. daCosta, C.J.B., Ogrel, A.A., McCardy, E.A., Blanton, M.P., and Baenziger, J.E. (2002) Lipid-protein interactions at the nicotinic acetylcholine receptor: a functional coupling between nicotinic receptors and phosphatidic acid-containing lipid bilayers. *J Biol Chem.* 277, 201-208.
91. Labriola, J.M., daCosta, C.J., Wang, S., Figeys, D., Smith, J.C., Sturgeon, R.M., and Baenziger, J.E. (2010) Phospholipase C activity affinity purifies with the Torpedo nicotinic acetylcholine receptor. *J Biol Chem.* 285(14), 10337-10343.
92. Kamerbeek, C.B., Mateos, M.V., Valles, A.S., Pediconi, M.F., Barrantes, F.J., and Borroni, V. (2015) Diacylglycerol levels modulate the cellular distribution of the nicotinic acetylcholine receptor. *Int J Biochem Cell Biol.* DOI: 10.1016/j.biocel.2016.02.010.
93. Bhushan, A. and McNamee, M.G. (1990) Differential scanning calorimetry and Fourier transform infrared analysis of lipid-protein interactions involving the nicotinic acetylcholine receptor. *Biochim Biophys Acta.* 1027(1), 93-101.
94. daCosta, C.J.B. and Baenziger, J.E. (2009) A lipid-dependent uncoupled conformation of the acetylcholine receptor. *J Biol Chem.* 284(26), 17819-17825.

95. Methot, N., Demers, C.N. and Baenziger, J.E. (1995) Structure of both the ligand- and lipid-dependent channel-inactive states of the nicotinic acetylcholine receptor probed by FTIR spectroscopy and hydrogen exchange. *Biochemistry.* 34, 15142-15149.
96. Hamouda, A.K., Sanghyi, M., Sauls, D., Machu, T.K., and Blanton, M.P. (2006) Assessing the lipid requirements of the Torpedo californica nicotinic acetylcholine receptor. *Biochemistry*. 45(13), 4327-4337.
97. Katz, B. and Thesleff, S. (1957) A study of the desensitization of produced by acetylcholine at the motor end-plate. *J Physiol.* 138, 63-80.
98. Boyd, N.D. and Cohen, J.B. (1980) Kinetics of binding of [^{3}H]acetylcholine and [^{3}H]carbamylcholine to *Torpedo* postsynaptic membranes: slow conformational transitions of the cholinergic receptor. *Biochemistry*. 19, 5344-5353.
99. Herz, J.M., Johnson, D.A., and Taylor, P. (1987) Interaction of noncompetitive inhibitors with the acetylcholine receptor. *J Biol Chem.* 262(15), 7238-7247.
100. Hénault, C.M., Sun, J., Therien, J.P.D., daCosta, C.J.B., Carswell, C.L., Labriola, J.M., Juranka, P.F., and Baenziger, J.E. (2015) The role of the M4 lipid-sensor in the folding, trafficking, and allosteric modulation of nicotinic acetylcholine receptors. *Neuropharmacol.* 96, 157-168.
101. Antollini, S.S., Xu, Y., Jiang, H., and Barrantes, F.J. (2005) Fluorescence and molecular dynamics studies of the acetylcholine receptor γM4 transmembrane peptide in reconstituted systems. *Mol Membr Biol.* 22, 471-483.
102. Xu, Y., Barrantes, F.J., Luo, X., Chen, K., Shen, J., and Jiang, H. (2005) Conformational dynamics of the nicotinic acetylcholine receptor channel: a 35-ns molecular dynamics simulation study. *J Am Chem Soc.* 127, 1291-1299.
103. Bouzat, C., Roccamo, A.M., Garbus, I., and Barrantes, F.J. (1998) Mutations at lipid eposed residues of the acetylcholine receptor affects its gating kinetics. *Mol Pharmacol.* 54, 146-153.
104. Lasalde, J.A., Tamamizu, S., Butler, D.H., Vibat, C.R., Hung, B., and McNamee, M.G. (1996) Tryptophan substitutions at the lipid-exposed transmembrane segment M4 of Torpedo californica acetylcholine receptor govern channel gating. *Biochemistry.* 35, 14139-14148.
105. Lee, Y.H., Li, L., Lasalde, J., Rojas, L., McNamee, M., G., Ortiz-Miranda, S.I., and Pappone, P. (1994) Mutations in the M4 domain of Torpedo californica acetylcholine receptor dramatically alter ion channel function. *Biophys J.* 66, 646-653.
106. Shen, X.M., Deymeer, F., Sine, S.M., and Engel, A.G. (2006) Slow-channel mutation in acetylcholine receptor alpha M4 domain and its efficient knockdown. *Ann Neurol.* 60, 128-136.
107. Zimmermann, I. and Dutzler, R. (2011) Ligand activation of the prokaryotic pentameric ligand-gated ion channel ELIC. *PLoS biology.* 9, e1001101.
108. Gonzalez-Gutierrez, G., Lukk, T., Agarwal, V., Papke, D., Nair, S.K., and Grosman, C. (2012) Mutations that stabilize the open state of the *Erwinia chrisanthemi* ligand gated ion channel fail to change the conformation of the pore domain in crystals. *Proc Natl Acad Sci USA.* 109, 6331-6336.
109. Haeger, S., Kuzmin, D., Detro-Dassen, S., Lang, N., Kilb, M., Tsetlin, V., Betz, H., Laube, B., and Schmalzing, G. (2010) An intramembrane aromatic network determines pentameric assembly of Cys-loop receptors. *Nat Struct Mol Biol.* 17, 90-98.

110. Carswell, C.L., Sun, J., and Baenziger, J.E. (2015) Intramembrane aromatic interactions influence the lipid sensitivities of pentameric ligand-gated ion channels. *J Biol Chem.* 290(4), 2496-2507.

111. Castillo, R.I., Rojo, L.E., Henriquez-Henriquez, M., Silva, H., Maturana, A., Villar, M.J., Fuentes, M., and Gaspar, P.A. (2016) From molecules to the clinic : linking schizophrenia and metabolic syndrome through sphingolipids metabolism. *Front Neurosci.* 10, 488.

112. Monteir-Cardoso, V.F., Oliveria, M.M., Melo, T., Domingues, M.R., Moreira, P.I., Ferreiro, E., Peixoto, F., and Videira, R.A. (2015) Cardiolipin profile changes are associated to the early synaptic mitochondrial dysfunction in Alzheimer's disease. *J Alzheimers Dis.* 43(4), 1375-1392.

113. Mahley, R.W. (2016) Central nervous system lipoproteins : ApoE and regulation of cholesterol metabolism. *Arterioscler Thromb Vasc Biol.* 36(7), 1305-1315.

114. Li, P. and Steinbach, J.H. (2010) The neuronal nicotinic αβ2 receptor has a high maximal probability of being open. *Br J Pharmacol.* 160(8), 1906-1915.

115. Fenster, C.P., Whitworth, T.L., Sheffield, E.B., Quick, M.W., and Lester, R.A. (1999) Upregulation of surface alpha4beta2 nicotinic receptors is initiated by receptor desensitization after chronic exposure to nicotine. *J Neurosci.* 19(12), 4804-4814.

116. Vallejo, Y.F., Buisson, B., Bertrand, D., and Green, W.N. (2005) Chronic nicotine exposure upregulates nicotinic receptors by a novel mechanism. *J Neurosci.* 25(23), 5563-5572.

117. Ngolab, J., Liu, L., Zhao-Shea, R., Gao, G., Gardner, P.D. and Tapper, A.R. (2015) Functional upregulation of α4* nicotinic acetylcholine receptors in VTA GABAergic neurons increases sensitivity to nicotine reward. *J Neurosci.* 35(22), 8570-8578.

118. Renda, A. and Nashmi, R. (2014) Chronic nicotine pretreatment is sufficient to upregulate α4* nicotinic receptors and increase oral nicotine self-administration in mice. *BMC Neurosci.* 15(89), doi: 10.1186/1471-2202-15-89.

119. Borroni, V. and Barrantes, F.J. (2011) Cholesterol modulates the rate and mechanism of acetylcholine receptor internalization. *J Biol Chem.* 286, 17122-17132.

120. Baier, C.J., Gallegos, C.E., Levi, V., and Barrantes, F.J. (2010) Cholesterol modulation of nicotinic acetylcholine receptor surface mobility. *Eur Biophys.* 39, 213-227.

121. Labriola, J.M., Pandhare, A., Jansen, M., Blanton, M.P., Corringer, P.J., and Baenziger, J.E. (2013) Structural sensitivity of a prokaryotic pentameric ligand-gated ion channel to its membrane environment. *J Biol Chem.* 288(16), 11294-11303.

122. daCosta, C.J.B., Sturgeon, R.M., Hamouda, A.K., Blanton, M.P., and Baenziger, J.E. (2011) Structural characterization and agonist binding to human α4β2 nicotinic receptors. *Biochm Biophys Res Commun.* 407, 456-460.

123. Methot, N., Ritchie, B.D., Blanton, M.P., and Baenziger, J.E. (2001) Structure of the pore-forming transmembrane domain of a ligand-gated ion channel. *J Biol Chem.* 276, 23726-23732.

124. Baenziger, J.E. and Methot, N. (1995) Fourier transform infrared and hydrogen/deuterium exchange reveal an exchange-resistant core of α-helical peptide hydrogens in the nicotinic acetylcholine receptor. *J Biol Chem.* 270, 29129-29137.

125. Morales, A., Aleu, J., Ivorra, I., Ferragut, J.A., Gonzales-Ros, J.M., and Miledi, R. (1995) Incorporation of reconstituted acetylcholine receptors from *Torpedo* into *Xenopus* oocyte membrane. *Proc Natl Acad Sci USA.* 92, 8468-8472.

126. Carswell, C.L., Hénault, C.M., Murlidaran, S., Therien, J.P.D., Juranka, P.F., Surujballi, J.A., Brannigan, G., and Baenziger, J.E. (2015) Role of the fourth transmembrane α-helix in the allosteric modulation of pentameric ligand-gated ion channels. *Structure*. 23(9), 1655-1664.
127. Hénault, C.M., Juranka, P.F., and Baenziger, J.E. (2015) The M4 transmembrane α-helix contributes differently to both the maturation and function of two prokaryotic pentameric ligand-gated ion channels. *J Biol Chem.* 290(41), 25118-25128.
128. Baenziger, J.E., Hénault, C.M., Therien, J.P., and Sun, J. (2015) Nicotinic acetylcholine receptor-lipid interactions: mechanistic insight and biological function. *Biochim Biophys Acta.* 1848, 1806-1817.
129. Barrantes, F.J. (2015) Phylogenetic conservation of protein-lipid motifs in pentameric ligand-gated ion channels. *Biochim Biophys Acta.* 1848, 1796-1805.
130. Jha, A., Cadugan, D.J., Purohit, P., and Auerbach, A. (2007) Acetylcholine receptor gating at extracellular transmembrane domain interface: the cys-loop and M2-M3 linker. *J Gen Physiol.* 130, 547-558.
131. Lummis, S.C., Beene, D.L., Lee, L.W., Lester, H.A., Broadhurst, R.W, and Dougherty, D.A. (2005) Cis-trans isomerisation at a proline opens the pore of a neurotransmitter-gated ion channel. *Nature.* 438, 248-252.
132. Blanton, M.P. and Cohen, J.B. (1992) Mapping the lipid-exposed regions in the *Torpedo californica* nicotinic acetylcholine receptor. *Biochemistry*. 31, 3738-3750.
133. Gonzalez-Gutierrez, G. and Grosman, C. (2010) Bridging the gap between structural models of nicotinic receptor superfamily ion channels and their corresponding functional states. *J Mol Biol.* 403, 693-705.
134. Baenziger, J.E. Ryan, S.E., Goodreid, M.M., Vuong, N.Q., Sturgeon, R.M., and daCosta, C.J.B. (2008) Lipid composition alters drug action at the nicotinic acetylcholine receptor. *Mol Pharmacol.* 73, 880-890.
135. Lurtz, M.M. and Pedersen, S.E. (1999) Aminotriarylmethane dyes are high-affinity noncompetitive antagonists of the nicotinic acetylcholine receptor. *Mol Pharmacol.* 55, 159-167.
136. Arias, H.R., Bhumireddy, P., Spitzmaul, G., Trudell, J.R., and Bouzat, C. (2006) Molecular mechanisms and binding site location for the noncompetitive antagonist crystal violet on nicotinic acetylcholine receptors. *Biochemistry.* 45, 2014-2026.
137. Fernandez-Nievas, G.A., Barrantes, F.J., and Antollini, S.S. (2008) Modulation of nicotinic acetylcholine receptor conformational state by free fatty acids and steroids. *J Biol Chem.* 283, 21478-21486.
138. McCarthy, M.P. and Moore, M.A. (1992) Effects of lipids and detergents on the conformation of the nicotinic acetylcholine receptor from *Torpedo californica. J Biol Chem.* 267, 7655-7663.
139. Heidmann, T., Oswald, R.E., and Changeux, J.P. (1983) Multiple sites of action for noncompetitive blockers on acetylcholine receptor rich membrane fragments from *Torpedo marmorata. Biochemistry.* 22, 3112-3127.
140. daCosta, C.J.B., Medaglia, S.A., Lavigne, N., Wang, S., Carswell, C.L., and Baenziger, J.E. (2009) Anionic lipids allosterically modulate multiple nicotinic acetylcholine receptor conformational equilibria. *J Biol Chem.* 284, 33841-33849.
141. Beckstein, O. and Sansom, M.S. (2006) A hydrophobic gate in an ion channel: the closed state of the nicotinic acetylcholine receptor. *Phys Biol.* 3, 147-159.

142. Hilf, R.J. and Dutzler, R. (2009) Structure of a potentially open state of a proton-activated pentameric ligand-gated ion channel. *Nature.* 457, 115-118.

143. Prevost, M.S., Sauguet, L., Nury, H., Van Renterghem, C., Huon, C., Poitevin, F., Baaden, M., Delarue, M., and Corringer, P.J. (2012) A locally closed conformation of a bacterial pentameric proton-gated ion channel. *Nat Struct Mol Biol.* 19, 642-649.

144. Unwin, N. and Fujiyoshi, Y. (2010) Gating movement of acetylcholine receptor caught by plunge-freezing. *J Mol Biol.* 422, 617-634.

145. Arias, H.R., McCardy, E.A., Gallagher, M.J., and Blanton, M.P. (2001) Interaction of barbiturate analogs with the *Torpedo californica* nicotinic acetylcholine receptor ion channel. *Mol Pharmacol.* 60(3), 497-506.

146. Arias, H.R., Bhumireddy, P., and Bouzat, C. (2006) Molecular mechanisms and binding site locations for noncompetitive antagonists of nicotinic acetylcholine receptors. *Int J Biochem & Cell Biol.* 38, 1254-1276.

147. Fryer, J.D. and Lukas, R.J. (1999) Antidepressants noncompetitively inhibit nicotinic acetylcholine receptor function. *J Neurochem.* 72, 117-1124.

148. Arias, H.R. (1999) Role of local anesthetics on both cholinergic and serotonergic ionotropic receptors. *Neurosci and Behav Rev.* 23, 817-843.

149. Middleton, R.E., Strnad, N.P., and Cohen, J.B. (1999) Photoaffinity labeling the *Torpedo* nicotinic acetylcholine receptor with [^{3}H]tetracaine, a nondesensitizing noncompetitive antagonist. *Mol Pharmacol.* 56, 290-299.

150. Gallagher, M.J. and Cohen, J.B. (1999) Identification of amino acids of the *Torpedo* nicotinic acetylcholine receptor contributing to the binding sites for the noncompetitive antagonist [^{3}H]tetracaine. *Mol Pharmacol.* 56(2), 300-307.

151. Blanchard, S.G., Elliott, J., and Raftery, M.A. (1979) Interaction of local anesthetics with *Torpedo californica* membrane-bound acetylcholine receptor. *Biochem.* 18(26), 5880-5885.

152. Pandhare, A., Hamouda, A.K., Staggs, B., Aggarwal, S., Duddempudi, P.K., Lever, J.R., and Blanton, M.P. (2012) Bupropion binds to two sites in the *Torpedo* nicotinic acetylcholine receptor transmembrane domain: a photoaffinity labeling study with the bupropion analog [^{125}I]-SADU-3-72. *Biochemistry.* 51(12), 2425-2435.

153. Krodel, E.K., Beckman, R.A., and Cohen, J.B. (1979) Identification of a local anesthetic binding site in nicotinic post-synaptic membrane isolated from *Torpedo marmorata* electric tissue. *Mol Pharmacol.* 15(2), 294-312.

154. Boyd, N. D. and Cohen, J.B. (1984) Desensitization of membrane-bound *Torpedo* acetylcholine receptor by amine noncompetitive antagonists and aliphatic alcohols: studies of [^{3}H]acetylcholine binding and ^{22}Na$^+$ion fluxes. *Biochemistry.* 23, 4023-4033.

155. White, B.H., Howard, S., Cohen, S.G., and Cohen, J.B. (1991) The hydrophobic photoreagent 3-(trifluoromethyl)-3-m-([^{125}I]iodophenyl) diazirine is a novel noncompetitive antagonist of the nicotinic acetylcholine receptor. *J Biol Chem.* 266(32), 21595-21607.

156. Wu, G., Raines, D.E., and Miller, K.W. (1994) A hydrophobic inhibitor of the nicotinic acetylcholine receptor acts on the resting state. *Biochemistry.* 33(51), 15375-15381.

157. Garcia-Colunga, J., Awad, J.N., and Miledi, R. (1997) Blockage of muscle and neuronal nicotinic acetylcholine receptor by fluoxetine (Prozac). *Proc Natl Acad Sci USA.* 94, 2041-2044.

158. Arias, H.R. and Bhumireddy, P. (2005) The antidepressant binding site on the nicotinic acetylcholine receptor. *Biophys J.* 88, 555.

159. Wohri, A.B., Hillertz, P., Eriksson, P.O., Meuller, J., Dekker, N., and Snijder, A. (2013) Thermodynamic studies of ligand binding to the human homopentameric glycine receptor using isothermal titration calorimetry. *Mol Membr Biol.* 30(2), 169-183.
160. Pratt, M.B., Pedersen, S.E., and Cohen, J.B. (2000) Identification of the sites of incorporation of [^{3}H]ethidium diazide within the *Torpedo* nicotinic acetylcholine receptor ion channel. *Biochemistry*. 39, 11452-11462.
161. Hamouda, A.K., Stewart, D.S., Chiara, D.C., Savechenkov, P.Y., Bruzik, K.S., and Cohen, J.B. (2014) Identifying barbiturate binding sites in a nicotinic acetylcholine receptor with [^{3}H]allyl *m*-trifluoromethyldiairine mephobarbital, a photoreactive barbiturate. *Mol Pharmacol.* 85(5), 735-746.
162. Gallagher, M.J., Chiara, D.C., and Cohen, J.B. (2001) Interactions between 3-(trifluoromethyl)-3-(*m*-[^{125}I]iodophenyl diazirine and tetracaine, phencyclidine, or histrionicotoxin in the *Torpedo* series nicotinic acetylcholine receptor ion channel. *Mol Pharmacol*. 59(6), 1514-1522.
163. Arias, H.R., McCardy, E.A., Bayer, E.Z., Gallagher, M.J., and Blanton, M.P. (2002) Allosterically linked noncompetitive antagonist binding sites in the resting nicotinic acetylcholine receptor ion channel. *Arch Biochem Biophys.* 403, 121-131.
164. Arias, H.R., Trudell, J.R., Bayer, E.Z., Hester, B., McCardy, E.A., and Blanton, M.P. (2003) Noncompetitive antagonist binding sites in the *Torpedo* nicotinic acetylcholine receptor ion channel: structure-activity relationship studies using adamantine derivatives. *Biochemistry*. 42, 7358-7370.
165. Ryan, S.E., Blanton, M.P., and Baenziger, J.E. (2001) A conformational intermediate between the resting and desensitized states of the nicotinic acetylcholine receptor. *J Biol Chem.* 276, 4796-4803.

Appendix

A. CHAPS Correction for Free Crystal Violet

My preliminary titrations with crystal violet yielded a K_d for aso-nAChR pre-incubated with agonist about 10x higher than was reported by Lurtz and Pedersen (127). This is likely because we did not further purify our crystal violet to control for degradation and did not correct for nonspecific binding to the lipid membrane, glass and plastic surfaces, etc. The concentration of free crystal violet is not equal in this case to bound crystal violet subtracted from the concentration of added crystal violet. A standard curve was therefore constructed to determine the concentration of free crystal violet in samples with nAChR.

Duplicate samples containing 1mM carbamylcholine ±20nM nAChR were made up in TRB to a total volume of 2ml and incubated for 30 min with 5, 10, 25, 50, 100, 200, 398, or 794 nM crystal violet (these concentrations are corrected for dilution). 1.4ml of each sample was centrifuged in a tabletop centrifuge at max speed for 30 min at 4^oC. 1.25ml of the supernatant containing free crystal violet was then mixed with 0.75ml of 2.67% CHAPS in TRB to obtain 2ml of 1% CHAPS, which was read in the Cary spectrophotometer (used for all fluorescence experiments presented in this dissertation) at excitation/emission = 590/630nm and slits 10/20nm (Fig. A.1).

The above plot shows that a significant amount of free CrV fluorescence is lost after incubation with nAChR, indicating depletion of CrV in solution through binding to nAChR. Assuming that for CrV in TRB (black squares), the concentration of CrV added is equal to the concentration of free CrV, we can calculate the concentration of free CrV after incubation with nAChR (white circles) from the fluorescence intensity. Free CrV with nAChR was then plotted against the concentration of CrV added to derive a slope of 0.7967 (Fig. A.2). Multiplying the

Figure A.1.

Fluorescence intensity of free CrV with (open white circles) and without nAChR (solid black squares). Data acquired with 20nM nAChR and 1mM Carb.

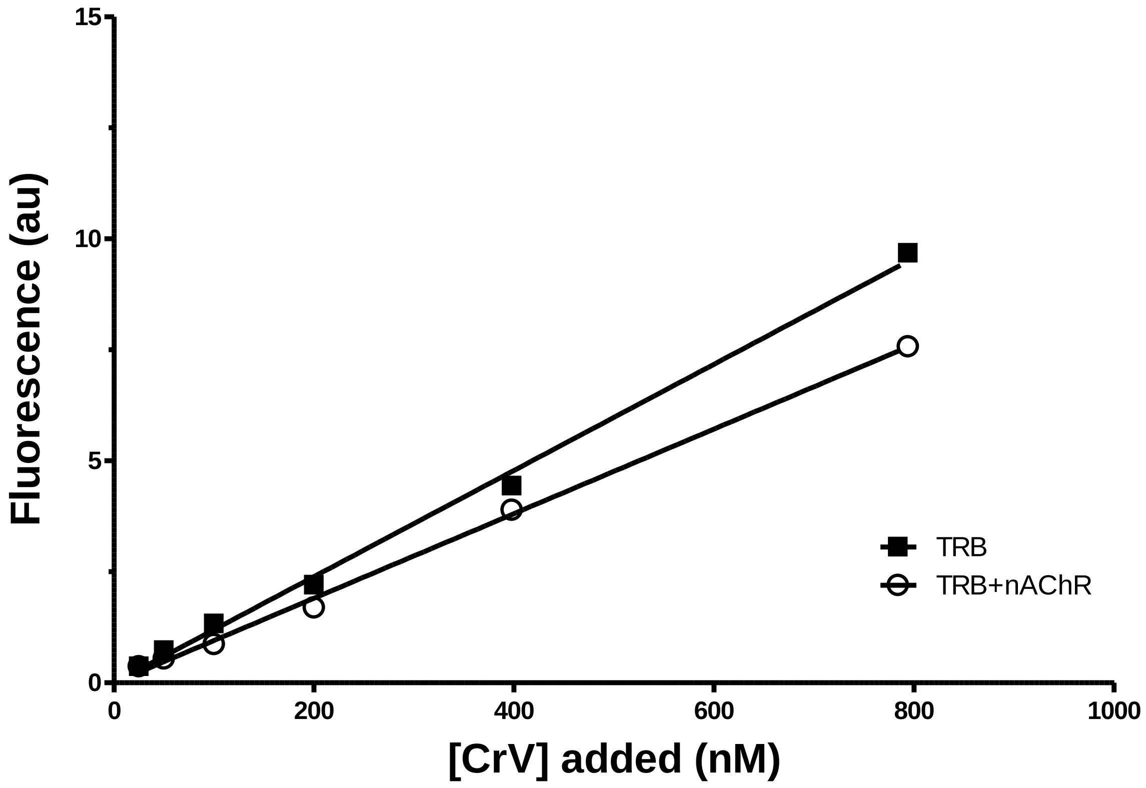
15
10
5
0
Fluorescence (au)
0
200
400
600
800
1000
[CrV] added (nM)
TRB
TRB+nAChR

Figure A.2.

Plot of free CrV in a sample with 20nM nAChR against CrV added. The slope is 0.7967.

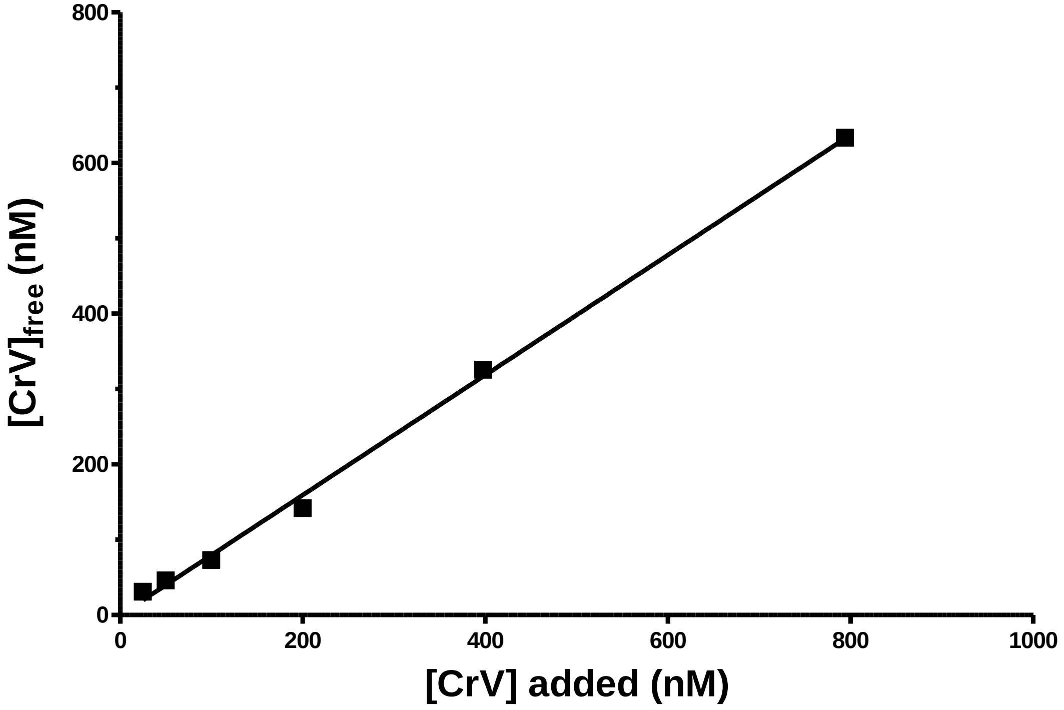

800
600
400
200
0
0
200
400
600
800
1000
$[CrV]_{free}$ (nM)
[CrV] added (nM)

concentration of CrV added by this correction factor yields the concentration of free CrV for a sample with 20nM nAChR.

B. Supporting data for CrV Binding Experiments

Kinetic binding data was obtained for CrV at 80 nM (~K_d of the desensitized conformation). CrV kinetic traces displayed similar patterns of activity as those obtained for ethidium bromide (Fig. B.1). Note that due to the high affinity of CrV for desensitized nAChR, initial mixing caused a large shift in the conformational equilibrium toward the desensitized state, and a large proportion of receptors bound to CrV. This results in a relatively small proportion of nAChR remaining in the resting state and thus sensitive to the addition of Carb. Note also that dibucaine addition slightly increases the fluorescence signal through light scattering upon interaction with aso-nAChR membranes. Furthermore, at the concentration of dibucaine used (500 μM), only about 50% of CrV fluorescence can be displaced from desensitized nAChR, and displacement from resting nAChR is negligible (from CrV competition data, see Chapter 4 Pore pharmacology of reconstituted nAChR).

We also considered the possibility that the binding detected to the resting state was due to high concentrations of CrV, which stabilize the desensitized state when bound, competing allosterically with α-BTX. CrV may shift the conformational equilibrium in favor of the desensitized state, and the observed binding may thus be due to a small population of desensitized nAChRs rather than to resting nAChRs.

The data suggest this is not the case – if CrV binds to resting nAChR and shifts them to the desensitized conformation, then a sigmoidal binding curve should be observed. If insufficient

Figure B.1.

CrV kinetic binding experiments showing agonist-induced fluorescence increase and displacement by dibucaine in aso-nAChR (i), aso-nAChR pre-incubated with 20x the molar concentration of α-BTX (ii), and PC-nAChR (iii).

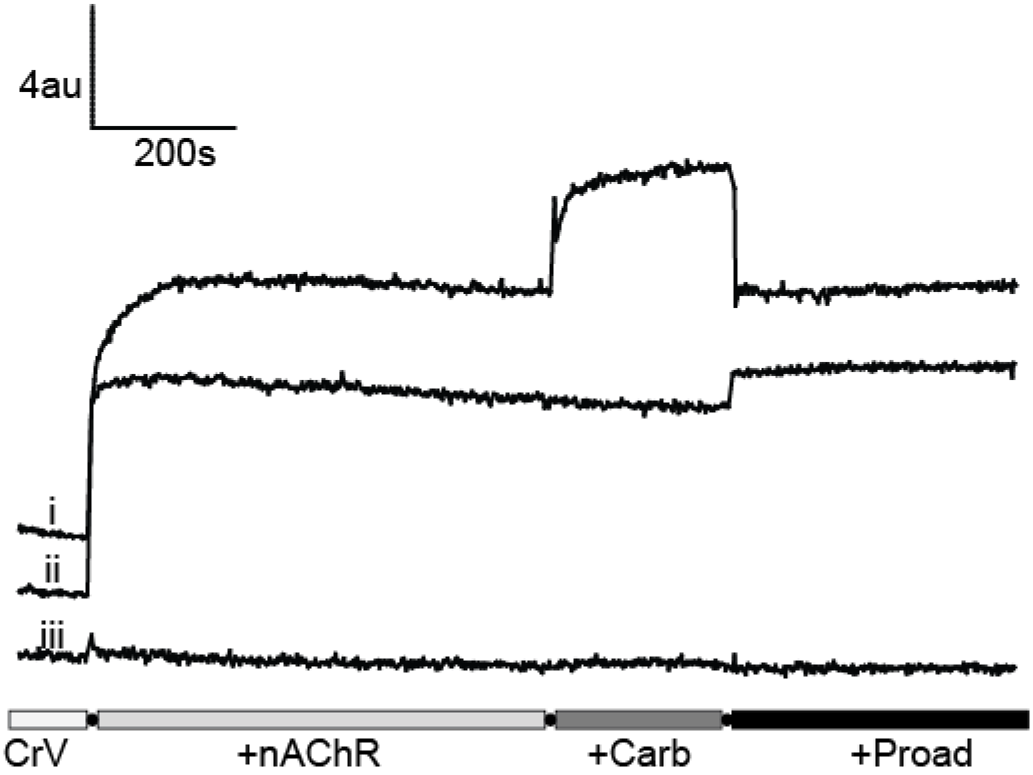
4au
200s
i
ii
iii
CrV
+nAChR
+Carb
+Proad

α-BTX was added and only a proportion of receptors were stabilized in the R state, then a sigmoidal curve with a reduced B_{max} value should be observed, reflecting binding of CrV to the portion of receptors stabilized in the desensitized state. The B_{max} values for the curve fits for CrV binding to aso-nAChR in both the presence of Carb and α-BTX are nearly identical, indicating that the number of CrV sites available is the same between the two samples. Note that the same nAChR reconstitutions were used for both binding curves.

I performed additional controls to ensure that sufficient α-BTX was used to stabilize the resting conformation. I recorded fluorescence emission scans after incubation of 50nM nAChR samples with increasing concentrations of BTX. At the concentration of BTX used in the titration experiments (10x the molar concentration of aso-nAChR), we should ideally see the same fluorescence intensity as at higher concentrations, indicating that the BTX binding is saturated (Fig. B.2).

The scans showed that increasing amounts of BTX increasingly inhibited CrV fluorescence (albeit minimally) up to >8uM, or about 160x the molar concentration of nAChR. A plot of the BTX concentration against peak fluorescence (measured from scans shown in Fig. B.2) shows that fluorescence plateaus at about 18 au (Fig. B.3). Since the light scattering effect from receptor in solution has been subtracted from these traces, and CrV has negligible fluorescence in solution, this fluorescence can be attributed to binding to the R state. Note that points for both 50nM aso-nAChR with 80nM CrV and 50nM aso-nAChR with 80nM CrV and 0.5mM Carb were plotted at [BTX]=0. Also note that these two traces were taken at 80nM CrV (the K_d of the desensitized state) instead of 240nM (K_d of the resting state).

Figure B.2.

Emission scans of CrV bound to resting state nAChR. 50 nM nAChR was pre-incubated with 500 μM Carb (+carb), buffer (-carb, -BTX), or increasing concentrations of α-BTX. The trace labeled (+BTX) is pre-incubated with α-BTX at 10x the molar concentration of nAChR (500 nM). Every successive trace going from top to bottom contains double the concentration of α-BTX as the previous one (20x molar concentration, 40x, etc.). Each trace is the average of 3 scans.

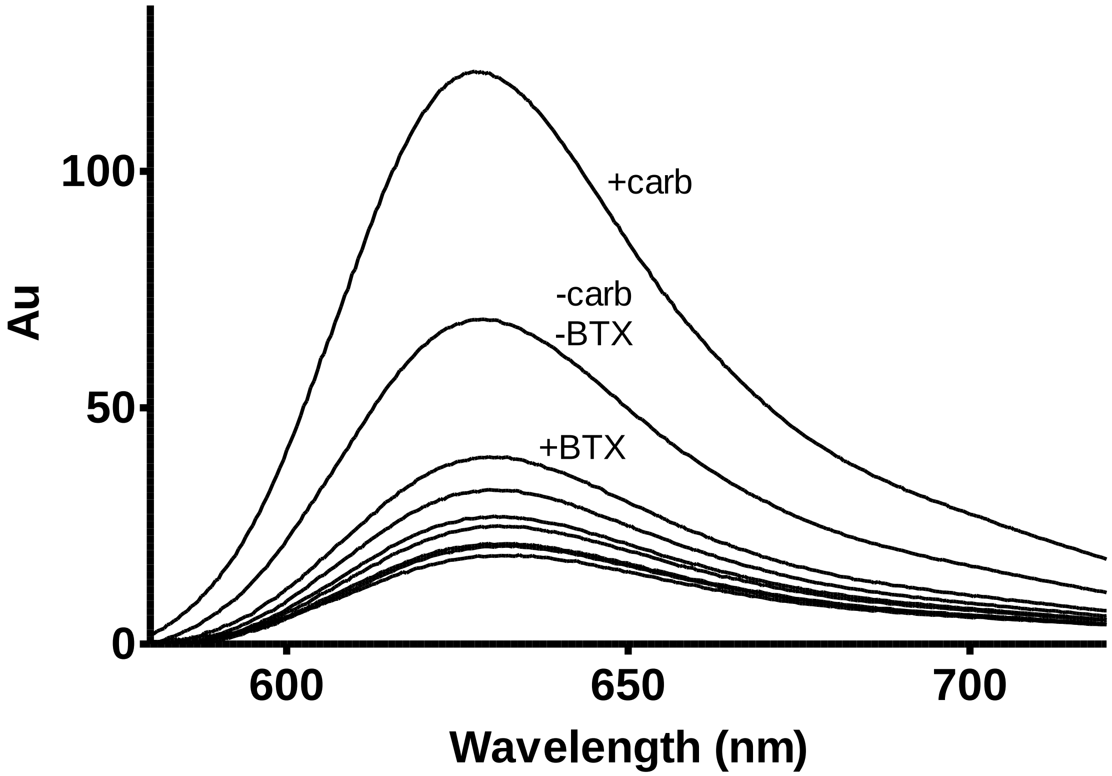

Au
0
50
100
600
650
700
Wavelength (nm)
+carb
-carb
-BTX
+BTX

Figure B.3.

Peak fluorescence of traces in Figure B.2 plotted against concentration of α-BTX (A) and the log of the α-BTX concentration (B). The fluorescence plateaus at ~18 au and corresponds to binding in the resting state. The (+carb) trace, which corresponds to aso-nAChR incubated with Carb in the absence of α-BTX, is included at 1nM α-BTX as a tether. Curve fit gives an EC_{50} of around 100 nM α-BTX.

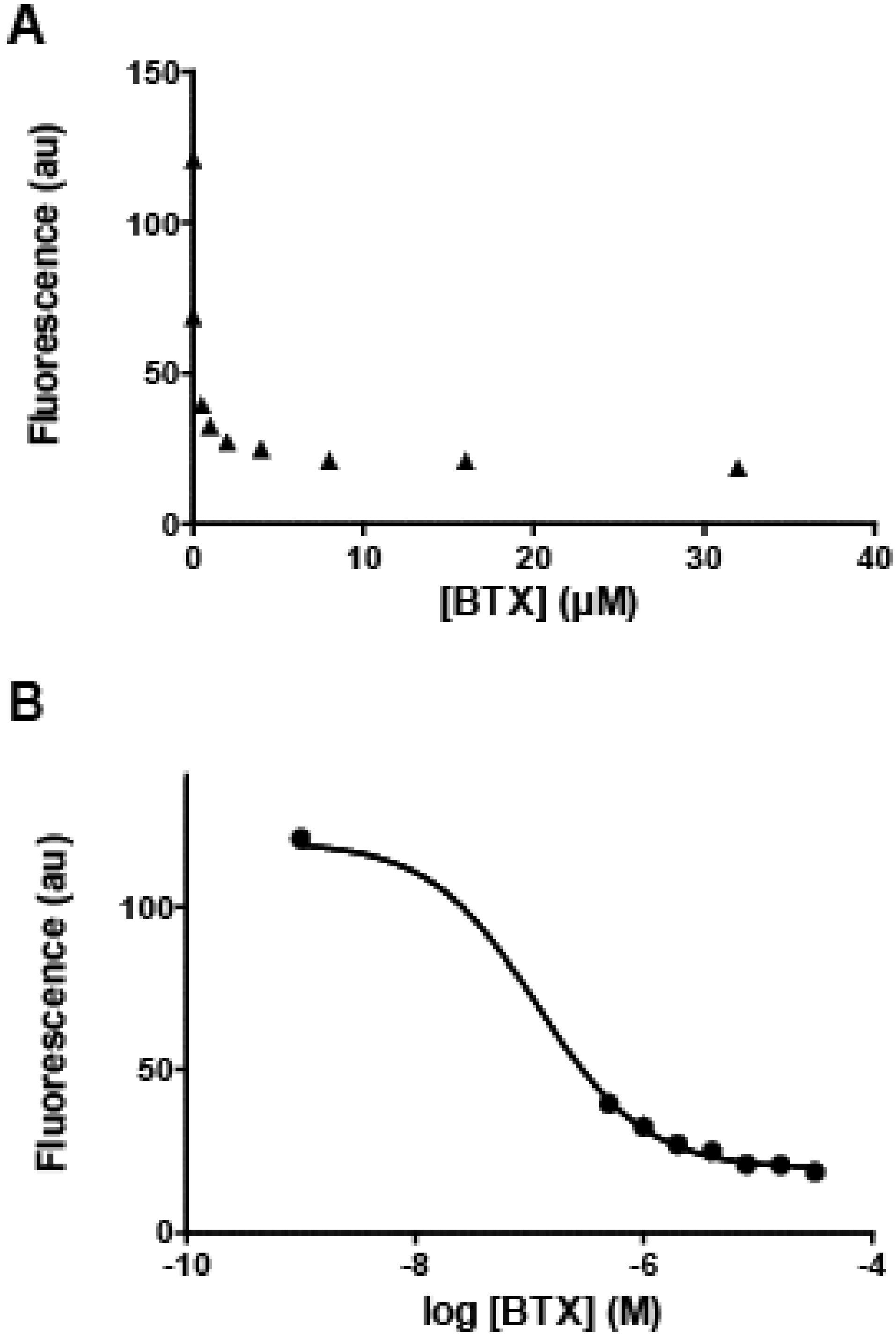
A
Fluorescence (au)
150
100
50
0
0
10
20
30
40
[BTX] (µM)
B
Fluorescence (au)
100
50
0
-10
-8
-6
-4
log [BTX] (M)

The plot in Fig. B.3 can be interpreted as follows: At a concentration of α-BTX = 0, 100% of receptors are stabilized in the desensitized conformation (au = 120). The plot reaches an asymptote, at which 100% of receptors are stabilized in the resting conformation by α-BTX (au = 20). At a concentration of α-BTX that is 20x the molar concentration of aso-nAChR, the fluorescence intensity is ~30au, which would correspond to about 90% of receptors stabilized in the resting state. This would suggest that I have used enough BTX to fully (within reason) stabilize the R state.

A log plot of the same data was constructed by constraining the top plateau to the value of the +carb trace, corresponding to 100% desensitized receptor. The point was placed at log value -9 (1nM) to tether the plot for presentation purposes (curve fit changes depending on where this point is tethered, but the analysis does not significantly change). The curve fit suggests that the EC_{50}, which is presumably when the receptor is stabilized half in D and half in R, occurs at ~100nM BTX, or 2x the molar concentration of receptor.

Curriculum Vitae

Name: Jiayin Sun

Degrees Obtained:

B.Sc. Neuroscience (Honours, High Distinction)
University of Toronto, 2013.

Research Experience:

2013 – 2016	Graduate thesis: “Structural characterization of a lipid-dependent uncoupled conformation of the nicotinic acetylcholine receptor.” Carried out under the supervision of Dr. John Baenziger, University of Ottawa.
2013	Summer research student – Continuation of work from 2011.
2012	Summer research student – Identifying the role of small Rho GTPases in the motility of cancer cells. Carried out under supervision of Dr. Stephen Gee, University of Ottawa.
2011	Summer research student – Characterization of the binding of ethidium to a pore site in different conformations of the nicotinic acetylcholine receptor. Carried out under the supervision of Dr. John Baenziger, University of Ottawa.

Scholarships and Awards:

2016	2nd Place (Biochemistry Master’s Student) in Graduate Poster Session, 2016
2014	CIHR Training Program in Neurodegenerative Lipidomics Scholarship
2013	University of Ottawa Graduate Admission Scholarship
2011	CIHR Summer Research Student Award in Neurodegenerative Lipidomics Scholarship

Publications:

Papers published in refereed journals:

1. **Jiayin Sun**, Frederique Comeau, and John E. Baenziger. (2016) Fluorescent channel blockers exhibit distinct pharmacologies for uncoupled, resting, and desensitized nicotinic acetylcholine receptors. *BBA-Biomembranes.* 1859(2), 146-154.

2. Carswell, C.L., **Sun, J.**, and Baenziger, J.E. (2015) Intramembrane aromatic interactions influence the lipid sensitivities of pentameric ligand-gated ion channels. *J Biol Chem.* 290(4), 2496-2507.

3. Baenziger, J.E., Hénault, C.M., Therien, J.P., and **Sun, J.** (2015) Nicotinic acetylcholine receptor-lipid interactions: mechanistic insight and biological function. *Biochim Biophys Acta.* 1848, 1806-1817.

4. Hénault, C.M., **Sun, J.,** Therien, J.P.D., daCosta, C.J.B., Carswell, C.L., Labriola, J.M., Juranka, P.F., and Baenziger, J.E. (2015) The role of the M4 lipid-sensor in the folding, trafficking, and allosteric modulation of nicotinic acetylcholine receptors. *Neuropharmacol.* 96, 157-168.

Conference Presenstations:

1. **Jiayin Sun**, Casey L. Carswell, and John E. Baenziger. (2014). Engineering Lipid Sensitivity in Prokaryotic Ligand-Gated Ion Channels. Poster presentation delivered at the Protein Engineering Conference in Ottawa, Canada on June 21, 2014.

2. **Jiayin Sun** and John E. Baenziger. (2014). Structural Insight into the Uncoupled Conformation of the Nicotinic Acetylcholine Receptor. Poster presentation delivered at the Annual Canadian Association for Neuroscience Meeting in Montreal, Canada on May 27, 2014.